Electron transfer between the reductase and ferredoxin component of toluene dioxygenase

Dissertation

zur Erlangung des akademischen Grades
doctor rerum naturalium
(Dr. rer. nat.)
im Fach Biologie
eingereicht an der

Mathemathisch-Naturwissenschaftlichen Fakultät I
der Humboldt-Universität zu Berlin
von

Dipl.-Biol. Tzong-Yuan Lin

Präsident der Humboldt-Universität zu Berlin
Prof. Dr. Jan-Hendrik Olbertz

Dekan der Mathematisch-Naturwissenschaftlichen Fakultät I
Prof. Stefan Hecht, PhD

Gutachter/in:
1. Prof. Dr. Holger Dobbek
2. Prof. Dr. Wolfgang Lockau
3. Prof. Dr. Silke Leimkühler

Tag der mündlichen Prüfung: 13.08.2012

Die zur Untersuchung vorliegende Arbeit wurde von September 2006 bis April 2010 an der Universität Bayreuth und von Mai 2010 bis März 2011 an der Humboldt-Universität zu Berlin unter der Leitung von Herrn Prof. Dr. Holger Dobbek durchgeführt.

The investigations of the present work were accomplished from September 2006 until April 2010 at the University of Bayreuth and from May 2010 until March 2011 at the Humboldt-University of Berlin under the supervision of Prof. Dr. Holger Dobbek.

The whole is more than the sum of its parts.

Aristotle (382 BC - 322 BC)

CONTESTS

ABBREVIATIONS

APS	**ammonium persulfate**
A_x	**absorption at x nm**
BESSY	**Berliner Elektronenspeicherring-Gesellschaft für Synchrotronstrahlung**
bp	**base pairs**
BPDO	**biphenyl dioxygenase**
BSA	**bovine serum albumin**
CAM	**chloramphenicol**
Cb	**carbenicillin**
CT	**charge transfer**
cv	**column volume, column volumes**
Dye_{OX}	**oxidized redox dye**
Dye_{RED}	**reduced redox dye**
DCPIP	**dichlorophenol indophenole**
DNA	**deoxyribonucleic acid**
dNTP	**deoxynucleoside triphosphate**
DTT	**2,3-dithiothreitol**
DT	**sodium dithionite**
EDTA	**ethylenediaminetetraacetic acid**
Enz_{OX}	**oxidized enzyme**
Enz_{RED}	**reduced enzyme**
Enz-$FAD^{\cdot}$	**flavoprotein, red semiquinone**
FAD	**flavin adenine dinucleotide**
FMN	**flavin mononucleotide**
FAD	**oxidized flavin adenine dinucleotide**
$FADH_2$	**two-electrons reduced flavin adenine dinucleotide, protonated, hydroquinone**

$FADH^{\cdot}$	**flavin adenine dinucleotide radical, blue semiquinone**
$FAD^{\cdot}$	**flavin adenine dinucleotide radical, red semiquinone**
FPLC	**fast protein liquid chromatography**
HEPES	**4-(2-hydroxyethyl)-1 piperazineethanesulfonic acid**
IPTG	**Isopropyl β-d-1-thiogalactopyranoside**
KHCNF	**potassium hexacyanoferrat**
MOPS	**3-(n-morpholino)propanesulfonic acid**
M_r	**relative molecular mass**
NAD^+	**oxidized nicotinamide adenine dinucleotide**
NADH	**reduced nicotinamide adenine dinucleotide**
NBDO	**nitrobenzene dioxygenase**
NDO	**naphthalene dioxygenase**
OD_x	**optical density at x nm**
PCR	**polymerase chain reaction**
PEG	**polyethylene glycol**
RED_{TOL}-FAD	**flavoprotein, oxidized**
RED_{TOL}-$FADH_2$	**flavoprotein, two-electron reduced, hydroquinone**
RED_{TOL}-$FADH^{\cdot}$	**flavoprotein, blue semiquinone**
RO	**Rieske non-heme iron dioxygenase**
RMSD	**root mean square deviation**
SDS	**sodium dodecyl sulfate**
PAGE	**polyacrylamide gel electrophoresis**
TAE buffer	**tris-acetate-EDTA buffer**

TDO	**toluene dixoygenase**
TEMED	**tetramethylethylenediamine**
TRIS	**2-amino-2-hydroxylmethyl-propane 1,3 diol**
U	**unit (enzyme activity in µmol of substrate consumed per min)**
UV	**ultraviolet**
UV/Vis	**ultraviolet-visible**
v/v	**volume per volume**
w/v	**weight per volume**
ε_x	**extinction coefficient at x nm**
λ	**wavelength**

INTRODUCTION

1 Aerobic degradation of aromatic hydrocarbons

Aromatic hydrocarbons are organic molecules with one or more aromatic rings. They can be classified into three groups, polycyclic aromatic hydrocarbons (PAH), heterocyclics and substituted aromatics (Ceraglia, 1992). They are known to be widespread anthropogenic pollutants and constitute a major environmental and health threat due to their carcinogenic, mutagenic and toxic character (Ceraglia, 1992).

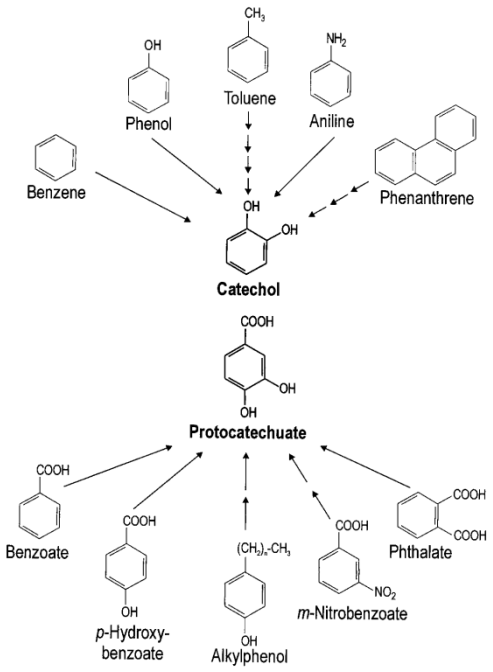

Figure 1. Aerobic degradation of aromatic hydrocarbons. Aromatic hydrocarbons are converted to one of the two key intermediates, catechol or protocatechuate. Figure is taken from Fritsche and Hofrichter (Fritsche & Hofrichter, 2000).

Many bacteria are capable of degrading aromatic compounds. The common strand for all microorganisms, which degrade aromatic hydrocarbons aerobically, is the initial step. The addition of molecular oxygen to the aromatic nucleus yields *cis*-diol.

The hydroxylated compounds are further converted to catechol or protocatechuate which are the two key intermediates in the aerobic degradation of aromatic hydrocarbons (Fig. 1). These key intermediates are substrates of ring-cleaving enzymes that utilize molecular oxygen to open the aromatic ring either between the hydroxyl groups (meta-cleavage), catalyzed by intradiol dioxygenases, or nearby one of the two hydroxyl groups (ortho-cleavage), catalyzed by extradiol dioxygenases (Harayama & Timmis, 1992). A Krebs cycle intermediate is formed *via* central pathways involving several more enzyme reactions. The Rieske non-heme iron dioxygenases belong to the family of enzymes that catalyze the initial step in the aerobic degradation of aromatic hydrocarbons. They are multi-component systems comprising of flavoproteins and iron-sulfur proteins.

2 Rieske non-heme iron dioxygenase

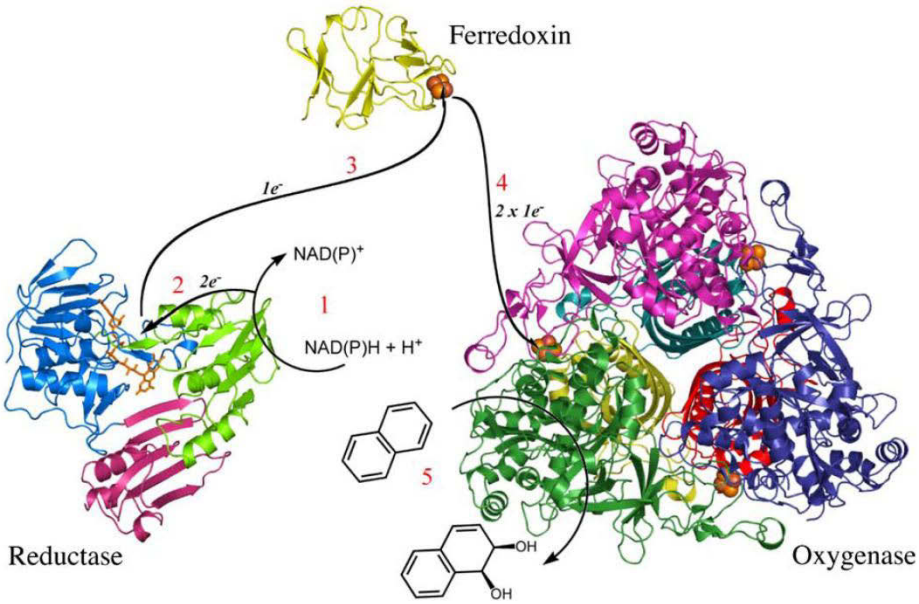

Figure 2. Electron transfer chain of the naphthalene dioxygenase. Electrons originate from NAD(P)H (1) and are passed to the flavin (2). The electrons are transferred to two ferredoxins in two subsequent one-electron steps (3). Ferredoxin shuttles the electrons to the Rieske-type [2Fe-2S] cluster of the oxygenase (4). The mononuclear iron center in the oxygenase component accepts the electrons and

catalyzes the conversion of naphthalene to its *cis*-dihydrodiol form by incorporating two oxygen atoms from dioxygen (5). Figure is taken from Ferraro *et al.* (Ferraro *et al*., 2005).

Table 1. Classification of ROs based on their components. Table is modified from Ferraro *et al*. (Ferraro *et al*., 2005).

Proteins	Class	Reductase	Ferredoxin	Oxygenase	Example
Two	IA	FMN $[2Fe\text{-}2S]_P$		$[2Fe\text{-}2S]_R$ Fe^{2+}	PDO
	IB	FAD $[2Fe\text{-}2S]_P$		$[2Fe\text{-}2S]_R$ Fe^{2+}	OMO
Three	IIA	FAD	$[2Fe\text{-}2S]_P$	$[2Fe\text{-}2S]_R$ Fe^{2+}	Dibenzofuran DO
	IIB	FAD	$[2Fe\text{-}2S]_R$	$[2Fe\text{-}2S]_R$ Fe^{2+}	Toluene DO
	III	FAD $[2Fe\text{-}2S]_P$	$[2Fe\text{-}2S]_R$	$[2Fe\text{-}2S]_R$ Fe^{2+}	Naphthalene DO

$[2Fe\text{-}2S]_P$ = plant-type ferredoxin; $[2Fe\text{-}2S]_R$ = Rieske-type ferredoxin; MO = monooxygenase system; DO = dioxygenase, PDO = phthalate dioxygenase, OMO = oxoquinoline monooxygenase

Table 2. Classification of ROs classified based on their substrates. Table is modified from Ferraro *et al*. (Ferraro *et al*., 2005).

Rieske non-heme oxygenase family	Example substrate	Example members
Naphthalene	Naphthalene, indole, Nitroarenes, phenanthrene	Naphthalene DO nitrobenzene DO
Toluene/biphenyl	Toluene, cumene, biphenyl PCBs	benzene DO toluene DO, biphenyl DO, cumene DO
Benzoate	Benzoate, toluate	Benzoate DO
Phthalate	Phthalate	Phthalate DO, 2-oxoquinoline-8 MO

$[2Fe\text{-}2S]_P$ = plant-type ferredoxin; $[2Fe\text{-}2S]_R$ = Rieske-type ferredoxin; MO = monooxygenase system; DO = dioxygenase

The enzymes of the Rieske non-heme iron dioxygenase (RO) system can be grouped by the number of their components. Two-component systems can be distinguished by the type of flavin, FAD or FMN that is present in the reductase component. Three-component systems are divided by the presence of a plant-type or Rieske-type ferredoxin component and furthermore by the presence or absence of an additional [2Fe-2S] cluster in the flavoprotein component (Tab. 1) (Ferraro *et al.*, 2005). Another classification of the RO system is based on the substrate specificity of the oxygenase component (Ferraro *et al.*, 2005) (Tab. 2).

3 **Flavoproteins in ROs**

A flavin-containing reductase is the first component of the system to accept electrons belonging either to the family of glutathione reductase (GR, e.g. toluene dioxygenase reductase) or to the family of ferredoxin-NADP reductase (e.g. phthalate dioxygenase reductase). Typical for a member of the glutathione reductases, simple flavoproteins contain only FAD as a prosthetic group and can be structurally divided into three domains, an FAD-binding, an NADH-binding and a C-terminal domain. $Reductase_{TOL}$ (RED_{TOL}) transfers the electrons from NADH to the ferredoxin. Members of this family include the reductase component of the naphthalene and benzene dioxygenase system (Gibson *et al.*, 1968). The reductase component of the toluene dioxygenase has an FAD redox center and possesses typical absorption spectrum maxima at 375 nm and 450 nm (Subramanian *et al.*, 1981). The FMN-containing putidaredoxin reductase has an analogous function in the cytochrome-$P\text{-}450_{CAMPHOR}$ hydroxylase (Koga *et al.*, 1989; Roome *et al.*, 1983).

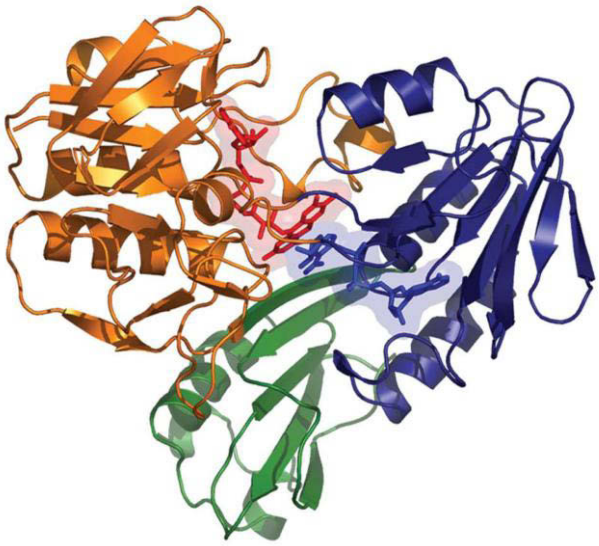

Figure 3. Overall structure of reductaseTOL. The FAD-binding domain is colored in blue, the NADH-binding domain colored in orange and the C-terminal domain is depicted in green. FAD and nicotinamide molecules are shown as red and blue stick models, respectively. Figure is taken from Friemann *et al*. (Friemann *et al*., 2009).

A structural feature of the GR family members is the possession of two ADP binding sites, one for FAD and one for NAD. The amino acid sequences of both binding sites are highly conserved. The FAD-binding site has the characteristic sequence of $GXGX_2GX_3AX_6G$, where X represents any amino acid. $GXGX_2G$ is part of a loop that connects the first β–strand and an α-helix causing a typical $\beta\alpha\beta\alpha$ fold (Scrutton *et al*., 1990). The $GXGX_2GX_3AX_6G$ sequence, close to the N-terminus, is typically the FAD-binding site. Around 140 residues downstream of the first conserved glycin another conserved dinucleotide binding consensus sequence can be found which represents the NAD-binding site. Compared to the conversed amino acid sequence for FAD binding, the alanine residue is exchanged by a glycine. There is a conserved glutamate seven residues along the alanine. The third glycine residue is replaced by an alanine followed by other four alanine residues (Senda *et al*., 2000).

The overall structure of reductaseTOL shows high similarity to bovine adrenodoxin reductase (AdR), putidaredoxin reductase (Pdr) and biphenyl dioxygenase reductase (BphA4) which both belong to the glutathione reductase family (Fig. 3) (Friemann *et*

al., 2009; Karplus & Schulz, 1987; Senda *et al*., 2000; Sevrioukova *et al*., 2004). In BphA4 from *Acidovorax sp*. transient protein-protein interactions have shown dependency on the redox state of the BphA4 (Senda *et al*., 2007). This suggests that the redox state of flavins and iron-sulfur clusters have a huge impact on the interplay of these proteins and the binding of a ligand leads to conformational changes to support protein-protein interactions (Senda *et al*., 2007).

3.1 Chemistry of flavin

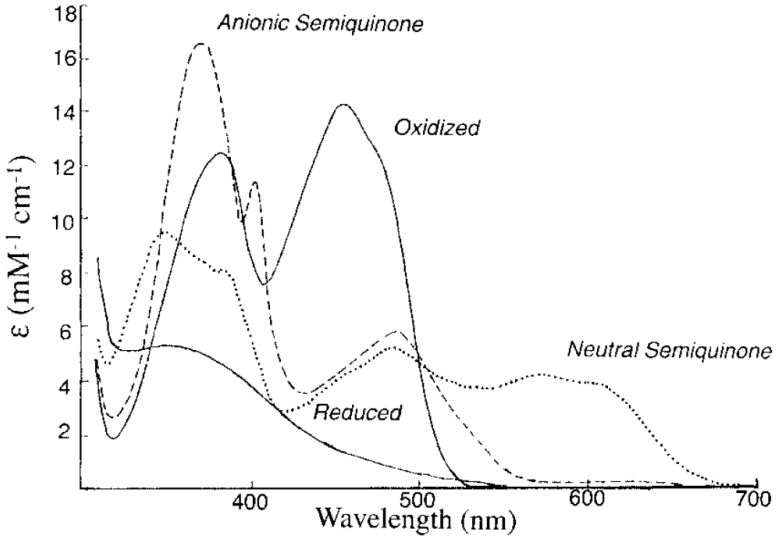

Figure 4. **UV/Vis spectrum of a flavoprotein** in its oxidized and reduced (both solid lines), anionic semiquinone (dashed) and neutral semiquinone (dotted) form. Figure is taken from Massey (Massey, 2000).

The flavin contributes to the characteristic UV/Vis spectrum of a flavoprotein with maxima at around 360 nm and 450 nm in oxidized state (Fig. 4). The chromophoric moiety has an amphoteric character. The pyrimidine nucleus is hydrophilic and the xylene ring is lipophilic making the pyrimidine ring the reactive part of the flavin. The redox chemistry of a flavoprotein is solely limited to the isoalloxazine ring, more precisely to the position N1-C4a-N5 where electron uptake and donation takes place

(Fig. 5) (Ghisla & Massey, 1989). The N10 ribityl side chain of the flavin is responsible for the interaction of the flavin with the protein (Fig. 5) (Massey, 2000).

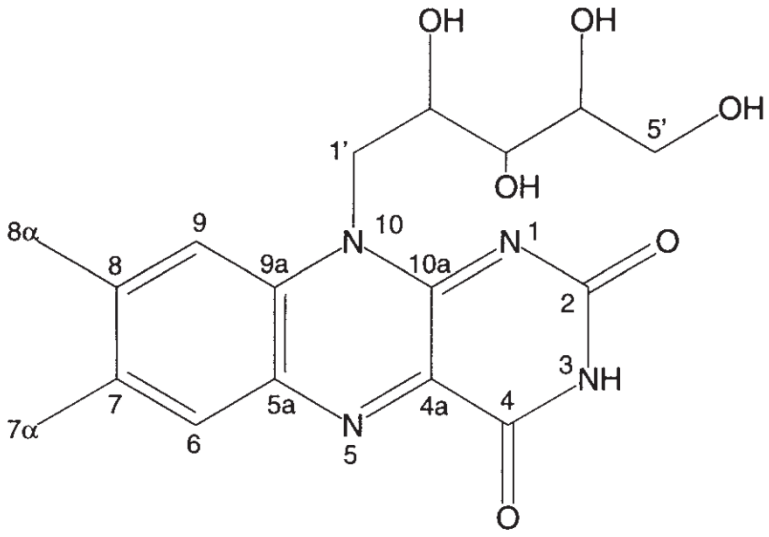

Figure 5. Structure of riboflavin. Figure taken from Macheroux (Macheroux, 1999).

The reduction of the oxidized flavin (quinone, Fl_{ox}) to the fully reduced flavin (hydroquinone, Fl_{red}) requires two electrons. The complete reduction of flavin can be achieved by either two one-electron steps or by a one two-electrons step (Fig. 6). The two one-electron steps allow the existence of a one electron reduced radical, namely semiquinone (Fl_{sq}), which is further reduced to Fl_{red} (Fig. 5). Free oxidized and reduced flavins in solution are rapidly at equilibrium with a certain portion of semiquinoid species (Ghisla & Massey, 1989). There are two species of semiquinone known, a blue (neutral) and an anionic (red) species (Fig. 5) (Hemmerich *et al.*, 1970). The neutral semiquinone shows a planar structure with a hydrogen bond to the N5 atom. The anionic semiquinone has a bend structure and a hydrogen bond to the N1 atom (Hemmerich *et al.*, 1970). The protein environment of the enzyme-bound flavin influences the stabilization of the flavin semiquinone. In some enzymes the neutral semiquinone is stabilized by a pK_a notably increased from pH 8.5. Other proteins have an anionic semiquinone stabilizing environment around the flavin with a

significantly decreased pK_a. The UV/Vis spectra of flavin semiquinones show different characteristics than the spectra of reduced or oxidized flavin making it easier to distinguish it between the species (Fig. 4) (Heelis, 1982).

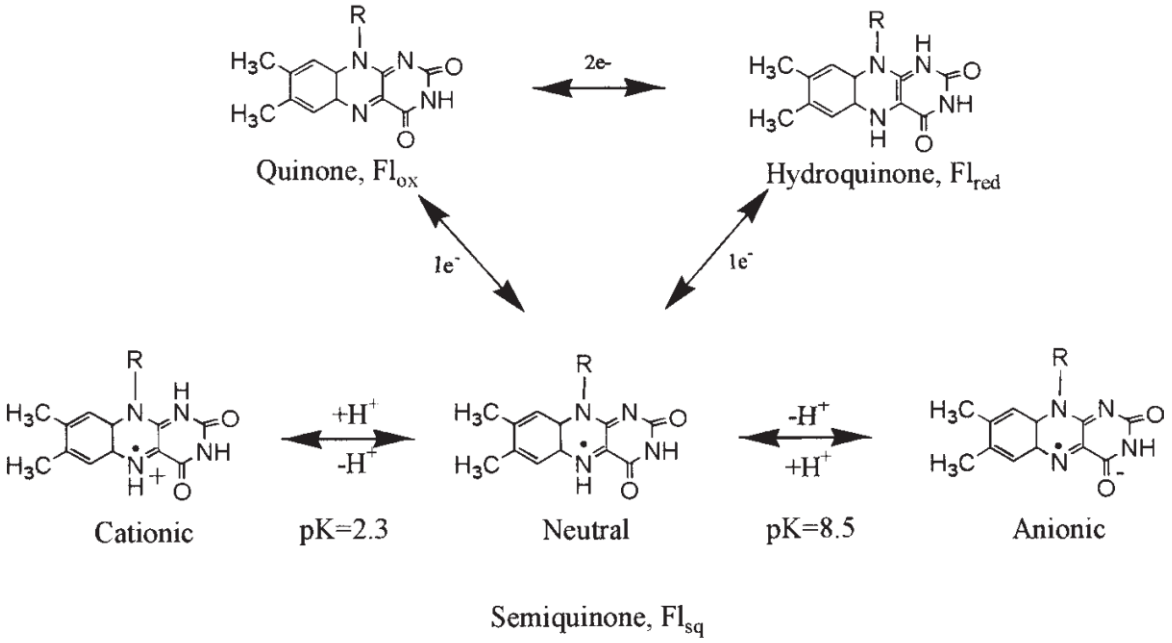

Figure 6. Redox states of flavin in dependency of *pK*. Fl_{ox} means flavin in oxidized state, Fl_{red} is for fully reduced flavin and Fl_{sq} stands for flavin semiquinone. Figure is taken from Edwards (Edwards, 2007).

As the pyrimidine nucleus of the three-membered ring system is hydrophilic and electron-deficient it was termed an "electron sink" by Ghisla and Massey (Ghisla & Massey, 1989). Consequently, any interaction lowering its negative charge density results in an increase of the redox potential. The Fl_{red} consists of an electron-rich phenylenediamine moiety complexed with a (4,5-diamino)-uracil. Stabilization or destabilization of the negative charge largely influences the redox potential. Therefore positive charges in the protein environment around the pyrimidine ring increase the redox potential whereas negative charges or a hydrophobic environment decrease it (Ghisla & Massey, 1989; Fraaije & Mattevi, 2000).

3.2 Charge transfer complex flavin-nicotinamide adenine dinucleotide

Due to the characteristic UV/Vis absorption spectra of oxidized and reduced flavins, anionic and neutral semiquinones (Fig. 4), another characteristic absorption spectrum of flavin could be distinguished. When the reduced melilotate hydroxylase was mixed with NAD^+, it exhibited a long wavelength absorption band that was also observed in oxidized protein titrated with equimolar NADH (Strickland & Massey, 1973). Titration of NADH to the oxidized flavoprotein resulted in a decrease of absorption at 340 nm and 450 nm. A concomitant increase at longer wavelength centered at 750 nm was observed. It was concluded that the decrease of absorption at 340 nm and 450 nm (reduction of flavin and oxidation of NADH, respectively) was in direct correlation to the increase of the absorption at longer wavelength. This finding was interpreted as a result of a charge transfer (CT) interaction between the hydroquinone of flavin and NAD^+ (Strickland & Massey, 1973).

Based on studies with covalently linked coenzyme-complexes, the long wavelength absorption intermediate was identified as a CT complex between the reduced pyridine nucleotide and the oxidized flavin. This implicates a second complex between oxidized pyridine nucleotide and reduced flavin, which has already been identified in the case of lipoyl dehydrogenase with numerous modified pyridine nucleotides (Massey and Palmer, 1962).

The role of the CT complex has rigorously been discussed. In some examples the CT complex has no catalytic function as it has been demonstrate in the case of glutathione reductase and lipoyl dehydrogenase (Massey & Palmer, 1962; Massey & Veeger, 1961). The CT complex of lactate monooxygenase functions as a catalytic intermediate as the binding of the substrate influences the outcome of the product and the enzyme's reactivity with oxygen (Massey & Ghisla, 1973).

3.3 The redox potential and oxygen reactivity of flavoproteins

The reaction of flavoproteins can be divided into reductive and oxidative half reaction. In the reductive half reaction, the oxidized flavin (Fl_{ox}) is reduced by an electron donor. The two-electrons reduced flavin (Fl_{red}) is reoxidized by an electron acceptor in the oxidative half-reaction. Molecular oxygen (O_2) can act as an electron acceptor and reacts with Fl_{red} (Fig. 6). The reaction is spin forbidden because protein-bound Fl_{red} is in singulet state and the oxygen is in triplet state. The problem can be overcome by successive one-electron transfer steps resulting in the generation of a radical pair, a semiquinone species of flavin (Fl_{sq}) and the superoxide anion of oxygen ($O_2^{\cdot-}$) (Malmström, 1982; Kemal *et al.*; 1977, Massey, 1994). From this point the radical pair can either dissociate to generate an oxygen radical or it can collapse into the C4a peroxide which can further dissociate to generate hydrogen peroxide (Fig. 7) (Massey, 1994; Massey, 2002).

The enormous difference in reactivity of flavoproteins with O_2 could stem from the thermodynamic driving force, e.g. the different redox potentials of flavin and the oxygen couples. The midpoint potential of Fl_{ox}/Fl_{red} is -207 mV, of Fl_{sq}/Fl_{red} around -101 mV and of $flavin_{Q}/flavin_{SQ}$ -313 mV (Mayhew, 1999). The redox potential of $O_2/O_2^{\cdot-}$ is approximately -160 mV and of $O_2^{\cdot-}/HO_2^{\cdot-}$ around +890 mV (Wood, 1988). Therefore the thermodynamic driving force is weak.

Fl_{sq} is often stabilized thermodynamically by the surrounding protein environment, consequentially increasing the reactivity with O_2 when the redox potential of free $flavin_{SQ}/flavin_{HQ}$ is lower than that of the $O_2/O_2^{\cdot-}$ couple (Massey, 2002).

However, oxygen reactivity of a flavoprotein cannot be solely justified by the thermodynamic driving force. The redox potential of $enzyme_{sq}/enzyme_{red}$ of D-amino acid oxidase (DAAO) with -204 mV is much more favorable than the one of glucose oxidase with -65 mV. Nevertheless, DAAO reacts 50 times slower with oxygen than glucose oxidase (Massey, 2002). Taking into consideration that the flavin at the active site is surrounded by a hydrophobic environment, desolvation is an explanation, as it

lowers the redox potential of the O_2/O_2^- and therefore increases the oxygen reactivity of the protein. Desolvation can be a result of ligand binding causing a decrease in polarity of the active site. This is based on the observation in the crystal structure of the pig kidney acyl-CoA dehydrogenase showing numerous water molecules in the active site when substrate is absent (Powell *et al.*, 1987; Kim *et al.*, 1993). The o-hydroxybenzoate hydroxylase shows opposite effect. The binding of substrate brings no large change in the redox potential and in the stabilization of flavin semiquinone (Entsch *et al.*, 1995). However, the reduced enzyme is more oxygen sensitive upon binding of substrate (Entsch *et al.*, 1976).

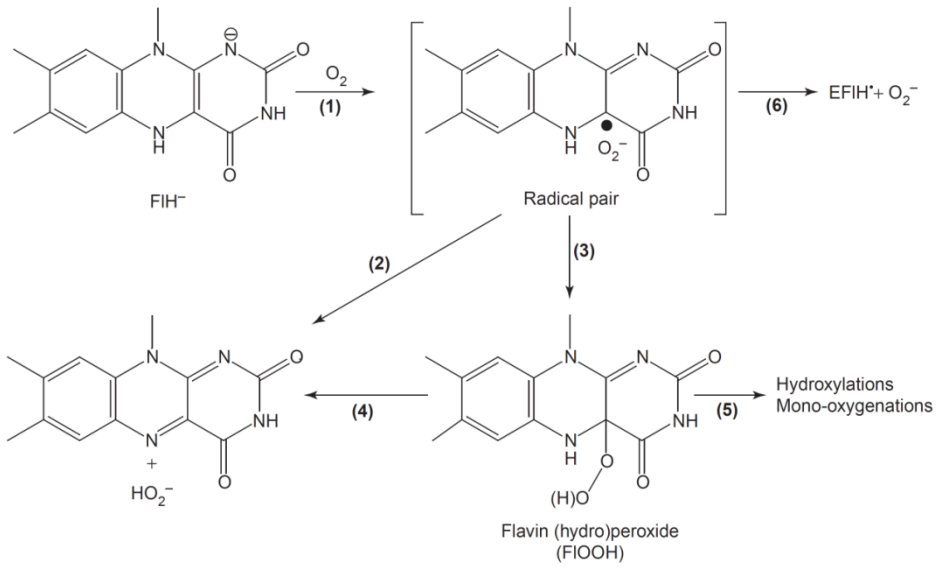

Figure 7. The reaction of reduced flavin with oxygen. The first step is a one-electron transfer from reduced flavin which results in a caged radical pair of either neutral semiquinone or superoxide anion. Figure is taken from Mattevi (Mattevi, 2006).

These examples are informative that thermodynamic driving force, desolvation or ligand binding in the active site is not an all-inclusive explanation. On the contrary, a mixture of these factors accounts for the large difference in oxygen reactivity of flavoproteins.

4 Rieske-type ferredoxin in ROs

The flavoproteins in ROs are reoxidized by ferredoxins that are hydrophilic one-electron carriers containing a [2Fe-2S] cluster. Iron-sulfur clusters are usually coordinated by cysteine residues commonly found in the form of [2Fe-2S], [3Fe-4S] or [4Fe-4S] clusters (Cammack *et al*., 1999) [2Fe-2S] clusters can be divided into two groups: (a) plant-type [2Fe-2S] and (b) adrenodoxin-type [2Fe-2S] cluster.

In 1964 Rieske discovered a different type of [2Fe-2S] cluster, the so called Rieske-type [2Fe-2S] cluster. One of the irons (Fe-1) is coordinated by 2 cysteines and the other iron (Fe-2) by 2 histidine residues (Rieske *et al.*, 1964). Two labile sulfur atoms bridge the Fe-1 and the Fe-2 forming the center of a tetrahedron with two histidine and two cysteines as endogenous ligands. The planarity of the tetrahedron is interrupted by the geometry around the His-coordinated Fe-2 (Kauppi *et al.*, 1998). The UV/Vis absorption spectrum of a Rieske-type [2Fe-2S] cluster in oxidized state has typical characterics with peak maxima at 325 nm and 460 nm with a shoulder at 560 nm (Ensley *et al.*, 1982)

The molecular weight of ferredoxins in the ROs is in the range of 12 - 15 kDa (Mason & Cammack, 1992). They do not have enzymatic activity by themselves. Rieske-type [2Fe-2S] cluster proteins can be distinguished by their redox potential. There are high reduction potential Rieske-type [2Fe-2S] cluster proteins with a redox potential in the range of +150 mV to +490 mV and Rieske-type [2Fe-2S] cluster proteins with low reduction potential of -150 mV to -50 mV (Cosper *et al*. 2002). The Fe-1 remains ferric upon reduction whereas the histidine-coordinated Fe-2 is reduced to ferrous (Cline *et al*., 1985; Kuila *et al*., 1986). Rieske-type [2Fe-2S] clusters are widespread in plants, animals and bacteria (Brown *et al*., 2008). Originally found in ubiquinole-cytochrome c reductase, the high potential Rieske-type [2Fe-2S] cluster protein acts as a one-electron transporter from ubiquinole to the cytochrome c subunit (Kurowski *et al*., 1987). In ROs, such as the toluene dioxygenase, the Rieske-type [2Fe-2S] cluster ferredoxin acts as a one-electron mediator between reductase and oxygenase

component. In these ring-hydroxylating systems the ferredoxin components are found to have a specific interaction with their reductase and oxygenase component as they could not be replaced by other ferredoxins, e.g. replacement of ferredoxin of naphthalene dioxygenase by ferredoxin of toluene dioxygenase (Haigler & Gibson, 1990).

Figure 8. Overall structure of ferredoxin$_{TOL}$. The large domain is colored in grey, the cluster-binding domain in light gray. The Rieske iron-sulfur cluster is shown in stick presentation with iron (margenta), sulfur (orange) and nitrogen (blue). The figure is taken from Friemann *et al.* (Friemann *et al.*, 2009).

Ferredoxin$_{TOL}$ (FER$_{TOL}$) has numerous properties of Rieske-type [2Fe-2S] ferredoxins participating in the pyrazon and benzene dioxygenase systems (Sauber *et al.*, 1977; Axcell & Geary, 1975). It possesses a characteristic Rieske-type [2Fe-2S] cluster spectrum with maxima at 277, 327 and 460 nm. The structure of ferredoxin$_{TOL}$ shares the highest similarity to naphthalene dioxygenase ferredoxin and biphenyl dioxygenase ferredoxin (Subramanian *et al.*, 1985; Karlsson *et al.*, 2002; Colbert *et al.*, 2000).

Ferredoxin$_{TOL}$ is found as monomer in solution and in the crystal structure (Roome *et al.*, 1983). The structure can be divided into two domains: a large domain and a cluster-binding domain. The large domain is dominated by two β-sheets, in which

each of them is comprised of three antiparallel β-strands connected by two short α-helices (Fig. 8). The cluster-binding domain has a four-stranded β-sheet, followed by an α-helix and a Rieske center (Fig. 8) (Friemann *et al.*, 2009).

5 The oxygenase component in ROs

The oxygenase is the terminal component in Rieske non-heme iron dioxygenases which accepts the electron from the ferredoxin component. It is an iron-sulfur protein consisting of a Rieske-type [2Fe-2S] cluster and a mononuclear iron. The oligomeric oxygenases with a M_R of 150 to 200 kDa can occur as tetramers or dimers of trimers (Mason, 1988; Batie *et al.*, 1991). The Rieske-type [2Fe-2S] cluster and the mononuclear iron are in the α-subunit (Fig. 9) (Friemann *et al.*, 2009; Ferraro *et al.*, 2005). In some oxygenases a β-subunit is evident and suggested to have a structural function (Beil *et al.*, 1998; Friemann *et al.*, 2005; Jiang *et al.*, 1999; Kauppi *et al.*, 1998; Parales, Parales *et al.*, 1998).

The mononuclear Fe(II) in the α-subunit is coordinated by two His and one Asp or Glu, the so called 2-His-1-facial triad motif (Hegg & Que, 1997; Que, 2000) (Fig. 10). The mononuclear iron creates a platform where oxygen can bind. The iron here can bind up to three exogenous ligands (Gibson *et al.*, 1970; Jerina *et al.*, 1971). The reaction usually starts with a six-coordinated Fe(II) center which has a moderate reactivity towards O_2. Upon substrate binding the iron center becomes five-coordinate yielding in an increased affinity towards molecular oxygen. The binding of molecular oxygen then triggers the oxidative reaction that differs from enzyme to enzyme (Que, 2000).

The mononuclear iron is more than 40 Å apart from the Rieske cluster within one subunit (Kauppi *et al.*, 1998). The distance is unfavourable for direct electron transfer (Moser *et al.*, 1992). This problem can be obviated in that the electron transfer proceeds from the mononuclear iron of one α-subunit to the Rieske cluster of the adjacent α-subunit (Fig. 10). The distance between the mononuclear iron and the

Rieske cluster here is around 12 Å (Kauppi *et al.*, 1998). An aspartate lies between the mononuclear iron and the Rieske cluster and is in van der Waals contact with a histidine ligand of the mononuclear Fe(II) and a histidine ligand of the Rieske cluster (Fig. 10). Therefore it was postulated that the electron transfer is facilitate by this aspartate as, for instance, found in NDO (Asp205) and PDO (Asp178) (Kauppi *et al.*, 1998; Tarasev *et al.*, 2006).

The oxygenase component of the toluene dioxygenase (ISP_{TOL}) is a dimer of trimers consisting of $\alpha_3\beta_3$ as found in NDO, NBDO and BPDO (Friemann *et al.*, 2009; Kauppi *et al.*, 1998; Friemann *et al.*, 2005; Furusawa *et al.*, 2004). It contains one $\alpha\beta$ heterodimer in the asymmetric unit. The overall structure of ISP_{TOL} is mushroom-shaped, in which the α-subunit represents the cap of the mushroom and the β-subunit the stem (Friemann *et al.*, 2009) (Fig. 9). The α-subunit contains a Rieske domain (residues 55 - 173) with a Rieske-type [2Fe-2S] cluster and a catalytic domain (residues 1 - 54 and 174 - 450) with a mononuclear iron (Friemann *et al.*, 2009) (Fig. 8 and 9). The Rieske domain has three antiparallel β-sheets and the Rieske cluster. The catalytic domain consists of a nine-stranded antiparallel β-sheet enclosed by 12 α-helices. Here, the mononuclear iron is coordinated by the conserved residues His222, His228 and Asp378, known as 2-His-1-carboxylate facial triad (Friemann *et al.*, 2009) (Fig. 9).

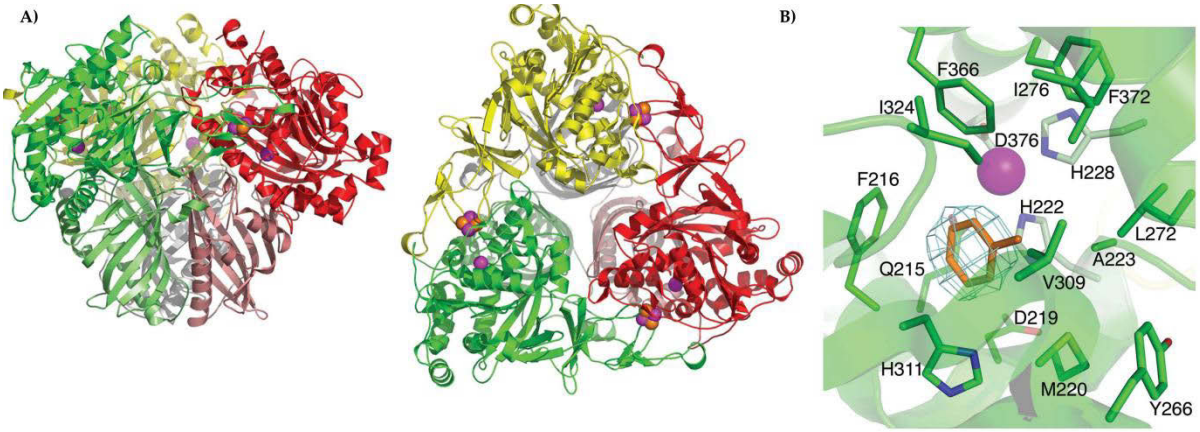

Figure 9. Overall structure and active site of ISP$_{TOL}$. A) ISP$_{TOL}$ is presented in side view (left) and top view (right). The α-subunits are colored in red, green and yellow, the β-subunit is depicted in pink, light green and gray. Fe and S atoms are colored in margenta and orange, respectively. Figure is modified from Friemann *et al*. (Friemann *et al*., 2009). B) The active site is complexed with toluene. The mononuclear iron is shown as a margenta sphere and the iron containing residues are colored in green. The $F_{obs} - F_{calc}$ map was computed before toluene was modeled. Figure is modified from Friemann *et al*. (Friemann *et al*., 2009).

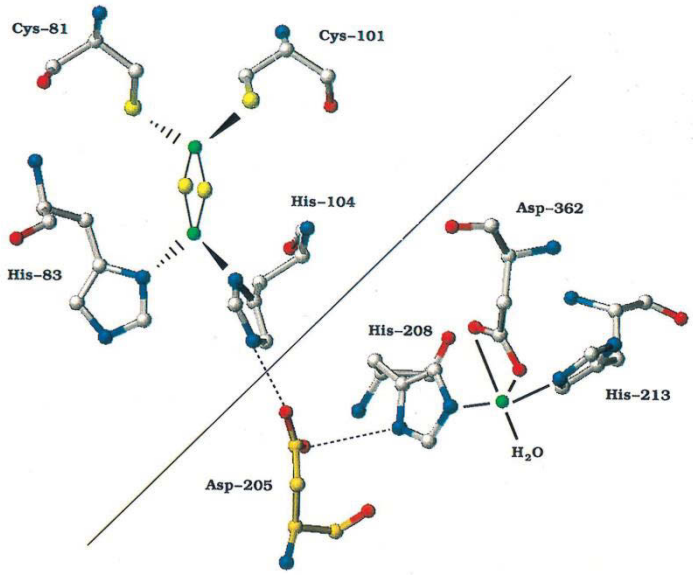

Figure 10. View of the active site of naphthalene dioxygenase. The Rieske cluster of one α-subunit is shown on the upper left side, the mononuclear iron center of the adjacent α-subunit on the lower right side. Dashed lines indicate the proposed electron transfer pathway via Asp205. Iron atom are depicted in yellow, sulfur atom is green, oxygen atoms in red and nitrogen in blue color. Figure is taken from (Parales *et al*., 1999).

6 Electron transfer in the toluene dioxygenase (TDO) from *Pseudomonas putida* F1

Pseudomonas putida F1 is able to degrade aromatic compounds and belongs to the family of Pseudomonadaceae with the genus *Pseudomonas*. This gram-negative, chemoautotrophic, rod-shaped soil bacterium was first isolated from a polluted creek

in Urbana, IL (Gibson *et al.*, 1968). It is one of the best studied bacterial strains involved in the degradation of aromatic hydrocarbons and is known to grow on benzene, toluene, ethylbenzene, isopropylbenzene and biphenyl (Gibson *et al.*, 1968). *Pseudomonas putida* F1 can grow on toluene as a sole carbon and energy source using enzymes needed for the degradation of toluene. TDO is responsible for the initial step in the degradation of toluene. TDO is a three-component system of the class IIB (Tab. 1) and catalyzes the dihydroxylation of toluene to yield *cis*-(1*R*,2*S*)-dihydroxy-3-methylcyclohexa-3,5-diene. In TDO, the flavin adenine dinucleotide ($FAD/FADH_2$) redox center of the reductase component accepts two electrons from soluble nicotinamide adenine dinucleotide ($NAD^+/NADH_2$) which are transferred to a Rieske-type [2Fe-2S] ferredoxin in a one-electron-transfer manner (Subramanian *et al.*, 1981). The ferredoxin component, in turn, transfers the electrons in two subsequent one-electron-transfer steps to the oxygenase component, where the dihydroxylation of toluene to its *cis*-dihydrodiol takes place at the mononuclear iron center. Studies of the α- and β-subunit gave insights into the electron transfer between ferredoxin and oxygenase component. The α-subunit alone could be reduced in the presence of reductase and ferredoxin component. However, toluene was not *cis*-dihydroxylated when the β-subunit was absent. Therefore the β-subunit was supposed to have a structural function by sustaining the contact between two adjacent α-subunits and consequently maintaining the catalytic activity (Jiang *et al.*, 1999).

6 Aim of this work

Previous studies on the toluene dioxygenase (TDO) gave biochemical insights into all three components (Subramanian *et al.*, 1979; Subramanian *et al.*, 1981; Subramanian *et al.*, 1985). Crystal structures of all components have been solved (Friemann *et al.*, 2009). The oxygenase$_{TOL}$ itself and its interaction with ferredoxin$_{TOL}$ have been under examination (Jiang *et al.*, 1996; Jiang *et al.*, 1998). However, the interplay of

reductase$_{TOL}$ with ferredoxin$_{TOL}$ remains to be elucidated. The question arises how the electron transfer between both proteins is regulated and which role the observed charge transfer complex of reductase$_{TOL}$ could play in the regulation. To study the mechanism of the electron transfer and the formation of the charge transfer complex, heterologous expression and purification of ferredoxin and reductase is mandatory. Various methods should be applied to characterize the relationship between the two-components of TDO such as UV/Vis spectroscopy, redox potential determination, transient kinetics and X-ray protein crystallography. UV/Vis spectroscopy is used to characterize the redox states of reductase$_{TOL}$ and ferredoxin$_{TOL}$. Knowledge of the UV/Vis spectroscopic characteristics of both proteins can be applied to a better understanding of the electron transfer kinetics. As the electron transfer reaction rate can be altered by a change of the thermodynamic driving force that a change of redox potential could bring, the redox potential of reductase$_{TOL}$ and reductase$_{TOL}$ with CT complex to be determined will be compared. The interaction of reductase$_{TOL}$ and ferredoxin$_{TOL}$ could also be explained from a structural point of view by the comparison of the reductase$_{TOL}$ structure to the reductase$_{TOL}$ charge transfer and the reductase$_{TOL}$-ferredoxin$_{TOL}$ complex.

MATERIAL AND METHODS

1 Chemicals and biochemicals

DNase-free water, T4 DNA ligase, *Taq* and *Pfu* DNA polymerase and restriction enzymes for molecular biology were purchased from Fermentas. Kits for plasmid purification were obtained from Fermentas. PCR purification and gel extraction kits were purchased from Qiagen. All gene amplifications were conducted using Master Cycler Personal from Eppendorf. UV/Vis spectroscopic studies were carried out with a SPECORD 40 Spectralphotometer from Analytik Jena. Stopped flow measurements were performed with an SX20MV from Applied Photophysics. Chromatography columns and column materials were obtained from GE Healthcare. Macro-prep ceramic hydroxyapatite (Type I, 20 μm) material was obtained from BIO-RAD. Electrophoresis materials and size markers for SDS-PAGE (RotiMARK standard) were supplied by Roth. All other chemicals used were of at least analytical grade and were obtained from Fluka, Sigma or Merck except for deazaflavin, which was given by Prof. Dr. Kroneck (Universität Konstanz). pET vectors were from Novagen. Crystallization solutions were prepared with chemicals of highest purity. Crystallization experiments were conducted in an anoxic glove box (model B, COY Laboratory Products Inc., Michigan, USA) under an atmosphere of 95 % N_2/5 % H_2 at 16 °C. Anaerobic solutions were prepared in a container (bottle, tube, or cuvette) equipped by a screwed cap with butyl rubber or silicon septum by successive cycles (at least 4 cycles) of evacuation and flushing with N_2 gas at a vacuum-gas line.

2 Molecular biology

The isolation of genomic DNA of *Pseudomonas putida* F1 is based on the publication of Chen and Kuo (Chen & Kuo, 1993). The genomic DNA was used as a template to amplify the genes encoding reductase$_{TOL}$ (*todA*) and ferredoxin$_{TOL}$ (*todB*) by PCR

including *Pfu* DNA polymerase and cloning primers. PCR mixtures, primer sequences and cycling conditions can be looked up in the appendix. Primers were synthesized by BIOMERS. Purification of PCR products were conducted as described in the manual (QIAquick PCR purification kit, Qiagen). The PCR products were restricted with fast digest *Nde*I and *Bam*HI enzymes and ligated into an *Nde*I/*Bam*HI-digested pET vector. The positive plasmid constructs were verified by DNA sequencing (AGOWA). The ligation products were transformed into an expression strain. The strains used in this thesis are listed in the appendix. Restriction of DNA was done according to the instruction manual of Fermentas. Ligation, determination of DNA concentration, preparation of competent cells and transformation were prepared as described in Sambook *et al*. (Sambrook *et al*., 1989). The procedure of purification of plasmid DNA can be looked up in the GeneJET manual (Fermentas).

3 Bacterial cultivation

Escherichia coli (*E. coli*) was used as a heterologous expression host. The genomic DNA for gene amplification was obtained from *Pseudomonas putida* F1 (*P. putida* F1). Bacteria were grown in test tubes and baffled shake flasks. Depending on the experiment bacteria were cultivated in lysogeny broth (LB), super optimal broth (SOB), double yeast extract trypton (dYT) or terrific broth (TB) medium containing appropriate antibiotics (Sambrook *et al*., 1989). The culture was incubated in a shaking incubator. LB agar plates were incubated in a drying cupboard at 37 °C. The optical density of the bacteria culture was monitored at a wavelength of 600 nm.

3.1 Cultivation of *Pseudomonas putida* F1

P. putida F1 was obtained as a dry pellet from DSMZ and rehydrated in LB medium containing 1 mM L-Cysteine. The rehydrated bacteria were plated on LB agar plates, incubated at room temperature over night and stored at 4 °C. Subsequently,

P. putida F1 was cultivated in LB medium in a shaking incubator at 28 °C. The liquid culture was mixed with equal volumes of LB medium and 30 % (v/v) glycerol (15 % (v/v) final concentration) for long time storage at -30 °C.

3.2 Heterologous expression in *Escherichia coli*

Plasmid constructs containing *todA* and *todB*, respectively, were transformed into *E. coli* BL21-CodonPlus(DE3)-RIL and plated on a LB agar plate after an 1 h incubation at 37 °C. The LB agar plates were put into an incubator at 37 °C over night. A single colony from LB agar was picked for the inoculation into an LB /chloramphenicol/carbenicillin medium (CAM, 34 μg/ml; Cb, 50 μg/ml). The preculture was grown at 37 °C over night. TB medium with CAM and Cb in baffled shake flask were mixed with the over night preculture with a ration of 50:1. When the culture reached the mid exponential phase (OD_{600} = 0.4 - 0.6) the cultivation temperature was shifted from 37 °C to 18 °C and the gene expression was induced by the addition of 0.5 mM IPTG. The culture was harvested 22 h after induction. After centrifugation the supernatant was discarded and the pellet was shock-frozen in liquid nitrogen and stored at -80 °C until use.

4 Protein purification

All purification steps were performed at 4 °C. Formulation of buffers used for purification is described in detail in the appendix.

4.1 Purification of reductase$_{TOL}$

The cultivation of *E. coli* BL21- CodonPlus(DE3)-RIL/pET15b*todA* was conducted as described in material and methods 3.2. The cell pellet containing the overproduced reductase$_{TOL}$ was washed and resuspended with buffer A. 20 g cells were sonified

(12 min, 50% duty cycle, microtip limit 7) and centrifuged (45 min, 18,000 rpm, 4°C). The supernatant was passed through a syringe loaded with 8 ml Nickel Sepharose Fast Flow equilibrated with buffer A. The column was washed with 3 column volumns (cv) of buffer A. The protein was eluted with increasing concentrations of imidazole in buffer B (buffer A with 30, 40, 80, 125, 250 mM imidazole). The purity of the protein was analyzed by using SDS PAGE. The purest fractions were pooled and directly loaded on a Q-Sepharose Fast-Flow column (20 ml) equilibrated with 60 ml buffer C. The wash was done with 2 cv of buffer C with a flow rate of 5 ml/min. The elution was performed with a linear gradient of 0 - 500 mM NaCl in buffer C. Reductase$_{TOL}$ was buffer exchanged on a Sephadex G-25 in buffer D. Purity of reductase$_{TOL}$ was monitored with SDS-PAGE. The combined fractions were concentrated to 23 mg/ml via ultrafiltration with Vivacell 70 (molecular weight cut off (MWCO), 30 kDa).

The measurement of activity was done according to Subramanian *et al.* (Subramanian *et al.*, 1981). DCPIP was used as electron acceptor and the activity was measured by following the reduction of DCPIP at an absorption of 600 nm (ε_{600} (DCPIP) = 21 mM^{-1} cm^{-1}). One unit of enzyme activity was defined as the amount of reductase$_{TOL}$ needed to reduce 1 µmol of DCPIP per min.

4.2 Purification of ferredoxin$_{TOL}$

E. coli BL21-CodonPlus(DE3)-RIL/pET11a*todB* was cultivated as described in material and methods 3.2. After induction with IPTG 0.2 mM $FeSO_4$ and 0.2 mM NaS_2 was added to the medium as a supplement. The cells were harvested, washed and resuspended in resuspension buffer. Cells were broken by sonification (0.5 min/1 g cell, 50% duty cycle, microtip limit 7) and centrifuged (45 min, 18,000 rpm, 4 °C). The supernatant was loaded on a DEAE-Sepharose Fast Flow column (50 ml) equilibrated with 2 cv of buffer E1 and washed with 3 cv of the same buffer. The protein was eluted with a linear gradient of 0 % - 100 % buffer E2. The flow velocity was 5 ml/min

and the fraction size 10 ml. The pooled fractions were loaded on a CHT™ Ceramic Hydroxyapatite (20 ml) equilibrated with buffer F1 and the protein was eluted with a linear gradient of 0 % - 100 % buffer F2 with a flow rate of 2 ml/min. The pooled fractions were optionally applied to a Superdex HR 200 (120 ml) in buffer G or directly buffer exchanged on a Sephadex G-25 column (50 ml) with buffer G. Ferredoxin$_{TOL}$ was concentrated by ultrafiltration with a Vivacell 70 (MWCO 10 kDA) to a final concentration of 10 mg/ml. Protein concentration was determined either by UV/Vis spectroscopy or by Bradford. After each purification step the purity of the protein was monitored by using SDS PAGE.

The activity of ferredoxin$_{TOL}$ was measured by monitoring the reduction of cytochrome c in the presence of NADH and reductase$_{TOL}$ corresponding to Subramanian *et al*. (Subramanian *et al.,* 1985). One unit of enzyme activity was defined as the amount of ferredoxin$_{TOL}$ needed to reduce 1 µmol of cytochrome c per min (ε_{600} (cytochrome c) = 21 mM^{-1} cm^{-1}).

4.3 Determination of protein concentration

4.3.1 Determination of protein concentration via Bradford

Protein concentration was determined by the method of Bradford (Bradford, 1976). A calibration curve needs to be established. Therefore different quantities of bovine serum albumin (BSA) in 50 µl H_2O in the range of 2 to 40 µg/ml was added up to 1000 µl with Bradford stock solution. Reference was 50 µl H_2O mixed with 950 µl Bradford stock solution. Each concentration was prepared and measured three times. The absorption values were measured at 595 nm (A_{595}) and the calibration curve was established by plotting the BSA concentration against the A_{595} values. The concentration of the sample could be determined by applying the measured absorption values at 595 nm to the linear equation derived from the calibration curve.

4.3.2 Determination of protein concentration via absorption of protein-bound flavin

The concentration of holoprotein (reductase$_{TOL}$ with FAD) was determined by measuring the absorption at 450 nm. Therefore the protein was diluted in 50 mM Tris-HCl pH 8.0 insofar as the absoption value at 450 nm was in the range of 0.1 to 0.9. Same buffer without protein was taken as a reference. Concentration was calculated by applying the measured absorption value to the Lambert-Beer equation.

$$A = c \cdot \varepsilon \cdot d \qquad (1)$$

where A is the abbreviation for absorption. ε stands for the molar extinction coefficient ($M^{-1}\,cm^{-1}$), d for the path length of the cuvette (cm) and c for the protein concentration.

4.4 Determination of flavin content

4.4.1 Determination of flavin content by SDS treatment

The flavin content was determined as described by Aliverti *et al.* (Aliverti *et al.*, 1999). SDS treatment releases the flavin and allows the determination of the flavin content as well as the type of flavin plus the determination of its extinction coefficient. 10 µM of protein was mixed with 50 mM Tris-HCl (pH 8.0) in a 1 ml Quartz cuvette. Same buffer also served as a reference. A protein spectrum was measured. After the addition of 10 % SDS a spectrum was captured every minute until no change could be observed.

4.4.2 Determination of flavin content via heat denaturation

A spectrum of 10 µM protein was measured. Protein mixed with 50 mM Tris-HCl (pH 8.0) was taken as a reference. The solution was transferred to a 1.5 ml tube and incubated for 10 min at 100 °C. The denatured protein solution was cooled down and centrifuged for 10 min at 13000 rpm. A spectrum of the supernatant was measured. Data was evaluated by using the extinction coefficient of protein bound FAD and free FAD (ε_{450} = 11.3 mM^{-1} cm^{-1}).

4.5 Iron determination

The determination of the non-heme iron content of protein was followed by the method of Fish using Ferene S as a specific Fe(II) chelator (Fish, 1988). The iron-containing protein was treated with hydrochloric acid (0.1 %) and incubated at 80 °C for 10 min. After heat treatment the samples were cooled down on ice for 5 min. Ammonium acetate (3.25 %) was added to neutralize the excess acid, ascorbic acid (0.4 %) to reduce the loosened iron. Addition of SDS (0.1 %) ensured that all of the iron was completely unbound. Ferene S (0.15 %) was added to the solution which was subsequently incubated for 10 min. Then the absorbance at 593 nm was measured and the stoichiometric amount of iron in the protein was calculated using the standard curve. The standard curve of known $FeSO_4$ concentration was established under the same procedure.

5 Photoreduction of reductase$_{TOL}$

Photoreduction experiments of reductase$_{TOL}$ were conducted using the deazaflavin-EDTA couple as electron generator to determine the semiquinone species. This method is used to ascertain semiquinone formation *via* single electron transfer steps. Photoreduction was carried out according to Massey and Hemmerich (Massey & Hemmerich, 1978). A 2 ml solution with 1 mM EDTA, 1 µM deazaflavin and appropriate amount of protein in 50 mM Tris-HCl (pH 8.0) was prepared in a glass

tonometer with a Quartz cuvette. The solution was made anaerobic by repeated cycles of evacuation and equilibration with nitrogen gas at a vacuum-gas line. A spectrum in the range of 200 - 800 nm served as a reference. The reduction was started by light exposure of the solution in defined intervals. After every excitation period the solution was left for 2 min to ascertain equilibrium in solution. Then a spectrum was measured. The experiment was finished when no further reduction of the protein was observable.

6 Determination of redox potential

The determination of the redox potentials of reductase$_{TOL}$ and ferredoxin$_{TOL}$ was performed according to the methods of Stankovich and Sucharitakul *et al*. (Stankovich, 1980; Sucharitakul *et al*., 2005). The redox dye served as a redox potential reference. The redox potential of the protein to be examined should not differ more than 30 mV from the redox potential of the selected redox dye. In the experiment redox dye and protein had the same concentration. Phenosafranine or Safranin T was selected in the case of reductase$_{TOL}$, indigo-disulfonate for the redox potential determination of ferredoxin$_{TOL}$. Benzyl viologen acted as an electron mediator to ensure fast equilibration. 20 µM protein and 20 µM redox dye as well as 1 µM benzyl viologen and xanthine oxidase (0.003 U/ml) was added to the buffer in a gas tight Quartz cuvette. The solution was made anaerobic at the gas train by several cycles of evacuation and flushing with N_2 gas. The cuvette was introduced into an anoxic tent and put into a spectrophotometer. When the solution in the cuvette was tempered to 25 °C a spectrum in the range of 200 - 900 nm was measured as a reference. The reaction was started by the addition of xanthine (final concentration: 300 µM). Spectra were recorded in 3 min intervals. The experiment was stopped when no further change of absorption could be observed.

The concentration of the oxidized/reduced species could be calculated using equation 2 and 3 with the extinction coefficients of the used redox dye, of the protein and the values of the measured absorption.

$$A_{450} = \varepsilon_{450}^{E} \cdot c^{E} + \varepsilon_{450}^{D} \cdot c^{D}$$

or respectively (2)

$$A_{460} = \varepsilon_{460}^{E} \cdot c^{E} + \varepsilon_{460}^{D} \cdot c^{D}$$

$$A_{521} = \varepsilon_{521}^{E} \cdot c^{E} + \varepsilon_{521}^{D} \cdot c^{D}$$

or respectively (3)

$$A_{521} = \varepsilon_{522}^{E} \cdot c^{E} + \varepsilon_{522}^{D} \cdot c^{D}$$

or respectively

$$A_{610} = \varepsilon_{610}^{E} \cdot c^{E} + \varepsilon_{610}^{D} \cdot c^{D}$$

whereby

A_x	absorption at x nm
ε_x^E	extinction coefficient of enzyme at x nm
c^E	concentration of enzyme
ε_x^D	extinction coefficient of redox dye at x nm
c^D	concentration of redox dye

A plot of the logarithm of concentration of oxidized/reduced enzyme *versus* the logarithm of concentration of oxidized/reduced redox dye gave the difference of the redox potential of enzyme and redox dye (ΔE). ΔE was used to calculate the redox potential of enzyme E_E^0 by using the Nernst equation ($\Delta E = \log [E_{OX}/E_{RED}]$, equation 4).

$$E_E^0 = E_D^0 - {(2.303 \cdot R \cdot T)}/{(n \cdot F)} \cdot \log[{E_{OX}}/{E_{RED}}] \quad (4)$$

whereby

E_D^o	redox potential of dye

n	number of electrons
T	298.16 K
R	8.31447 J/mol K
F	96,485.34 C/mol

In case the spectra of protein and redox dye overlapped, the extinction coefficient was calculated at the selected wavelength. The absorption at the selected wavelength was measured with different concentrations of protein. There from a calibration curve (concentration of protein value plotted against the selected wavelength) was established where the slope represents the extinction coefficient. Same was done for the calculation of the extinction coefficient of the redox dye. Extinction coefficients of proteins and dyes are listed in the appendix.

The Gibbs free energy (ΔG) could be calculated with the determined redox potential using equation 5.

$$-\Delta G = n \cdot F \cdot E^0 \quad (5)$$

where n is the number of electrons (n = 2), F the Faraday constant and E^0 the determined redox potential.

The change of Gibbs free energy (ΔΔG) was calculated by the subtraction of two distinct Gibbs free energies ($\Delta\Delta G = \Delta G1 - \Delta G2$).

The influence of the change of Gibbs free energy on the electron transfer rate reaction (Δk) was calculated with the equation 6.

$$\Delta k = A \cdot e^{-\Delta\Delta G / RT} \quad (6)$$

where A is the pre-exponential factor, R the gas constant (8.314 J/K mol) and T the temperature (298 K).

7 Single turnover measurements

The stopped flow measurements were performed under anaerobic conditions with an SX20MV apparatus from Applied Photophysics equipped with a diode array (DA) or a photomultiplier tube (PMT). All measurements were carried out at 10 °C. Solutions were made anaerobic by several cycles of vacuum and equilibration with molecular nitrogen in gas-tight bottles. One hour prior to the measurements the stopped flow apparatus was flushed with anaerobization buffer (0.1 g glucose, 0.34 g sodium acetate in 50 ml ddH_2O pH adjusted to pH 5 with acetic acid) including 120 U/ml glucose oxidase. A buffer with 50 mM Tris-HCl (pH 8.0) was used as a reference.

7.1 Reductive half reaction

Reductase$_{TOL}$ in a glass tonometer and NADH stock solution (1.5 mM in 50 mM Tris-HCl, 150 mM NaCl, pH 7.2) were made anaerobic separately at a vacuum-gas line by several cycles of evacuation and equilibration with N_2 gas. A dilution series of different NADH concentrations in the same buffer were made of the NADH stock solution. The exact concentration deployed was calculated using the measured values at A_{340} (ε_{340} (NADH) = 6.2 $mM^{-1}\,cm^{-1}$) with the Lambert-Beer law (equation 1). A glass tonometer containing the protein solution and a gas-tight syringe including the NADH solution were applied to the stopped flow spectrophotometer. The reduction of the flavin by NADH was followed by the change of absorbance at 450 nm while the formation of the charge transfer complex was monitored at 690 nm. The Pro-Data software was used for data evalution (Applied Photophysics). The measured absorption changes at 450 nm and 690 nm were fitted to a single exponential expression to determine the observed rate constant (k_{obs}) using equation 7.

$$\Delta A = A_{(1)} \cdot e^{(-k_{obs} \cdot t)} + c \quad (7)$$

where ΔA is the change of absorption, $A_{(1)}$ the amplitude, k_{obs} the observed rate constant, t the time and c the offset. The k_{obs} values were plotted against the substrate concentration and the data were evaluated according to the following model

$$RED_{TOL}\text{-}FAD + NADH \underset{k_{-1}}{\overset{k_1}{\rightleftharpoons}} \underset{\textit{Michaelis complex}}{RED_{TOL}\text{-}FAD\text{-}NADH} \underset{k_{-2}}{\overset{k_2}{\rightleftharpoons}} \underset{\textit{charge transfer complex}}{RED_{TOL}\text{-}FADH^{-}\text{-}NAD^{+}}$$

where RED_{TOL}-FAD and NADH stands for enzyme and substrate, respectively, RED_{TOL}-FAD-NADH for the enzyme-substrate complex and RED_{TOL}-$FADH^{-}$-NAD^{+} for the intermediate. Under the assumption that the binding of NAD^{+} to RED_{TOL}-FAD is fast compared to the electron transfer step the k_{obs} value depends hyperbolically on the NAD^{+} concentration (equation 8) (Strickland, 1975).

$$k_{obs} = k_{-2} + \frac{k_2 \cdot [S]}{K_D + [S]} \quad (8)$$

whereby

k_{obs}	observed rate constant
k_2	limiting rate constant
[S]	NADH concentration
K_D	dissociation constant

7.2 Oxidative half reaction

Various concentrations of ferricyanide were in the same buffer as the protein. The protein solution in a glass tonometer and the NADH stock solution were made anaerobic at a vacuum-gas line. Before the measurement the NADH stock solution in a gas-tight syringe was titrated to the protein solution until no further reduction

could be observed at 450 nm. The tonometer with reduced reductase$_{TOL}$ was applied to the stopped flow apparatus. Ferricyanide solutions in syringes were flushed with molecular nitrogen for at least 10 min and also applied to the stopped flow apparatus. Oxidation of flavin was monitored at a wavelength of 450 nm while the decay of the charge transfer complex was observed at 690 nm and the formation of semiquinone was observed at 610 nm. An increase of absorption in the region of 570 – 600 nm typically accounts for the generation of neutral semiquinoid form of flavin (Beinert, 1956). The decay of charge transfer complex was noticed by recording the decrease of absorption at 690 nm.

Data were evaluated with the software Pro-Data (Applied Photophysics). A two step mechanism model for the reaction of enzyme with a one electron acceptor was assumed.

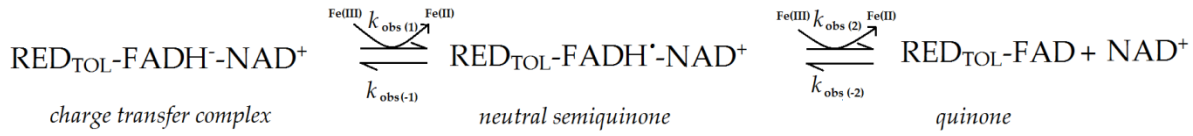

Fe(III) stands for the oxidized ferricyanide and Fe(II) for the reduced ferricyanide. The rate constants for the semiquinone formation and decay ($k_{obs(1)}$, resp. $k_{obs(2)}$) were determined by fitting the measured absorption changes (ΔA) at 450 nm, 690 nm and 610 nm to a double exponential function with an offset (c) and amplitude changes ($A_{(1)}$ and $A_{(2)}$) (equation 9).

$$\Delta A = A_{(1)} \cdot e^{(-k_{obs(1)}\,t)} + A_{(2)} \cdot e^{(-k_{obs(2)}\,t)} + c. \qquad (9)$$

8 Crystallography and data collection

Crystallization of oxidized reductase$_{TOL}$ was carried out by *hanging-drop* vapor-diffusion technique. Reductase$_{TOL}$ with a specific activity of 23 U/mg and a final

concentration of 23 mg/ml in 20 mM MOPS pH 7.2, 100 mM NaCl was used for crystallization experiments.

Crystallization of NAD^+-reductase$_{TOL}^{CT}$ under various conditions of index screen by Hampton Research was conducted in an anoxic tent by *hanging-drop* vapor-diffusion technique. 23 mg/ml of reductase$_{TOL}$ in 20 mM MOPS pH 7.2, 100 mM NaCl was treated with 3-fold the concentration of NADH prior to crystallization trials. Reductase$_{TOL}$-ferredoxin$_{TOL}$ complex was crystallized by the *sitting-drop* technique in an anoxic glove box. The reductase$_{TOL}$ was treated with 5-fold excess of NADH and subsequently mixed with equimolar concentration of ferredoxin$_{TOL}$.

All crystals were harvested in reservoir solutions containing 25 % (v/v) glycerol as a cryoprotectant, flash cooled and stored in liquid nitrogen.

The collection of diffraction data were performed at beam line BL14.2 (BESSY, Berlin, Germany). Diffraction data sets were integrated and scaled using XDS (Kabsch, 1993). All structures were solved using molecular replacement (Rossmann, 1990) using Patterson search techniques with the crystal structures of ferredoxin$_{TOL}$ (PDB-Id.: 3EF6) (Friemann *et al*., 2009) and reductase$_{TOL}$ (PDB-Id.: 3DQY) (Friemann *et al*., 2009) as homologous search models using PHASER (McCoy *et al*., 2007). All models were built with COOT (Emsley & Cowtan 2004). Positional and temperature factor and TLS refinements (Painter & Merritt, 2006) were carried out using PHENIX (Adams *et al*., 2010)

9 Computer Softwares

Alignment of amino acids were done with ClustalW, colored and edited manually (Chenna *et al*., 2003). Measured spectra were analyzed and presented by GraFit 5 (Leatherbarrow, 2001). Data from stopped flow measurements were evaluated and analyzed by Pro-Data Viewer (Applied Photophysics). Pictures of the structures solved in this thesis were prepared with PyMol (DeLano, 2002).

RESULTS AND DISCUSSION

1 *todA* and *todB* involved in the toluene degradation

Aromatic hydrocarbons such as benzene, benzoate, toluene, phthalate, naphthalene or biphenyl are widespread pollutants of soil and groundwater. Many bacteria degrade aromatic hydrocarbons to utilize them as a sole carbon and energy source. The first step in the aerobic degradation is often catalyzed by a multi-component Rieske non-heme iron dioxygenase. This enzyme family is therefore an attractive area of work as the elucidation of the mechanism could lead to the solution of environmental problems caused by aromatic hydrocarbons (Gibson & Parales, 2000). The toluene dioxygenase (TDO) was first characterized and isolated from *P. putida* F1 by Gibson *et al.* (Gibson *et al.*, 1970). The genes encoding the three enzymes of TDO were determined by Zylstra and Gibson (Zylstra & Gibson, 1989), of which the genes *todA* and *todB* encode the reductase$_{TOL}$ and the ferredoxin$_{TOL}$, respectively.

1.1 *todA* - the gene encoding reductase$_{TOL}$

Amino acid alignment of the *todA* product with Blast (http://blast.ncbi.nih.gov/Blast.cgi) predicts a protein belonging to the family of FAD-dependent pyridine nucleotide-disulfide oxidoreductases. It contains two conserved domains of Pyr_redox (nucleotide binding regions), one for FAD (at positions 4 - 35) and one for NAD (at positions 145 - 173). Alignment of the amino acid sequence of the *todA* product to homologous reductase components of ROs and other members of the glutathione reductase (GR) family found in bacteria and archea illustrates the conservation of residues coordinating the FAD and NAD binding. $GXGX_2GX_3AXG$ is a characteristic sequence for an FAD-binding site and is closely located at the N-terminus (Mason & Cammack, 1992). Two to three hydrophobic residues are situated before the first glycine (Fig. 11). The NAD-binding domain is usually represented by

a $GXGX_2GX_3AX_6E$ sequence (Fig. 11) (Benen *et al.*, 1989; Hanukoglu & Gutfinger, 1989).

Further conserved amino acids in ROs reductases of type IIB probably participate in the structural changes found in the CT complexes (Fig. 11, cyan boxes), the interaction between ferredoxin$_{TOL}$ and reductase$_{TOL}$ (Fig. 11, pink boxes) and the facilitation of electron transfer between the two cofactors in the complex (Fig. 11, dark red boxes).

The gene *todA* was cloned into a pET-15b vector with an N-terminal His6-Tag, designated as pET15b*todA*. The 1233 base pairs (bp) long *todA* encodes 410 amino acids of reductase$_{TOL}$. The nucleotide sequence from DNA sequencing matches the published sequence of *todA* (Zylstra & Gibson, 1989).

1.2 *todB* - the gene encoding ferredoxin$_{TOL}$

Amino acid alignment of *todB* predicts a protein with a [2Fe-2S] cluster binding site, termed Rieske RO ferredoxin. Sequence alignment to homologous ferredoxins of ROs exposes conserved residues that are responsible for the coordination of the Rieske-type [2Fe-2S] cluster (Fig. 13, yellow boxes). A proline (P79), a phenylalanine (F68) and threonine (T43) are conserved throughout the RO ferredoxins, e.g. P79's equivalent P80 in the biphenyl dioxygenase reductase (BphA4) (Fig. 11, dark red boxes). The phenylalanine (F68) and threonine (T43) partake in the hydrogen bonding network around the cluster. Conformational changes of their side chains are suspected to influence the redox potential of the RO ferredoxins and Rieske-type [2Fe-2S] cluster containing ferredoxins (Ferraro *et al.*, 2007). Other conserved amino acids appear to participate in the protein-protein interaction of reductase and ferredoxin components (Fig. 11, pink boxes).

The gene *todB* was cloned into a pET-15b and pET-11a vector and named pET15b*todB* and pET11a*todB*, respectively. These plasmids contain the 324 bp long *todB* gene. The nucleotide sequence from the DNA sequencing and the translated amino acid

sequences confirmed no mutation compared to the published sequence of *todB* (Zylstra & Gibson, 1989).

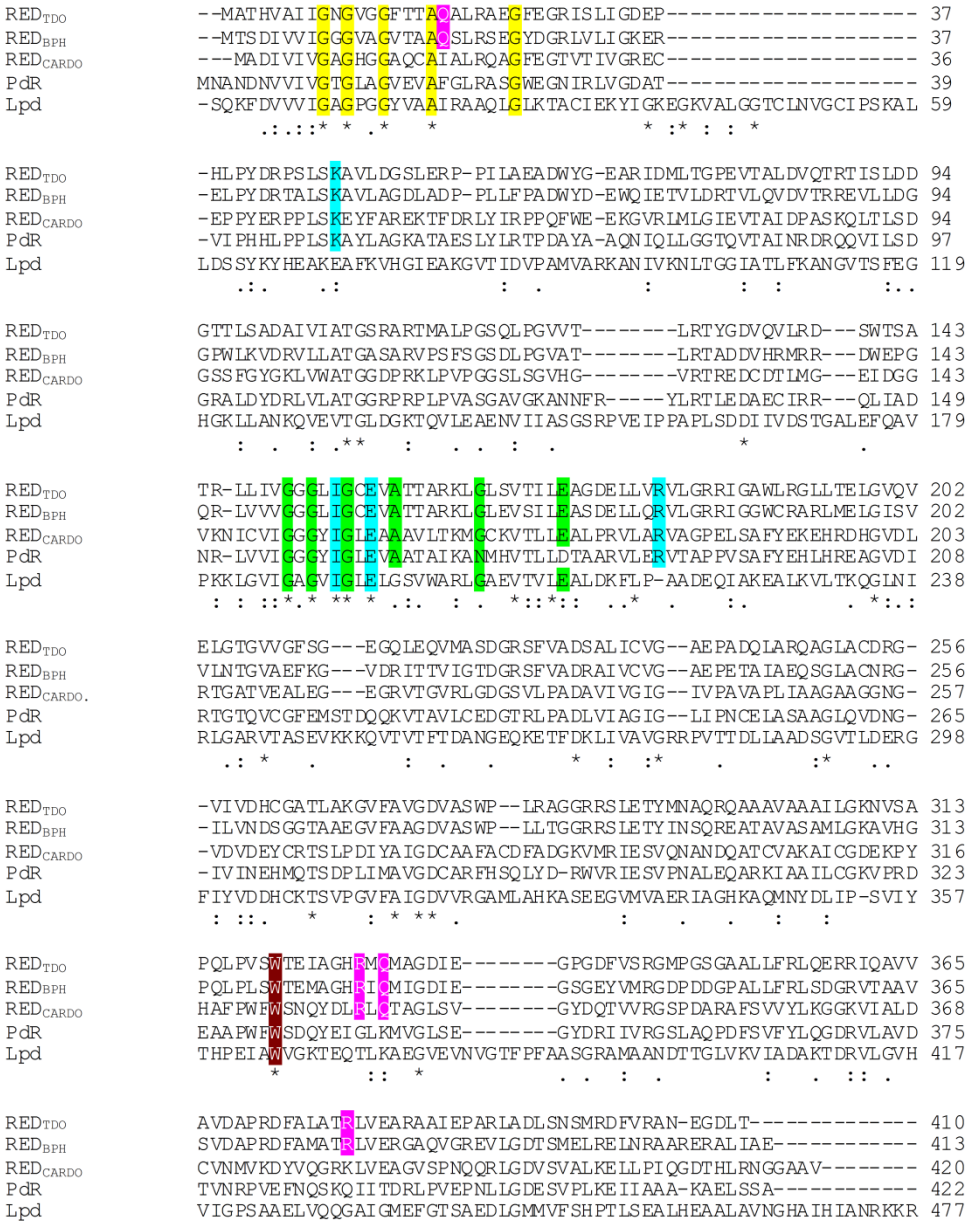

Fig 11. Alignment of amino acid sequence with reductase components of the Rieske non-heme iron dioxygenase family and members of glutathione reductase family. The conserved residues of bindings sites of FAD- and NAD(P)-binding sites are depicted in yellow and green, respectively. Amino acids colored in dark red seem to be involved in electron transfer between FAD and [2Fe-2S] cluster. Pink colored amino acids are likely involved in protein-protein interaction and cyan colored amino acids important for the CT complex formation. RED$_{TDO}$, reductase$_{TOL}$ from *Pseudomonas putida*; RED$_{BPH}$, biphenyl dioxygenase reductase from *Pseudomonas sp.*; RED$_{CARDO}$, carbazole dioxygenase

reductase from *Pseudomonas resinovorans*; PdR, putidaredoxin reductase from *Pseudomonas putida*; Lpd, lipoamide dehydrogenase from *Pseudomonas fluorescence.* Sequences were aligned with ClustalW (Chenna *et al*., 2003): *, fully conserved residues; : (colon), conservation of strong groups; . (period), conservation of weak groups.

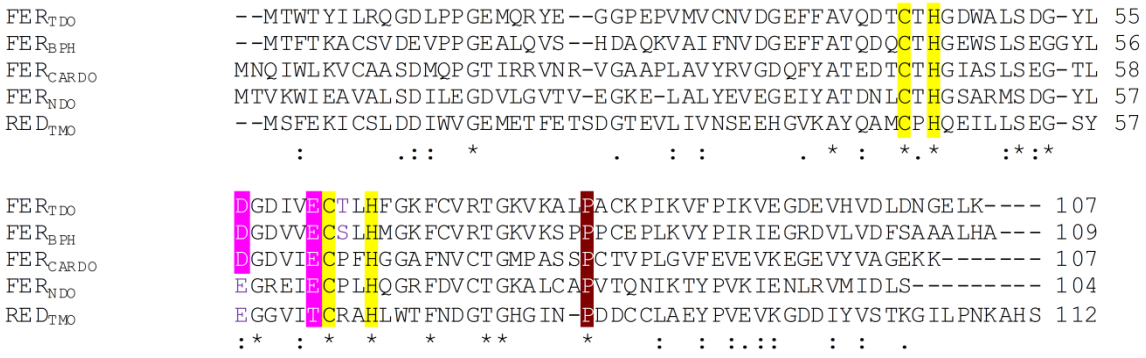

Figure 12. Alignment of amino acid sequence with homologues ferredoxin components of the Rieske non-heme iron dioxygenase system. The Rieske consensus sequence is colored in yellow. Amino acids colored in dark red seem to be involved in electron transfer between FAD and [2Fe-2S] cluster. Pink colored amino acids appear to be important for protein-protein interaction. FER$_{TDO}$, ferredoxin$_{TOL}$ from *Pseudomonas putida*; FER$_{BPH}$, biphenyl dioxygase ferredoxin from *Pseudomonas sp*; FER$_{CAR}$, carbazole dioxygenase ferredoxin from *Pseudomonas resinovorans*; FER$_{NDO}$, naphthalene dioxygenase ferredoxin from *Pseudomonas putida*; FER$_{TMO}$, ferredoxin of toluene monooxygenase from *Pseudomonas mendocina*. Amino acids sequences were aligned with ClustalW (Chenna *et al*., 2003): *, fully conserved residues; : (colon), conservation of strong groups; . (period), conservation of weak groups.

2 Expression and purification of reductase$_{TOL}$ and ferredoxin$_{TOL}$

The pET15b*todA* and pET15b*todB* constructs were transformed and expressed in *E. coli*. This section deals with the expression and purification of reductase$_{TOL}$, followed by the result and discussion of the ferredoxin$_{TOL}$ expression and purification.

2.1 Expression and purification of reductase$_{TOL}$

Even though heterologous expression and purification of the recombinant protein have already been performed by Lee *et al.* (Lee *et al.*, 2005) the His6-Tag affinity system was applied to optimize the purification of reductase$_{TOL}$.

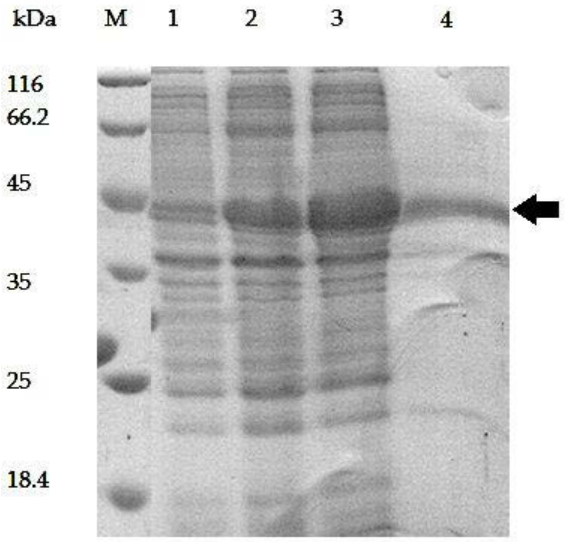

Figure 13. Coomassie stained 12 % SDS PAGE of heterologous expression of His6-tagged reductase$_{TOL}$. Lane 1 - 0 h, Lane 2 - 3 h, Lane 3 - 20 h after induction, Lane 4 - supernatant fraction after sonification, M is molecular protein weight marker from Roth. The arrow indicates the overproduced reductase$_{TOL}$ (45 kDa).

E.coli BL21 (DE3) harboring the pET15b*todA* construct was induced with different concentrations of IPTG (0.1 - 1 mM) in the mid (OD_{600} = 0.4 - 0.7), early (OD_{600} = 0.1 - 0.3) and late logarithmic phase (OD_{600} > 0.7). Reductase$_{TOL}$ was weakly produced in insoluble form. The solubility of the protein could not be enhanced by varying the fermentation conditions such as temperature, the choice of medium or inducer concentration. Overexpression of *todA* was achieved by changing the expression strain to *E.coli* CodonPlus(DE3)-RIL (Stratagene). This strain contains additional tRNA genes for arginine, isoleucine and leucin and is used for organisms with AT-rich genomes. Although His6-tagged reductase$_{TOL}$ was overproduced, the protein was mostly found in form of inclusion bodies. Cultivation experiments were

performed at lower temperatures than 37 °C after the time of induction. Temperature reduction is a well known way to reduce the aggregation of heterogously expressed proteins because of increased protein stability and a higher probability for correct folding (Schein, 1989). Highest solubility of reductaseTOL was achieved at a temperature of 20 °C. The choice of the cultivation media also had an impact on the protein yield. Overproduction of reductaseTOL was enhanced in enriched media such as dYT or TB.

40 % of soluble His6-tagged reductaseTOL was obtained after an around 20 h expression at 20 °C in TB medium induced with 0.5 mM IPTG in the mid logarithmic phase (Fig. 13, lane 4).

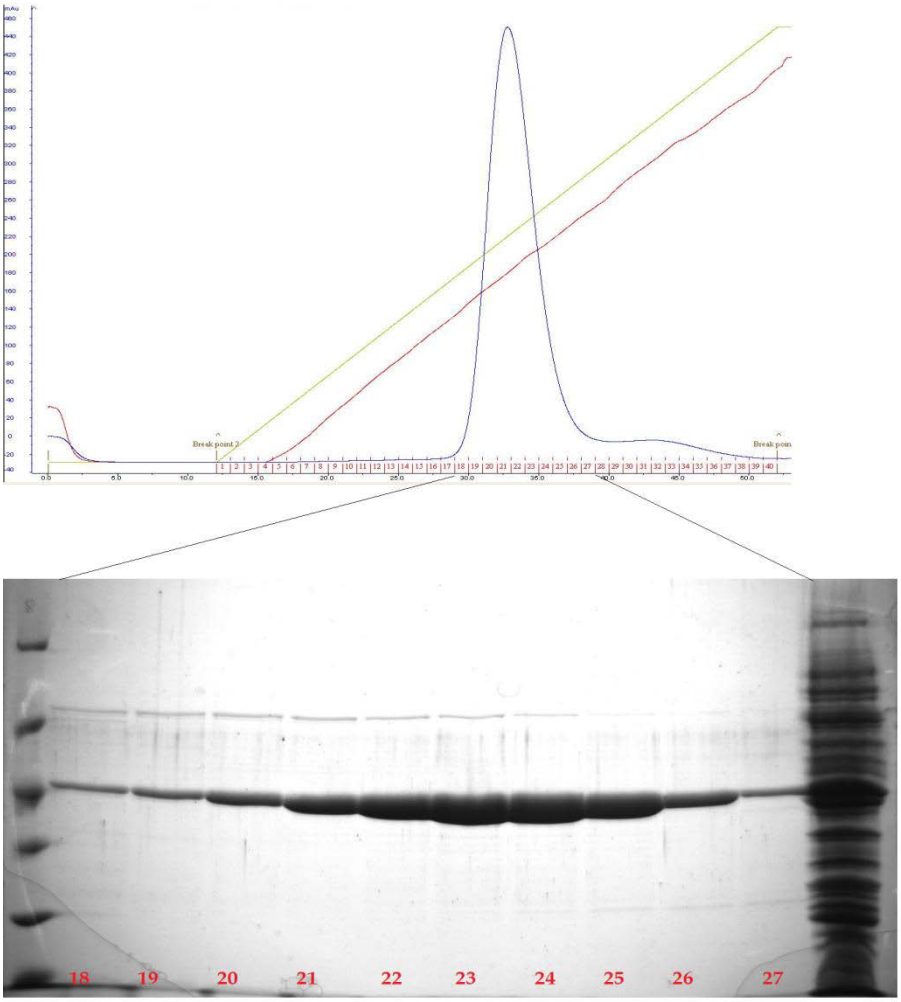

Figure 14. Coomassie stained 12 % SDS-PAGE of the purification of His-tagged reductase$_{TOL}$ on Q-Sepharose FF column. Lane 1 - 10, 5 µl samples of elution over a linear gradient of 0 - 500 mM NaCl (total volumn 200 ml) was loaded. Lane 11 shows the overproduced reductase$_{TOL}$. Red numbers indicate the fraction number shown in the elution profile. The green colored line shows the linear gradient of NaCl, the red line the conductivity. M is molecular protein weight marker from Roth.

His6-tagged reductase$_{TOL}$ was isolated as described in material and methods. The protein bound to the Ni^{2+} loaded chelating sepharose FF (fast flow). Major impurities were removed after a wash with three column volumes of washing buffer. Elution of the protein was conducted with a stepwise increase of the imidazole concentration (10 mM steps). Most of the protein was eluted at a concentration of 125 mM imidazole with a purity of around 90 %. In the Q-Sepharose purification step a peak with a shoulder was detectable (Fig. 14). Fractions collected from the peak contained reductase$_{TOL}$ with FAD (holo-reductase$_{TOL}$) and from the shoulder reductase$_{TOL}$ without FAD (apo-reductase$_{TOL}$) (Fig. 14). The reductase without FAD could be reconstituted by incubation with a 2-fold surplus of FAD. Excess, unbound FAD was removed by a passage through a Sephadex column. 60 mg of holo-reductase$_{TOL}$ could be obtained from 20 g wet weight of cell paste. Purified reductase$_{TOL}$ had a specific activity of 23 U/mg.

The choice of the pET-15b system facilitated the purification of reductase$_{TOL}$. The purification steps were reduced to two steps and allowed to quickly obtain active holo-reductase$_{TOL}$.

2.2 Expression and purification of ferredoxin$_{TOL}$

The purification strategy of reductase$_{TOL}$ was not applicable to ferredoxin$_{TOL}$. The purity of His6-tagged ferredoxin$_{TOL}$ was over 90 % but resulted in a protein without an intact iron cluster (apo-ferredoxin$_{TOL}$). This is proven by the colorlessness of the protein solution. A holo-ferredoxin$_{TOL}$ is usually brown in color derived from the presence of an intact Rieske-type [2Fe-2S] cluster (Subramanian *et al.*, 1985).

Supplementation of variable concentrations of 0.1 mM Na_2S and 0.1 mM $FeSO_4$ x 7 H_2O during expression did not result in the generation of holo-ferredoxin$_{TOL}$. Heterologous purification also did not yield His6-tagged holoprotein. The Rieske-type [2Fe-2S] cluster could not be reconstituted after purification as well. The structure of ferredoxin$_{TOL}$ published by Friemann *et al.* shows that the iron sulfur cluster is closely located at the N-terminal cluster-binding domain of the protein (Friemann *et al.*, 2009). The N-terminal His6-Tag probably hampers the assembly of the iron-sulfur cluster. This could also explain why supplement addition during expression and iron-sulfur cluster reconstitution experiments after purification were not effective.

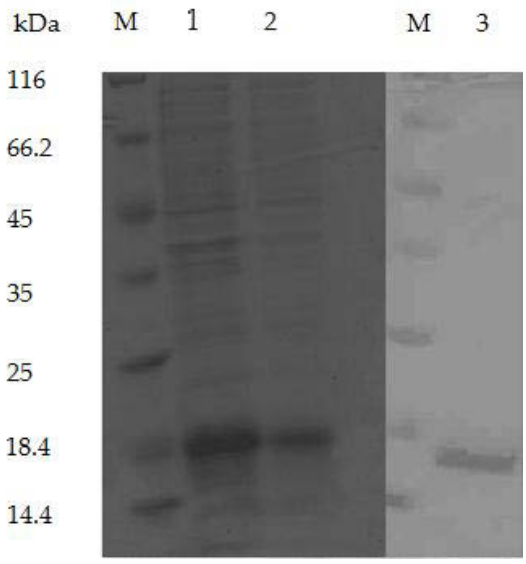

Figure 15. Coomassie stained 15% SDS-PAGE of heterologous expression and the final step in purification of ferredoxin$_{TOL}$. Lane 1 - insoluble fraction after 22 h expression, lane 2 - soluble fraction after 22 h expression, lane 3 - purified protein after Superdex HR 200, M is molecular protein weight marker from Roth.

Thus, the pET11a*todB* construct (without affinity tag) was used for the overproduction of ferredoxin$_{TOL}$. The expression condition of ferredoxin$_{TOL}$ resembled the expression condition of reductase$_{TOL}$. The solubility of ferredoxin$_{TOL}$ was dependent on the temperature after induction. No soluble protein could be detected

at higher temperature than 20 °C and no ferredoxin$_{TOL}$ was overproduced at temperature lower than 16 °C. Most of ferredoxin$_{TOL}$ was soluble at 18 °C. Protein expression was induced by the addition of 0.5 mM IPTG at OD_{600} = 0.5. Right before induction 0.1 mM Na_2S and 0.1 mM $FeSO_4$ x 7 H_2O were added and the expression temperature was shifted from 37 °C to 18 °C. Cells were harvested 20 h after induction. The overproduction of ferredoxin$_{TOL}$ was highly reproducible (Fig. 15, lane 1 and 2).

Ferredoxin$_{TOL}$ bound tightly to the DEAE-Sepharose FF column and was eluted at a concentration of 270 mM NaCl. The elution of the protein could be monitored by following the migration of the brown band on the column. The protein was then applied to a hydroxyapatite column. Even though ferredoxin$_{TOL}$ did not bind to hydroxyapatite this step had a purification effect on ferredoxin$_{TOL}$ because major impurities bound to the column. Ferredoxin$_{TOL}$ was collected from the flow-through. At that point of the purification the protein was around 80 % pure. A purification step with Superdex HR 200 helped to remove further impurities. In the end the protein was 85 % pure (Fig. 15, lane 3). 20 g cell gave approximately 10 mg brownish ferredoxin$_{TOL}$. The iron determination experiment revealed that the ferredoxin$_{TOL}$ possessed two irons and two sulfur atom per monomer indicating holo-ferredoxin$_{TOL}$. The expression of C-terminal His6-Tag ferredoxin$_{TOL}$ might be tested in order to get a higher protein yield. The purification of C-terminal His6-Tag ferredoxin$_{TOL}$ could result in His-tagged ferredoxin$_{TOL}$ with an intact iron-sulfur cluster as the C-terminal His-tag would not likely affect the formation of iron-sulfur cluster located at the N-terminus.

3 Structural characterization

Crystal structures of reductase$_{TOL}$ and NADH-reduced reductase$_{TOL}$ were solved in order to examine any structural changes of reductase$_{TOL}$ that are caused by the reduction with NADH. The structures of reductase$_{TOL}$ and reduced reductase

forming a charge transfer complex with NAD^+ (NAD^+:reductase$_{TOL}^{CT}$) are compared in the first part of this chapter. Second part of this chapter deals with the structural characterization of the complex between reductase$_{TOL}$ and ferredoxin$_{TOL}$.

3.1 Crystallization and structure of reductase$_{TOL}$ and NAD^+:reductase$_{TOL}^{CT}$

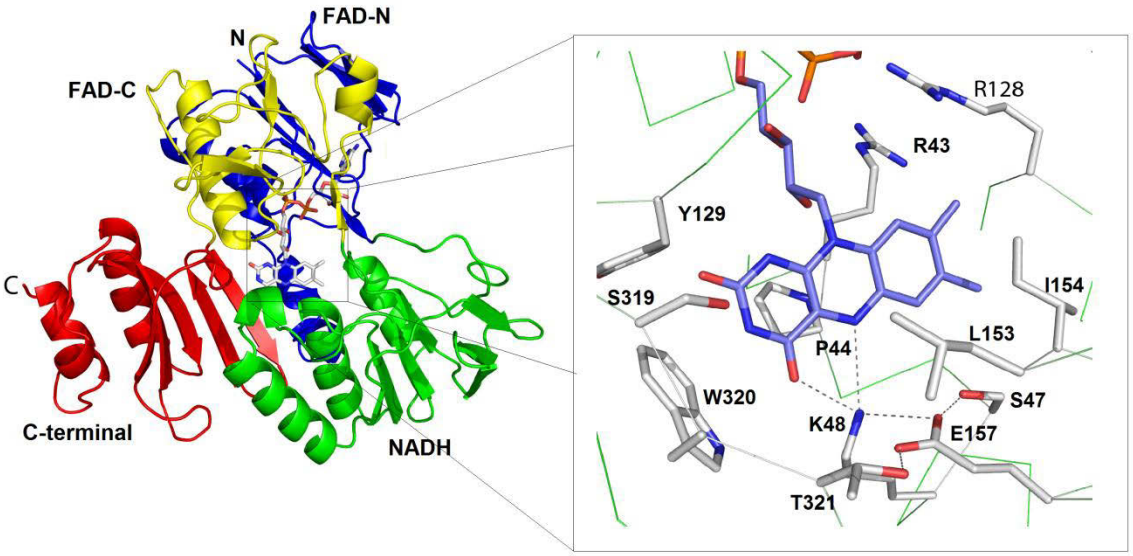

Figure 16. Overall structure and view of the active site of reductase$_{TOL}$. Reductase$_{TOL}$ is shown in cartoon representation. The N-terminal FAD-binding domain (FAD-N) is depicted in blue, the NADH-binding domain (NADH) in green, the C-terminal FAD-binding domain (FAD-C) is shown in yellow and the C-terminal domain (C) is colored in red. FAD in the overall structure (left) is in white carbons. In the enlarged figure (right) all carbon atoms of FAD have been depicted in blue and the active site residues in white. The dashed lines represent hydrogen-bonds.

The overall structure of reductase$_{TOL}$ solved in this work is identical to the structure of reductase$_{TOL}$ previously published (Friemann *et al.*, 2009). Yellow crystals of reductase$_{TOL}$ grew in 0.1 M Bis-Tris pH 6.5 and 1.4 M ammonium sulphate within three days. Slightly blue crystals of NADH-treated reductase$_{TOL}$ in 2.2 M sodium malonate pH 6.5 grew within one week. The crystals of reductase$_{TOL}$ and NADH-

treated reductase$_{TOL}$ belong to the space group $P4_12_12$ and contain one molecule per asymmetric unit (Tab. 3).

The overall structure of reductase$_{TOL}$ shows high similarity to bovine adrenodoxin reductase (AdR) and BphA4 (Fig. 16) (Schulz *et al.*, 1978; Karplus & Schulz, 1987). It consists of three domains: an FAD-binding domain, an NADH-binding domain and a C-terminal domain. The FAD-binding domain can be divided into an N-terminal (3 - 111) and a C-terminal part (239 - 317) (Fig. 15) and comprises of a central β-sheet build of five parallel β-strands, to which the N-terminal part contributes four β-strands and the C-terminal part one β-strand. This β-sheet is on one side enclosed by a β-sheet made of three antiparallel β-strands and on the other side by three α-helices (Fig. 15). Residues 36 - 61 between the second and the third β-strand of the N-terminal part of the FAD-binding domain form an extension that covers the pyrazine and dimethylbenzene portion on the *Si*-side of the isoalloxazine ring. The equivalent structural part has been termed "backrest subdomain" in the structure of BphA4 (Senda *et al.*, 2007).

Table 3. Statistics on diffraction data and structure refinement of reductase$_{TOL}$ and NAD$^+$:reductase$_{TOL}^{CT}$

Reductase$_{TOL}$		NAD$^+$:reductase$_{TOL}^{CT}$	
Wavelength	0.91841	Wavelength	0.91841
Space group	$P4_12_12$	Space group	$P4_12_12$
Cell constants (Å)	77.4, 77.4, 157.5	Cell constants (Å)	78.4, 78.4, 158.7
Total / unique refl.	273,927 / 75,479	Total / unique refl.	316,338 / 41,735
R_S [a] (%)	4.9 (46.1)	R_S [a] (%)	4.9 (46.1)
Resolution (Å)	20 – 1.88 (1.93-1.88)	Resolution (Å)	20 – 1.88 (1.93-1.88)
Completeness (%)	98.4 (97.5)	Completeness (%)	90.1 (99)
(I) / (I)	16.0 (2.8)	(I) / (I)	20.9 (2.8)
Model R / R_{free}-factor (%) [b]	19.3 / 23.5	Model R / R_{free}-factor (%) [b]	18.4 / 21.5
Rms deviation from ideal geometry		Rms deviation from ideal geometry	
Bonds (Å)	0.0011	Bonds (Å)	0.0011
Angles (°)	1.5	Angles (°)	1.779

Numbers in brackets denote the values found in the highest resolution shell.

[a] $Rs = \sum_h \sum_i | I_i(h) - \langle I(h) \rangle | / \sum_h \sum_i I_i(h)$; where i are the independent observations of reflection h.

[b] The R_{free} factor was calculated from 5 % of the data, which were removed at random before the refinement was carried out. The R factor has been calculated from the reflections of the working set and test set.

The same structural elements are found in the NADH-binding domain. The NADH-binding domain has a central parallel β-sheet build of four β-strands. The β-sheet is sandwiched by a two stranded antiparallel β-sheet and by three α-helices (Fig. 15). The C-terminal domain possesses an antiparallel five stranded β-sheet and three short α-helices (Fig. 16). N-terminal part and C-terminal part of the FAD-binding domain form a gap in which the FAD is bound to the N-terminal part of the FAD-binding domain with its ADP moiety. The isoalloxazine ring is situated near beneath the surface where all three domains intersect (Fig. 16). The pyrimidine part of the isoalloxazine ring points to the surface and opposes W320 that shields it from the solvent (Fig. 16). Other hydrophobic residues like P44 are part of the residues between the second and third β-strand of the N-terminal FAD-binding domain and shield the *Si*-side of the isoalloxazine ring from the solvent (Fig. 16). The isoalloxazine ring of FAD is in planar conformation (Fig. 16).
In spite of the relatively low sequence identities of 34 % (reductase$_{TOL}$ *vs.* BphA4) and 32 % (reductase$_{TOL}$ *vs.* AdR) the active site of these protein are quite similar. Residues within the substrate channel and active sites architecture of reductase$_{TOL}$, BphA4 and AdR are identical with a hydrogen bonding network around K48, E157 and S52, a cluster of arginine residues at the entrance of the substrate channel to facilitate steering of NADH into the active site and a hydrophobic path at the *Si*-side of the isoalloxazine ring that includes the side chains of P44 and W320.

The overall crystal structure of NAD^+:reductase$_{TOL}^{CT}$ is similar to the structure of reductase$_{TOL}$ but with an NAD^+ molecule in the active site. NAD^+ is lying in the

solvent accessible cavity facing the *Re*-side of the isoalloxazine ring. It shields the reactive N5-C4a part of FAD whose influencing is supposed to alter the oxygen sensitivity of the flavoprotein (Sun *et al.*, 1997) (Fig. 17). The carboxamide group of NAD^+ is directly opposite to the pyrimidine ring of the flavin. The pyridine ring of the nicotinamide is lying above the pyrazine ring of flavin. The N5 atom of the pyrazine ring of FAD and the C4 atom of the pyridine ring of NAD^+ are 3.2 Å apart (Fig. 17).

Structural changes can be found in the NADH-binding domain and are caused by the conformation changes of residues that interact with the diphosphate moiety of NAD^+ (Fig. 17). Upon NAD^+ binding the side chain of R181 moves, so the guanidinium group can form a salt bridge with the AMP-phosphate of NAD^+. R181 also participates in hydrogen-bonding to the ribose of NAD^+ (Fig. 18). Salt bridges and hydrogen bonds effect that the Cα-atom of Arg181 comes about 3.0 Å closer to the NAD^+. The movement of R181 causes a subsequent pull of the residues 170 - 199 (Fig. 18). The carboxylate group of E157 is in hydrogen bond distance to the carboxyamide group of NAD^+, 3.4 Å away from the hydride donor/acceptor atom of C4 (Fig. 18). NAD^+ seems to push the isoalloxazine ring resulting in a tilt of 10 ° compared to the isoalloxazine ring of oxidized reductase$_{TOL}$ (Fig. 17).

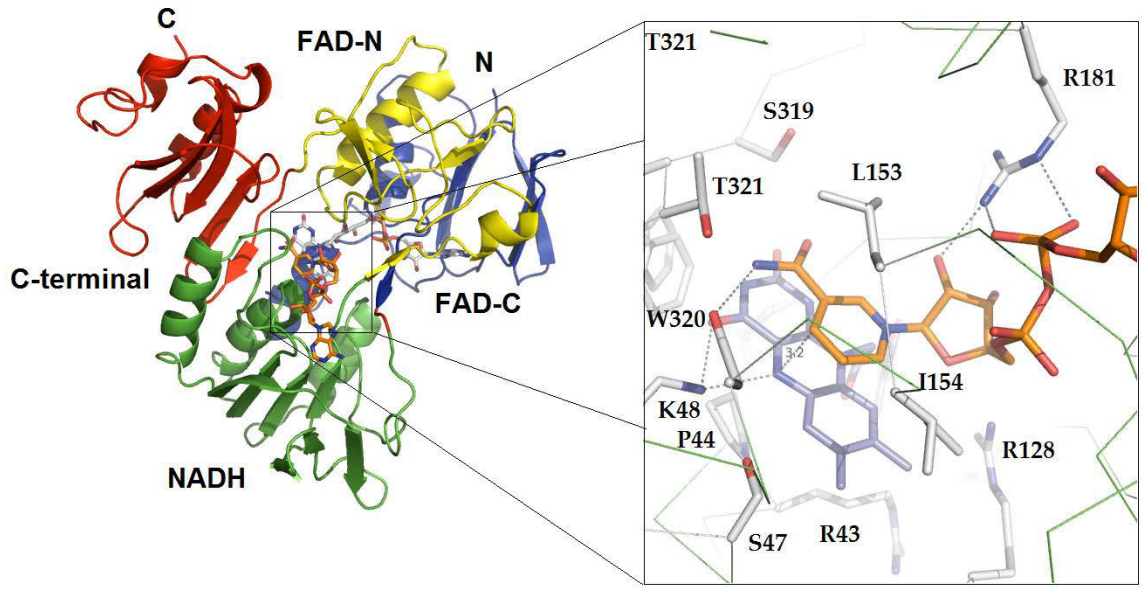

Figure 17. Overall structure and view of the active site of NAD⁺:reductase$_{TOL}^{CT}$. NAD⁺:reductase$_{TOL}^{CT}$ is shown in cartoon presentation. The N-terminal FAD-binding domain is depicted in blue and the C-terminal FAD-binding domain is shown in yellow. The NADH-binding domain is colored in green and the C-terminal domain in red. Carbon atoms of FAD and NAD⁺ shown as stick-model are depicted in white and orange, respectively. In the figure of the active site, carbon atoms of FAD are depicted in blue.

The N5 atom of FAD shifts by 0.5 Å from the C4 atom of NAD⁺ and the O4 atom of FAD by 0.7 Å from the carboxamide group of NAD⁺ (Fig. 16 and 17). NAD⁺ also pushes away I154 in the active site. In opposition to the side chain of K48 in the reductase$_{TOL}$ structure the side chain of K48 in the NAD⁺:reductase$_{TOL}^{CT}$ structure can be found in two conformations. One conformation is in hydrogen-bonding distance to the N5 atom of FAD (Friemann *et al.*, 2009).

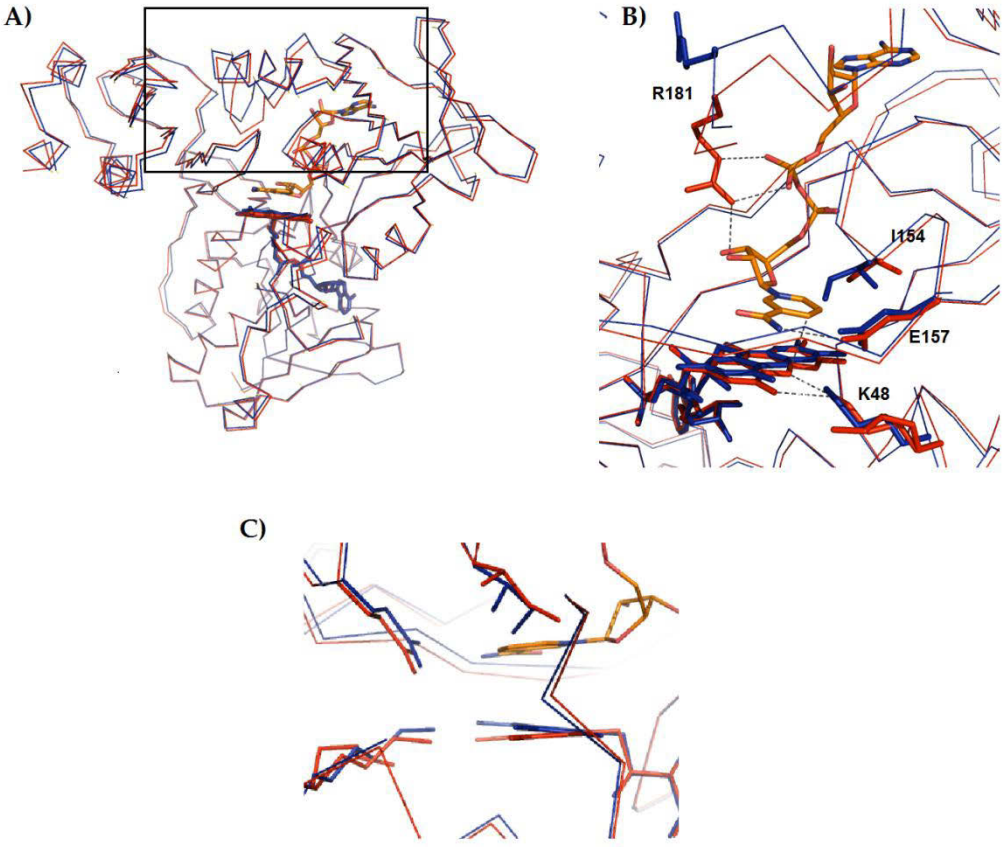

Figure 18. Superimposition of the overall structure and active site of reductase$_{TOL}$ and NAD$^+$:reductase$_{TOL}^{CT}$. Protein matrix is shown in ribbon presentation, for reductase$_{TOL}$ in blue, for NAD$^+$:reductase$_{TOL}^{CT}$ in red. Selected residues are represented as lines. Salt- and hydrogen bond interactions are shown in dashed lines. The marked area indicates the structural change in the protein matrix of the NADH-binding domain of NAD$^+$:reductase$_{TOL}^{CT}$ (A). Enlarged figure shows the isoalloxazine ring as blue sticks for reductase$_{TOL}$ and red sticks for NAD$^+$:reductase$_{TOL}^{CT}$. For NAD$^+$, carbons are depicted in orange, oxygen in red and nitrogen in blue color (B). The isoalloxazine ring in the NAD$^+$:reductase$_{TOL}^{CT}$ is tilted by ca. 10 ° compared to the isoalloxazine ring of reductase$_{TOL}$ (C).

The biphenyl dioxygenase reductase (BphA4) belongs to the same group of Rieske non-heme iron dioxygenase and was structurally characterized by Senda *et al.* (Senda *et al.*, 2007). The interaction between ferredoxin and reductase are redox dependent and structural changes upon FAD reduction could be observed in BphA4: a butterfly-like bent of the isoalloxazine ring, a flip of ribityl chain, a shift of "backrest subdomain" and a rotation of the NAD-binding and C-terminal domains. The redox dependent change of FAD triggers a conformation change of the NADH and C-terminal domain and thereby facilitates the binding of ferredoxin$_{TOL}$ to BphA4 (Senda *et al.*, 2007).

The isoalloxazine ring of FAD in NAD$^+$:reductase$_{TOL}^{CT}$ is coplanar with the nicotinamide ring of NAD$^+$ unlike the butterfly-bent shape conformation along the N10-N5 axis of the reduced flavin in BphA4. A flip of the ribityl chain cannot be seen (Senda *et al.*, 2007). The crystals of NAD$^+$:reductase$_{TOL}^{CT}$ were not yellowish, suggesting that the planar conformation of isoalloxazine ring is not consequence of flavin reoxidation. The planar conformation could be explained best by stabilization of the π-π donor-acceptor interaction in the charge transfer complex (Massey & Ghisla, 1974; Sakurai & Hosoya, 1966). Besides the above mentioned shielding of FAD from the solvent, NAD$^+$ forces the reduced FAD into a planar conformation which is energetically less favorable to react with oxygen (Massey & Ghisla, 1974). The C4NAD-N5FAD distance of NAD$^+$:reductase$_{TOL}^{CT}$ with 3.2 Å is comparable to the C4NAD-N5FAD distance in NAD$^+$:BphA4^{CT} with 3.4 Å (Senda *et al.*, 2007). R183 in

BphA4^{CT} seems to have a similar function as R181 in reductase$_{TOL}$. Yet, the movement caused by R183 does not resemble the drastic pull of R181 at the NADH-binding domain. Other amino acids such as I154, E157 and K48 in reductase$_{TOL}$ are equivalent to I156, E159 and K53 of BphA4. K53 of BphA4 is thought to be mainly responsible for the mobility of the backrest subdomain via hydrogen bonding to FAD (Senda *et al*., 2009). In the amino acid sequence alignment of the enzymes of the GR family the lysine is highly conserved (Fig. 11).

The redox-dependent rotation of NADH/CT domain of BphA4 (Senda *et al*., 2007) could not be observed with the CT complex structure of reductase$_{TOL}$. NAD^+ binding induces a conformation change of residues at the active site with a subsequent minimal change in the NADH-binding domain (Fig. 18). These changes are not caused by a conformational change of the isoalloxazing ring upon reduction but seem to be solely a consequence of the interaction between NAD^+ and residues in the active site. Accordingly, the conformational changes of the conserved residues could influence the affinity of NAD^+:reductase$_{TOL}^{CT}$ to ferredoxin$_{TOL}$. Mutation of the residues, such as K48, R181 and W320 could explain their function in the interaction between reductase$_{TOL}$ and ferredoxin$_{TOL}$.

3.2 Crystallization and structure of reductase$_{TOL}$-ferredoxin$_{TOL}$ complex

Orange crystals of reductase$_{TOL}$-ferredoxin$_{TOL}$ complex grew in 0.1 M Bis-Tris pH 6.5, 20 % (w/v) Polyethylene glycol monomethyl ether 5,000 within two to three weeks and diffracted to 2.4 Å resolution. The crystals belong to the space group $P6_5$ (Tab. 5). The reductase$_{TOL}$ in general reveals two major recesses on contrary sides of the surface of reductase$_{TOL}$ that are potential binding sites for ferredoxin$_{TOL}$ (Fig. 15, 16 and 19). One binding site is above the NADH-binding channel to the R*e*-face of the flavin, one is opposite to the NADH-binding channel facing the S*i*-side of the isoalloxazine ring (Fig. 15).

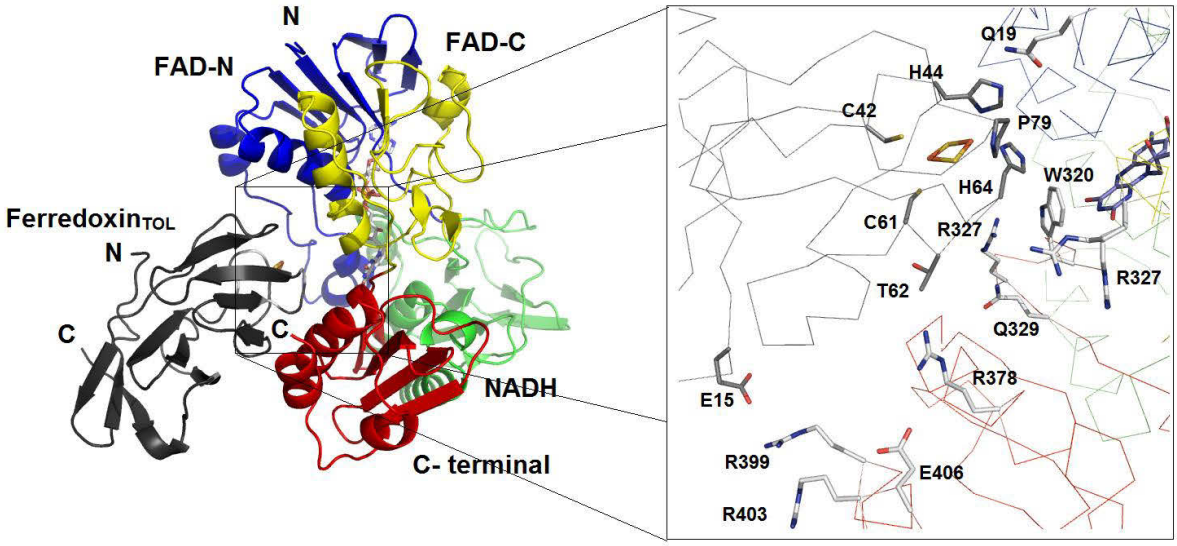

Figure 19. Overall structure and view of active site of reductase$_{TOL}$-ferredoxin$_{TOL}$ complex. The complex is shown in cartoon presentation. Each domain is colored as indicated. The N-terminal FAD-binding domain is depicted in blue, the NADH-binding domain in green, the C-terminal FAD-binding domain is shown in yellow and the C-terminal domain is colored in red. Ferredoxin$_{TOL}$ is colored in black. Carbon atoms of the residues of reductase$_{TOL}$ participating in the interaction are colored in white, carbon atoms of the residues of ferredoxin$_{TOL}$ in white. Protein backbone is presented in ribbon plot presentation. The domain is same colored as in cartoon representation. For FAD, all carbon atoms have been depicted in blue.

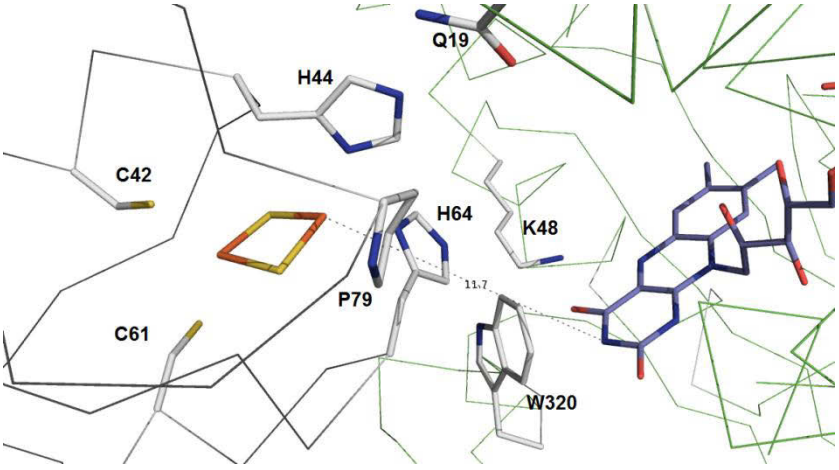

Figure 20. Distance between the two cofactors in the reductase$_{TOL}$-ferredoxin$_{TOL}$ complex. Carbon atoms of the residues of reductase$_{TOL}$ participating in the interaction are colored in white, carbon atoms of the residues of ferredoxin$_{TOL}$ in white. The protein backbone is presented in ribbon plot

presentation. The domain is same colored as in cartoon representation. For FAD, all carbon atoms have been depicted in blue. Iron atoms are colored in orange, sulfur atoms in yellow.

The reductase$_{TOL}$-ferredoxin$_{TOL}$ complex structure reveals that ferredoxin$_{TOL}$ binds to the recess close to the *Si*-side of FAD which is formed by the FAD-binding domain and the C-terminal domain of reductase$_{TOL}$ (Fig. 18). The complex is stabilized by Coulomb attraction between reductase$_{TOL}$ and ferredoxin$_{TOL}$. The charge of the interacting surface area of reductase$_{TOL}$ is largely positive, while the charge of the interacting surface area of ferredoxin$_{TOL}$ is negatively charged (Fig. 20 A and B). These attractive surface charges preliminarily allow both proteins to non-specifically orient to the right position (Fig. 21) (Prudêncio & Ubbink, 2004). A neutrally charged patch, which consist of hydrophobic interaction sites, acts as an entrance and exit for the electrons. It is located where both cofactors are closest (Prudêncio & Ubbink, 2004). Upon complexation 14 % of the solvent accessible surface area of ferredoxin$_{TOL}$ (759 from a total of 5,453 Å^2) and 4.4 % of reductase$_{TOL}$ (769 from a total of 17,522 Å^2) are covered. Ferredoxin$_{TOL}$ contributes around 20 residues and reductase$_{TOL}$ 30 residues to the protein-protein interface. The protein-protein interaction is likely stabilized by one short salt-bridge (R378 - E60), one long salt bridge (R378 - D55) and by hydrogen-bonding of T62 and P79 of ferredoxin$_{TOL}$ and R327, Q329 and Q19 of reductase$_{TOL}$ (Fig. 19). Formation of a salt bridge by R378 of reductase$_{TOL}$ with ferredoxin$_{TOL}$ causes a change of its side-chain conformation and an increased order of the C-terminal helix of reductase$_{TOL}$ around R378 (Fig. 19).

The shortest connection between the two cofactors, more precisely the distance between the histidine-coordinated iron ion of the [2Fe-2S] cluster and the N3 atom of the isoalloxazine ring is 11.7 Å (Fig. 20). The distance is in the range of physiological relevance for a fast electron transfer between the two centers, not exceeding the distance of 14 Å. Above this distance the electron tunneling is drastically decreased (Page *et al*., 1999). Similar distances between the cofactors for electron transfer have been found in BphA4-BphA3 (10 Å) and adrenodoxin reductase-adrenodoxin

(10.3 Å) complexes (Senda *et al.*, 2007; Müller *et al.*, 2001). The conservation of the tryptophan at position 320 between FAD of reductase$_{TOL}$ and [2Fe-2S] cluster of BphA4 (Fig. 10) could facilitate the electron transfer between both cofactors (Senda *et al.*, 2007). P79 (ferredoxin$_{TOL}$) is also conserved (Fig. 12). Two salt-bridges (R378-E60, R378-D55) and hydrogen-bonding of T62 and P80 of ferredoxin$_{TOL}$ with R327, Q329 and Q19 of reductase$_{TOL}$ are found to have a stabilizing effect on the complex. Equivalent amino acids are also found in reductase, respectively, ferredoxin components of biphenyl dioxygenase, naphthalene dioxygenase and carbazole dioxygenase (Senda *et al.*, 2007).

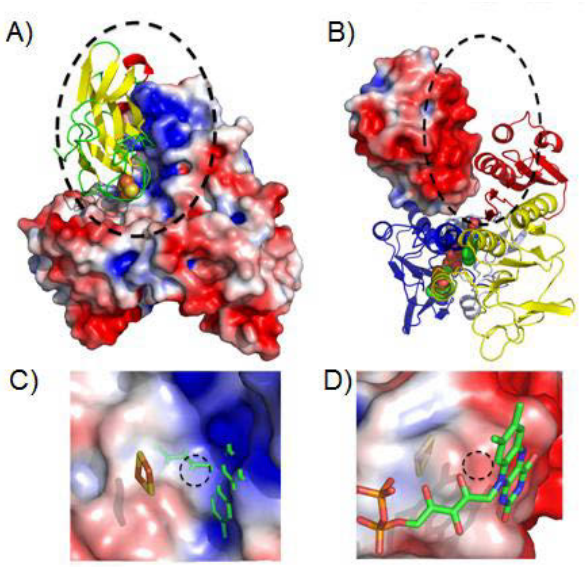

Figure 21. Electrostatic potential mapped on the solvent accessible surface of reductase$_{TOL}$ and ferredoxin$_{TOL}$. (A) shows the electrostatic potential of the solvent accessible surface of reductase$_{TOL}$ and ferredoxin$_{TOL}$ in cartoon presentation, (B) the other way round and (C) gives an enlarged view of the electrostatic potential map at the site of electron-transfer viewed from the [2Fe-2S] cluster in the direction of the isoalloxazine ring of FAD and (D) displayed from the FAD in direction of the [2Fe-2S] cluster. Broken-lined circles indicate where a line connecting the closest atoms between both cofactors would cross the displayed surfaces.

Comparison of the reductase$_{TOL}$ structure with complex structures of NAD$^+$:reductase$_{TOL}^{CT}$ and reductase$_{TOL}$-ferredoxin$_{TOL}$ indicate no large conformational

changes of the domains upon NAD^+ binding and complexation. It can be speculated that the large rotation of the NADH/CT-domain is not essential for binding of ferredoxin$_{TOL}$ as seen with the BphA4. The reductase$_{TOL}$-ferredoxin$_{TOL}$ complex differs from the BphA3-BphA4 complex in the positioning of the Rieske-type [2Fe-2S] cluster of the ferredoxin component. The distance between FAD and the Rieske-type [2Fe-2S] cluster is shifted 6.3 Å relative to the C-terminal domain. The small difference like the one descibed in the protein surfaces and the distance between both cofactors (11.7 Å in reductase$_{TOL}$-ferredoxin$_{TOL}$ complex *vs*. 10 Å in BphA4-BphA3 complex) could explain the specificity of the reductase component for its interacting ferredoxin component.

Table 5. Statistics on diffraction data and structure refinement of reductase$_{TOL}$- ferredoxin$_{TOL}$ complex

Wavelength	0.91841
Space group	$P6_5$
Cell constants (Å)	120.3, 120.3, 60.4
Total / unique refl.	84,338 / 19,644
R_S [a] (%)	15.2 (58.1)
Resolution (Å)	20 – 2.40 (2.40-2.40)
Completeness (%)	99.9 (100)
(I) / (I)	7.9 (2.9)
Model R / R_{free}-factor (%) [b]	16.7 / 22.8
Rms deviation from ideal geometry	
Bonds (Å)	0.004
Angles (°)	0.79

Numbers in brackets denote the values found in the highest resolution shell.

[a] $R_s = \sum_h \sum_i | I_i(h) - \langle I(h) \rangle | / \sum_h \sum_i I_i(h)$; where i are the independent observations of reflection h.

[b] The R_{free} factor was calculated from 5 % of the data, which were removed at random before the refinement was carried out. The R factor has been calculated from the reflections of the working set and test set.

4 Redox potential determination of reductase$_{TOL}$ and ferredoxin$_{TOL}$

Stabilization of FAD and the protein environment as a cause of CT complex formation were discerned. Again these structural changes could result in a change of the redox potential. Therefore the redox potential of reductase$_{TOL}$ and reductase$_{TOL}$ complexed with NAD^+ were determined.

4.1 Redox potential determination of reductase$_{TOL}$ and NAD^+:reductase$_{TOL}^{CT}$

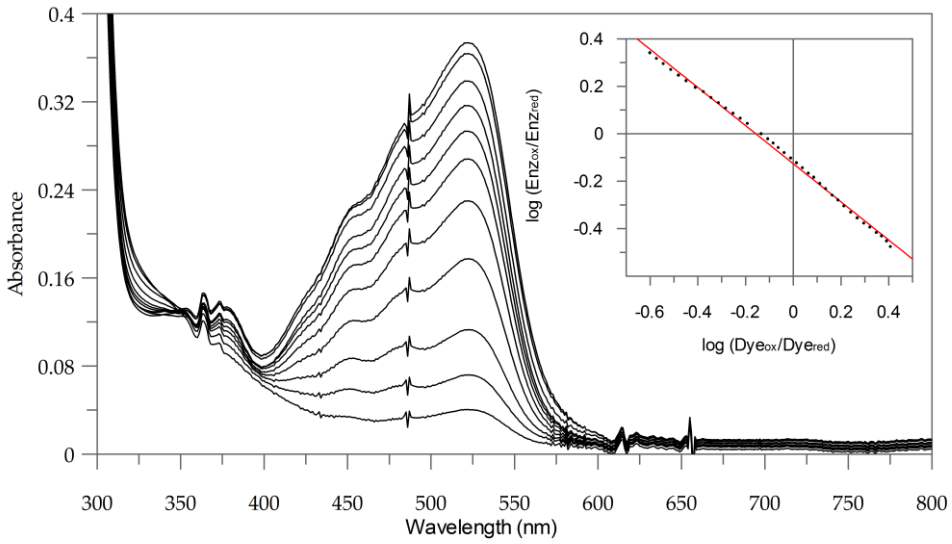

Figure 22. Redox potential measurement of reductase$_{TOL}$. 20 µM of reductase$_{TOL}$ with equal concentration of Safranin T mixed in 50 mM Tris-HCl pH 7.0, 0.15 M NaCl, 1 µM benzyl viologen, 0.05 U xanthine oxidase. Spectra were recorded every 2.5 min. Inset shows the plot log (Enz$_{OX}$/Enz$_{RED}$) *versus* log (Dye$_{OX}$/Dye$_{RED}$). The continuous line displays the linear fit with a slope of around -1. The redox potential was determined as -293 mV.

The measurement of the redox potential of reductase$_{TOL}$ was carried out in the presence of phenosafranine (-252 mV at pH 7; Loach, 1973). The enzyme was reduced much slower than the redox dye. This implies a more negative redox potential of reductase$_{TOL}$ than -252 mV (Fig. 22). The plot log(Enz$_{OX}$/Enz$_{RED}$) *versus* log (Dye$_{OX}$/Dye$_{RED}$) underpins this observation with a slope of ca. -0.5 indicating that

redox dye and enzyme were not equally reduced and that the electron transfer reaction was not at equilibrium (data not shown).

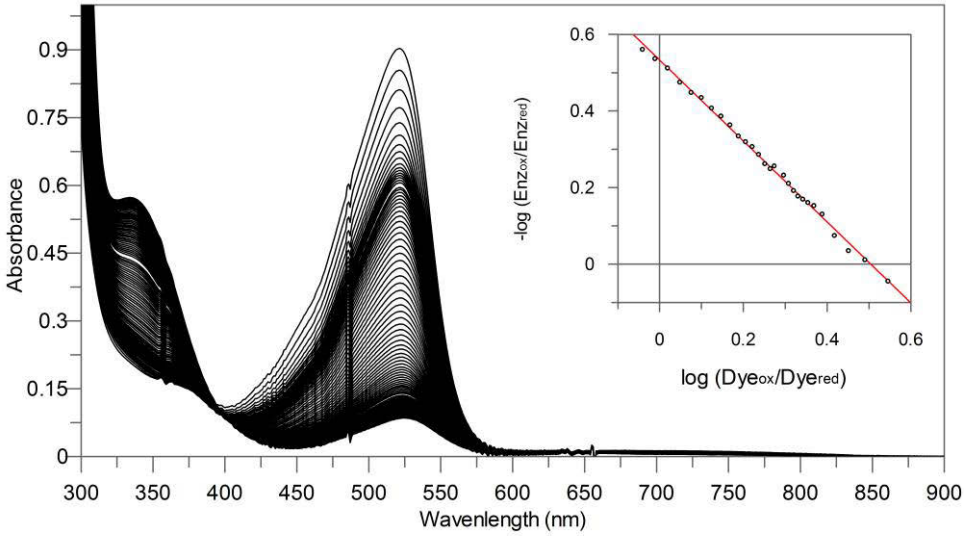

Figure 23. Redox potential measurement of reductase$_{TOL}$ with NAD$^+$. 20 µM of reductase$_{TOL}$ with equal concentration of phenosafranine were in 50 mM Tris-HCl pH 7.0, 0.15 M NaCl, 1 µM benzyl viologen, 1 mM NAD$^+$, 0.05 U xanthine oxidase. Spectra were recorded every 2.5 min. Inset shows the plot log (Enz$_{OX}$/E$_{RED}$) *versus* log (Dye$_{OX}$/Dye$_{RED}$). The continuous line displays the linear fit with a slope of around -1. The redox potential was determined as -233 mV.

Therefore the redox potential of reductase$_{TOL}$ was determined with Safranin T (-289 mV at pH 7; Clark, 1960). Reductase$_{TOL}$ and Safranin T had a similar reduction rate. The redox potential of reductase$_{TOL}$ in the absence of NAD$^+$ was calculated to be -293 mV. The linear regression of the plot log (Enz$_{OX}$/Enz$_{RED}$) against log(Dye$_{OX}$/Dye$_{RED}$) gives a slope of around -1 (Fig. 22, inset) indicating that the electron transfer reaction was at equilibrium.[-]

The redox potential of NAD$^+$:reductase$_{TOL}^{CT}$ was determined with phenosafranine. The reduction of NAD$^+$:reductase$_{TOL}^{CT}$ was minimally slower than that of the redox dye suggesting a value more positive than -252 mV. The interception of the ordinate was applied to the Nernst equation giving a redox potential of -233 mV (Fig. 23). The linear regression of the plot log (Enz$_{OX}$/Enz$_{RED}$) *vs.* log (Dye$_{OX}$/Dye$_{RED}$) gives a slope of

around -1 (Fig. 23, inset). This indicates that enzyme and dye were nearly equally reduced and the reaction was at equilibrium.

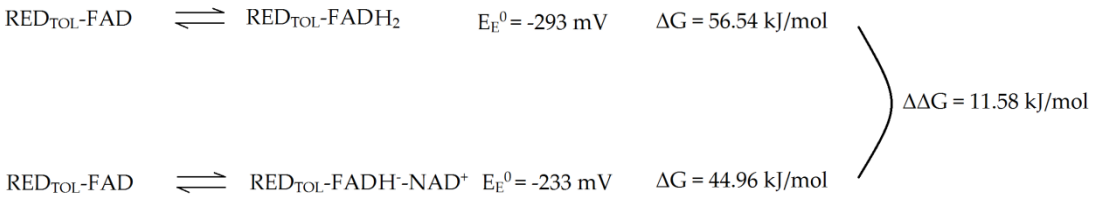

Figure 24. RED$_{TOL}$-FAD stands for the oxidized reductase$_{TOL}$, RED$_{TOL}$-FADH$_2$ is the reduced reductase$_{TOL}$. RED$_{TOL}$-FADH$^-$-NAD$^+$ is the reduced reductase in the presence of NAD$^+$. E_E^0 is the determined redox potential. ΔG is the change of Gibbs free energy calculated with formula $\Delta G = n F E_E^0$ (equation 5).

A difference of redox potential (ΔE^0) of +60 mV on the account of NAD$^+$ binding means a change of Gibbs free energy (ΔΔG) of 11.58 kJ/mol (Fig. 24). This value again means that the electron reaction rate is decreased by about 100-fold (Δk = 106).

The redox potential change might result from the stabilization of the positive charges in the active site and, in turn, of the negative charges of the FAD of NAD$^+$:reductase$_{TOL}^{CT}$ as a consequence of NAD$^+$ binding (Ghisla & Massey, 1989). The amino group of K48 is in hydrogen bond distance to the N5 atom of FAD. This lysine is found to be conserved in many members of the GR family and is believed to affect the redox potential of the protein (Pai & Schulz, 1983). Mutation of the lysine to an arginine in the lipoamide dehydrogenase resulted in an increase of redox potential and influenced the formation of the CT complex (Maede-Yorita *et al.*, 1994). The change of redox potential upon binding of NAD$^+$ can also be found in putidaredoxin reductase (PdR), a protein in the cytochrome P450-dependent monooxygenase system that transfers the electron from NADH to putidaredoxin (-369 ±10 mV at pH 7.0 to -230 ± 10 mV) (Reipa *et al.*, 2007).

4.2 Redox potential determination of ferredoxin$_{TOL}$

The determination of the redox potential of ferredoxin$_{TOL}$ was followed by the reduction of enzyme and redox dye at 325 and 600 nm, respectively. The simultaneous decrease of absorption of ferredoxin$_{TOL}$ spectrum at 325 nm and absorption changes of indigo-disulfonate at 600 nm (-109 mV at pH 7.5; Clark, 1960) indicate that enzyme and redox dye were reduced contemporaneously. The linear regression of the plot log (Enz$_{OX}$/Enz$_{RED}$) against log (Dye$_{OX}$/Dye$_{RED}$) gives a slope of around -1 (Fig. 25, inset). This provides information that enzyme and dye accepted approximately the same number of electrons and the reaction was at equilibrium. The interception of the ordinate is applied to the Nernst equation to give a redox potential (E^0) of -112 mV. The determined redox potential of -112 mV coincides with the previously estimated one of -109 mV (Subramanian *et al.*, 1985).

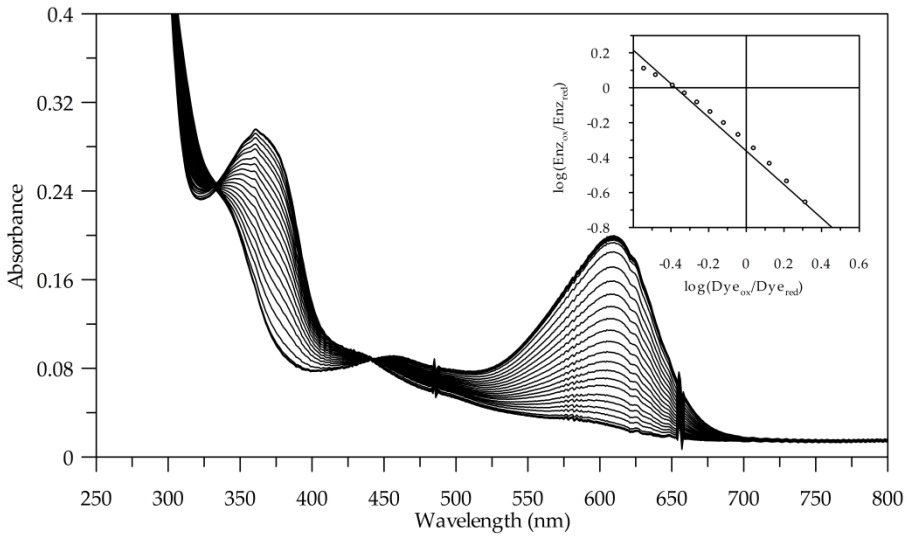

Figure 25. Redox potential measurement of ferredoxin$_{TOL}$. 15 μM of ferredoxin$_{TOL}$ with equal concentration of indigo-disulfonate were in 50 mM Tris-HCl pH 7.5, 0.15 M NaCl, 1 μM benzyl viologen, 0.05 U xanthine oxidase. Spectra were recorded every 3 min. Inset shows the plot log(Enz$_{OX}$/Enz$_{RED}$) *versus* log(Dye$_{OX}$/Dye$_{RED}$). The continuous line displays the linear fit with a slope of -1. The redox potential was -112 mV.

5 Spectroscopic characterization of reductase$_{TOL}$ and ferredoxin$_{TOL}$

The reductase$_{TOL}$ undergoes structural changes when complexed with NAD^+. CT complex formation results in a change of redox potential by +60 mV and leads to a calculated 100-fold decrease of the electron reaction rate. Stopped flow measurements were conducted to analyze whether electron transfer reaction rates between reductase$_{TOL}$ and its electron acceptor are constistent with the results of the structural characterization and determination of the redox potential. Therefore reductase$_{TOL}$ and ferredoxin$_{TOL}$ were first characterized *via* UV/Vis spectroscopy in order to simplify the evaluation of the data obtained in the reductive and oxidative half reaction of reductase$_{TOL}$.

5.1 UV/Vis spectroscopic characterization of reductase$_{TOL}$ and ferredoxin$_{TOL}$

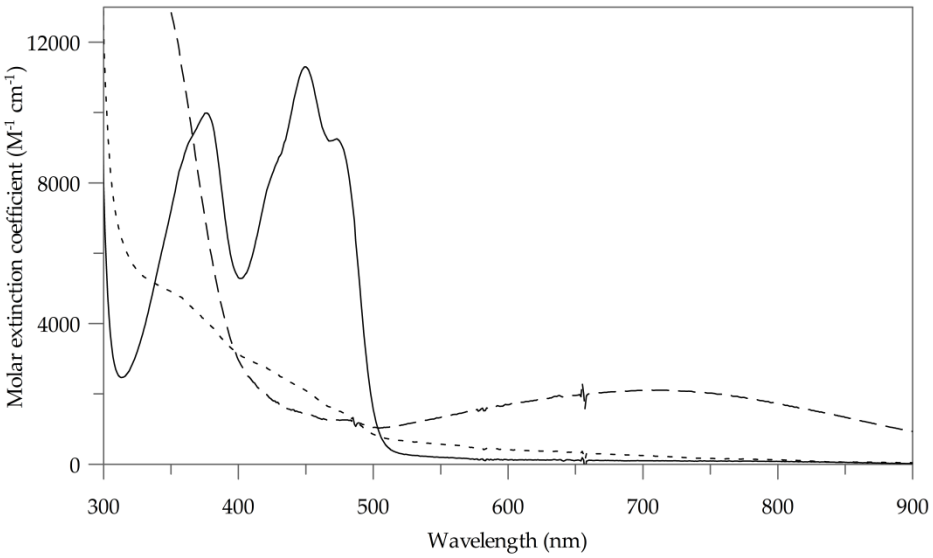

Figure 26. UV/Vis absorption spectra of oxidized and NADH-reduced reductase$_{TOL}$. Reductase$_{TOL}$ was mixed with 50 mM Tris-HCl pH 8.0. The spectrum of the oxidized enzyme is shown in solid, the spectrum of the NADH reduced enzyme is depicted in dashed lines. The DT-reduced reductase$_{TOL}$ is demonstrated in dotted lines.

The UV/Vis absorption spectrum of the oxidized reductase$_{TOL}$ features absorption properties typical for a flavoprotein. It has peak maxima at 377 nm and 450 nm with a shoulder centered at 473 nm (Fig. 26). Titration with an excess of NADH led to the bleaching of the peaks illustrating the complete reduction of FAD (FAD/$FADH_2$). The reduction of the flavin was followed by the appearance of a long wavelength absorption band in the range of 600 to 800 nm (Fig. 26). The long wavelength absorption band is attributed to the formation of a charge transfer (CT) complex between flavin and the pyridine nucleotide (Massey & Palmer, 1962). The involvement of reduced flavin and oxidized nicotinamide in the formation of CT complex was confirmed by experiments of lipoyl dehydrogenase with several NADH and NAD^+ analogues and emphasized by experiments with NADase, which is unable to hydrolyze reduced nicotinamide (Massey & Palmer, 1962). The calculated extinction coefficient of reductase$_{TOL}$ is 11,300 M^{-1} cm^{-1} at 450 nm (Subramanian *et al*., 1981). The calculated molar extinction coefficient of the charge transfer complex is 2,082 M^{-1} cm^{-1} at 690 nm (Fig. 26, dashed lines). Sodium dithionite (DT) reduced reductase$_{TOL}$ exhibited no CT absorption band (Fig. 25, dotted lines) and could only be detected after titration of NAD^+ (Fig. 27).

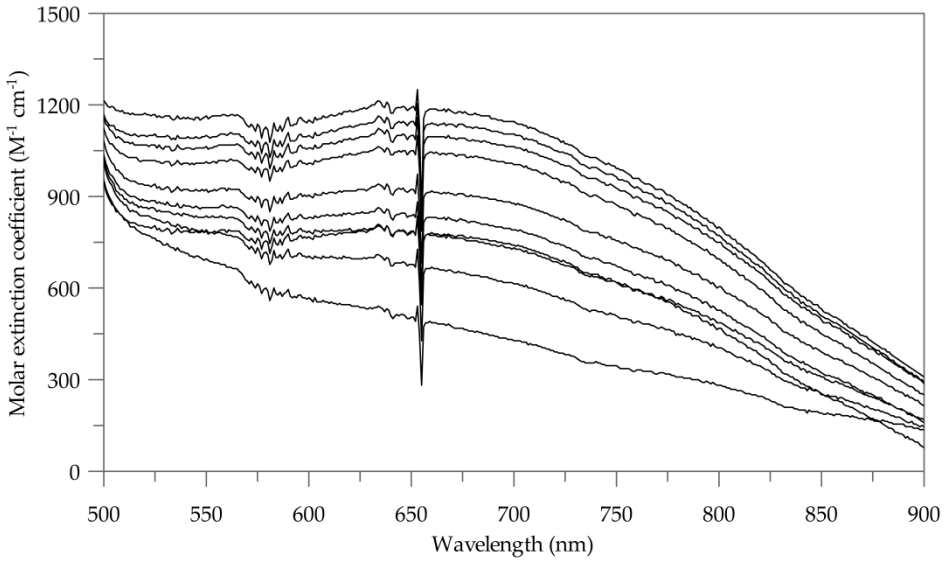

Figure 27. Titration of DT-reduced reductase$_{TOL}$ with NAD$^+$. Reductase$_{TOL}$ was in 50 mM Tris-HCl pH 8.0. DT-reduced reductase$_{TOL}$ was titrated with NAD$^+$ in steps of 2, 4, 8, 12, 16, 21.5, 29.1, 44, 92 and 220 μM final concentration of NAD$^+$.

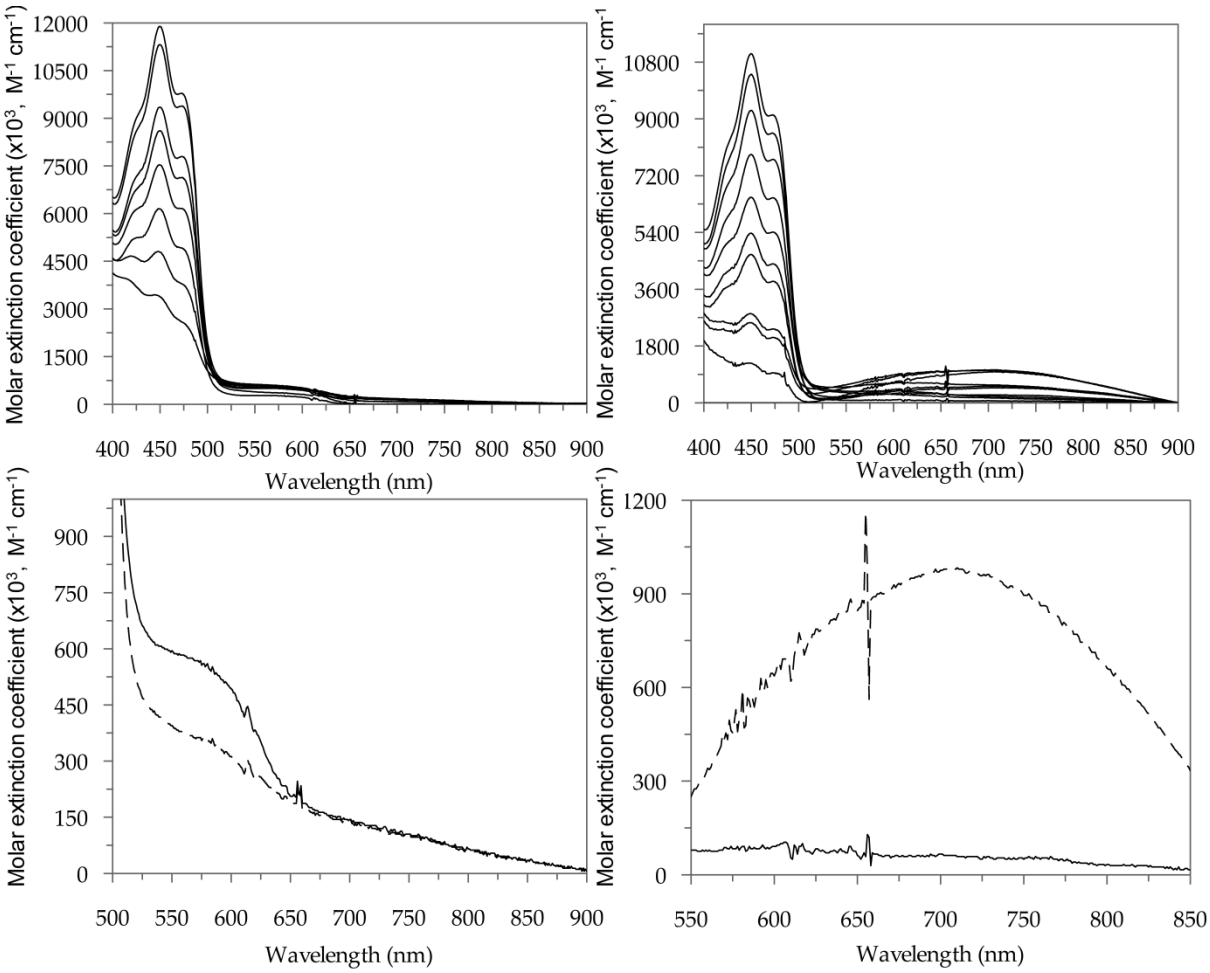

Figure 28. Photoreduction of reductase$_{TOL}$ in the absence and in presence of NAD$^+$. Left side of the figure shows reductase$_{TOL}$ mixed in 50 mM Tris-HCl pH 8.0, 1 mM EDTA as electron source and a catalytic amount of deazaflavin. Lower left figure shows a spectrum directly after (solid line) and after 2 min of illumination (dashed line) in the range of 550 – 850 nm, respectively. Right side of the figure reductase$_{TOL}$ mixed in 50 mM Tris-HCl pH 8.0, 1 mM NAD$^+$, 1 mM EDTA as electron source and a catalytic amount of deazaflavin. Lower right figure shows a spectrum directly after (solid line) and after 20 min of illumination (dashed line) in the range of 550 - 850 nm, respectively.

When reductase$_{TOL}$ was photoreduced in the presence of deazaflavin, the absorption maxima at 377 nm and 450 nm decreased and a corresponding absorption band in

the region of 530 to 630 nm appeared indicating the existence of a neutral semiquinone species (Beinert, 1956) (Fig. 28). The neutral semiquinone formed rapidly and dissociated gradually, just as it has been described in the case of the glucose oxidase (Massey & Palmer, 1966). However, the interpretation of the observation made with reductase$_{TOL}$ is not completely reliable as the formation and decay of the semiquinone could be falsified by slight traces of oxygen in the solution or accidental contact with light. $FADH_2$ would quickly be reoxidized to FAD. FAD and $FADH_2$ in solution could disproportionate to $FADH^{\cdot}$ (Massey & Palmer, 1966). The moderate intensity of the neutral semiquinone absorption band can be explained by the above mentioned factors and could also be dependent on the pH of the solution (pH 8) used in the photoreduction experiment. A solution at pH 8 rather favors the formation of anionic semiquinone (Massey & Palmer, 1966). In the presence of NAD^+, the semiquinone band was not detectable because it was covered by the prominent CT absorbance band (Fig. 28).

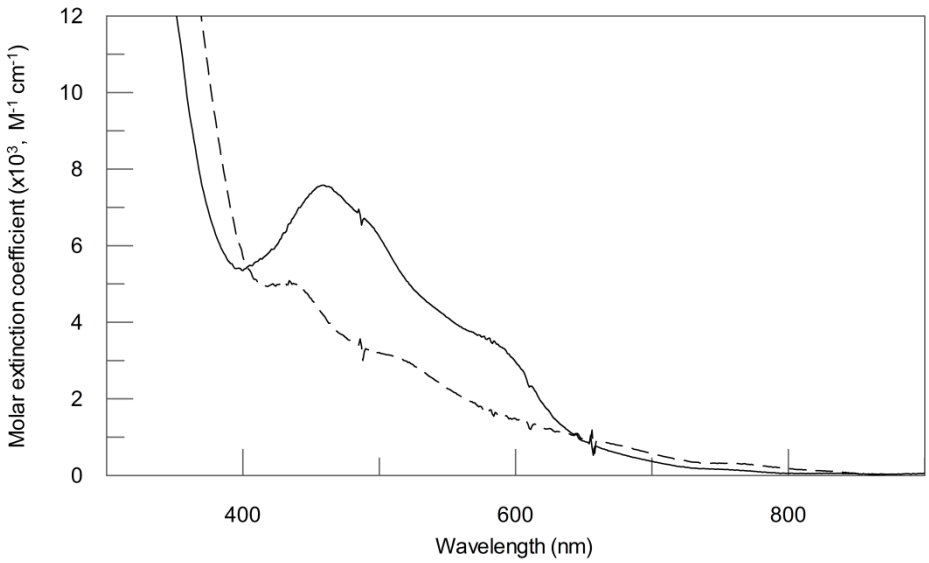

Figure 29. **UV/Vis absorption spectra of oxidized and reduced ferredoxin$_{TOL}$.** Ferredoxin$_{TOL}$ was in 50 mM Tris-HCl pH 7.5 with 400 nM reductase$_{TOL}$ and 67 µM NADH. The oxidized and reduced spectra are shown in solid and dashed lines, respectively.

The absorption spectrum of ferredoxin$_{TOL}$ shows peak maxima at 325 nm and 460 nm and shoulder at circa 575 nm. The spectrum is typical for a Rieske-type [2Fe-2S] cluster protein (Fig. 29) (Ensley *et al.*, 1982). The intensity of absorption maxima lowered, but not completely diminished during the time course of reduction. Rather a shift of maxima was perceivable. The reduced ferredoxin$_{TOL}$ features an additional peak at 438 nm (ε_{438} = 4,930 M^{-1} cm^{-1}) and a shoulder at 505 nm (ε_{505} = 2,980 M^{-1} cm^{-1}). The isosbestic point is at 402 nm (Fig. 29, dashed line). The calculated extinction coefficient is 15,880 M^{-1} cm^{-1} at 325 nm and 7,571 M^{-1} cm^{-1} at 460 nm (Fig. 29, solid line). These results of ferredoxin$_{TOL}$ are comparable to those of Subramanian *et al*. (Subramanian *et al*., 1981).

5.2 Reductive and oxidative half reaction

UV/Vis spectroscopic studies reveal that the reduction of the reductase$_{TOL}$ involves the one-electron reduced neutral semiquinone species and that a charge transfer complex is formed between fully reduced flavin and oxidized nicotinamide. The UV/Vis investigations also show that spectra of reductase$_{TOL}$ and ferredoxin$_{TOL}$ would overlap in spectroscopic interaction experiments making it difficult to attribute any observed spectral changes exclusively to the reductase$_{TOL}$, the CT complex or the ferredoxin$_{TOL}$. Therefore ferricyanide was used as a one electron acceptor in the oxidative half reaction. It does not interfere strongly with the spectrum of reductase$_{TOL}$ at longer wavelengths. Notwithstanding the fact that the reaction with the artificial electron acceptor ferricyanide does not equate to the reoxidation with ferredoxin$_{TOL}$, it can be used to mimic the reaction of reductase$_{TOL}$ with its physiological electron acceptor.

5.2.1 Reductive half reaction

The reductive half reaction of reductase$_{TOL}$ was analyzed according to the model mentioned in material and methods. NADH binds to the reductase with the consequence that a Michaelis complex is formed (FAD::NADH). The FAD of the reductase$_{TOL}$ is then reduced within the complex which results in a charge transfer interaction between flavin and nicotinamide ($FADH^{-}$::NAD^{+}). The dissociation constant (K_D) was calculated to be 41 ±4 μM. A limiting rate constant (k_2) of 152 ±4 μM was observed (Fig. 31). The observed rate constant at 450 (28.2 s^{-1}) and 690 nm (29.1 s^{-1}) are similar suggesting that the reduction of FAD is immediately followed by the formation of CT complex (Fig. 32, left side). Nearly 100 % of the CT intermediate was formed after 40 ms (Fig. 30 and 32).

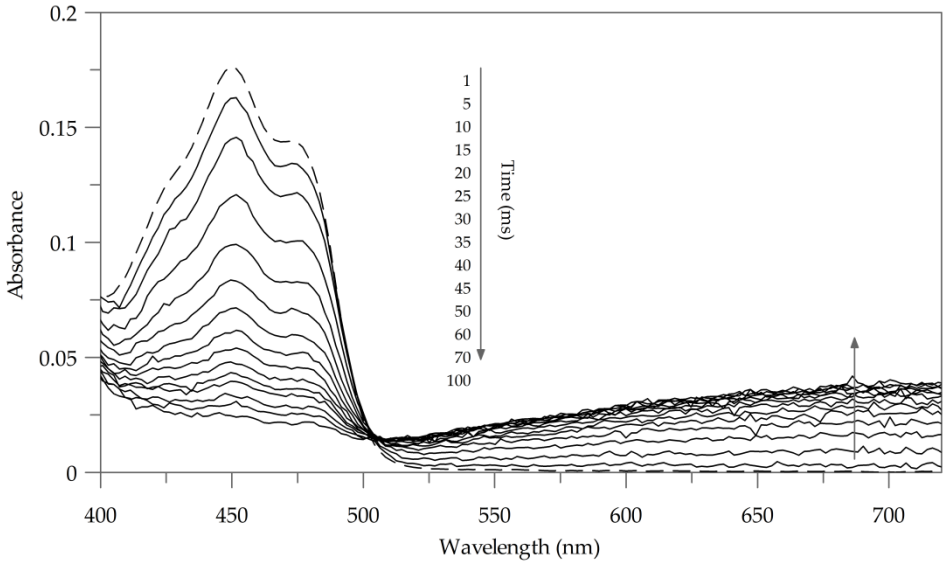

Figure 30. **Reduction of reductase$_{TOL}$ with NADH.** Spectra were recorded after mixing oxidized reductase$_{TOL}$ (15 μM) with NADH (30 μM) in the stopped flow spectrophotometer in 1 ms interval. Only selected spectra are shown. The spectrum of oxidized reductase$_{TOL}$ (dashed line) has been recorded by mixing 15 μM of reductase$_{TOL}$ with 50 mM Tris-HCl pH 7.2, 150 mM NaCl. Arrows indicate the directions of absorption changes and the times in milliseconds after mixing.

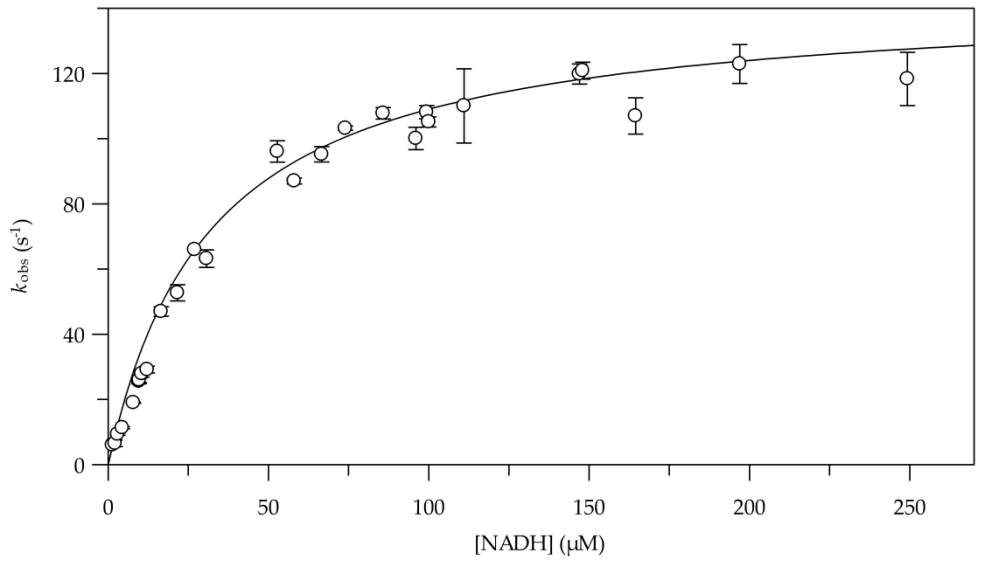

Figure 31. **Reaction traces of reductase$_{TOL}$ with NADH.** The observed hyperbolic relationship between the k_{obs} values and NADH concentrations was fitted assuming that a rapid equilibrium for the binding of enzyme and NADH, followed by a slow reaction.

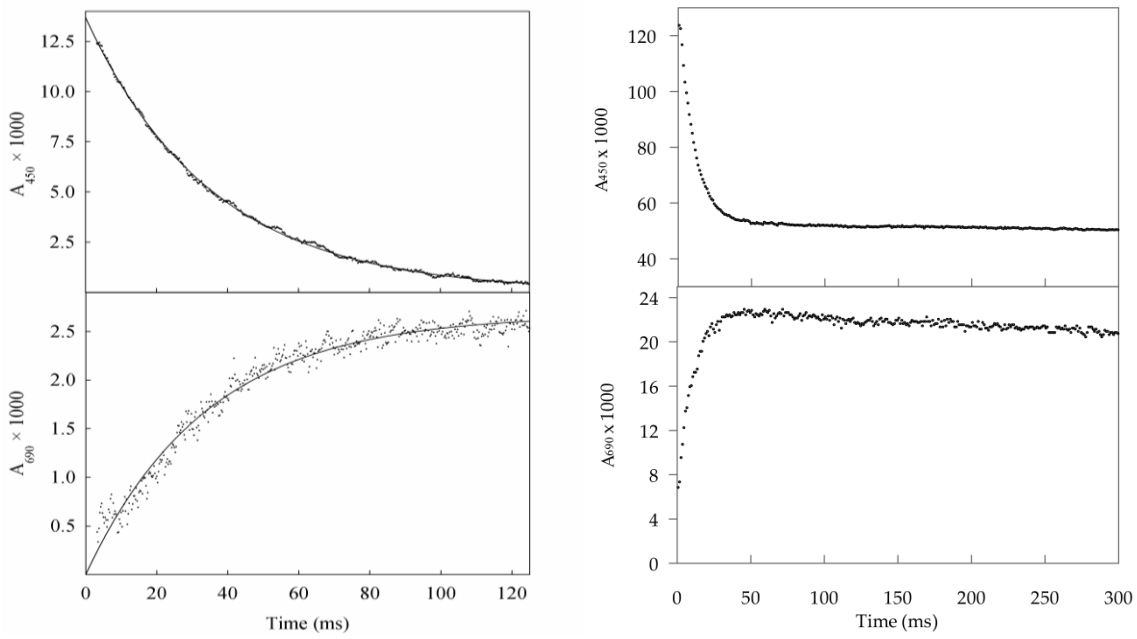

Figure 32. Spectral changes upon the reaction of reductase$_{TOL}$ with NADH at 450 and 690 nm, respectively. Left side of the figure shows 1.2 μM of reductase$_{TOL}$ mixed with 10 μM of NADH in 50 mM MOPS, pH 7.2, 150 mM NaCl. The reaction transients were fitted to a single exponential equation ($A\ (t) = A_{max} \exp(-k_{obs}\ t) + c$), to give the observed rate constants of 28.2 s^{-1} (450 nm) and 29.1 s^{-1}

(690 nm). Right side of the figure shows 7.5 µM of reductase$_{TOL}$ mixed with 15 µM of NADH in 50 mM MOPS, pH 7.2, 150 mM NaCl.

The reductive half reaction fits to the model with the exception that a slow NAD^+ dissociation was discernable after CT complex formation (Fig. 32, right side). The observed NAD^+ dissociation at the end of the reductive half reaction would most likely not appear under physiological condition with an intracellular NAD pool and could be circumvent by adding an excess of NAD^+ according to the LeChatelier's principle (Atkins, 1993).

The reaction of the reductive half reaction can be completed as follows.

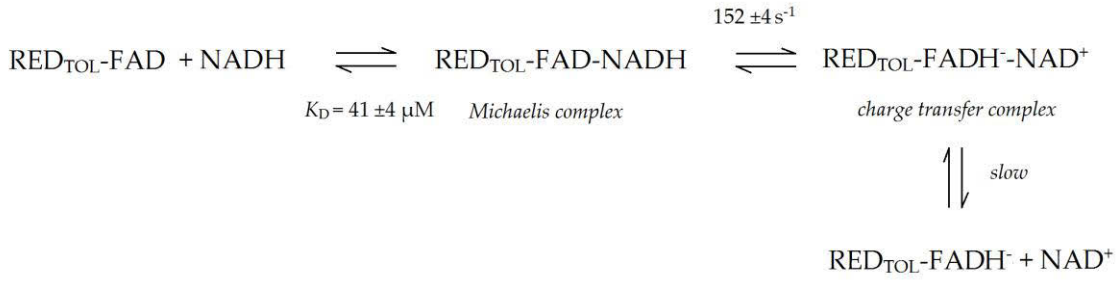

Reaction scheme 1. Reaction scheme of the reductive half reaction. RED$_{TOL}$-FAD describes the reductase in its oxidized state. Redox dependent changes can be found in the change of its prostestic group´s redox state: $FADH^-$ equals the reduced flavin.

5.2.2 Oxidative half reaction

The oxidative half reaction was analyzed under the assumption of the model given in material and methods. Ferricyanide binds to NAD^+:reductase$_{TOL}^{CT}$ and is reduced by the flavin hydroquinone resulting in generation of a neutral semiquinone species. Another molecule of ferricyanide is reduced by the neutral semiquinone leaving a flavin quinone. The reoxidation of the semiquinone is followed by a dissociation of NAD^+. The presumption of the existence of the neutral semiquinone intermediate

was based on the results of the photoreduction experiment of reductase$_{TOL}$ in the absence of NAD^+.

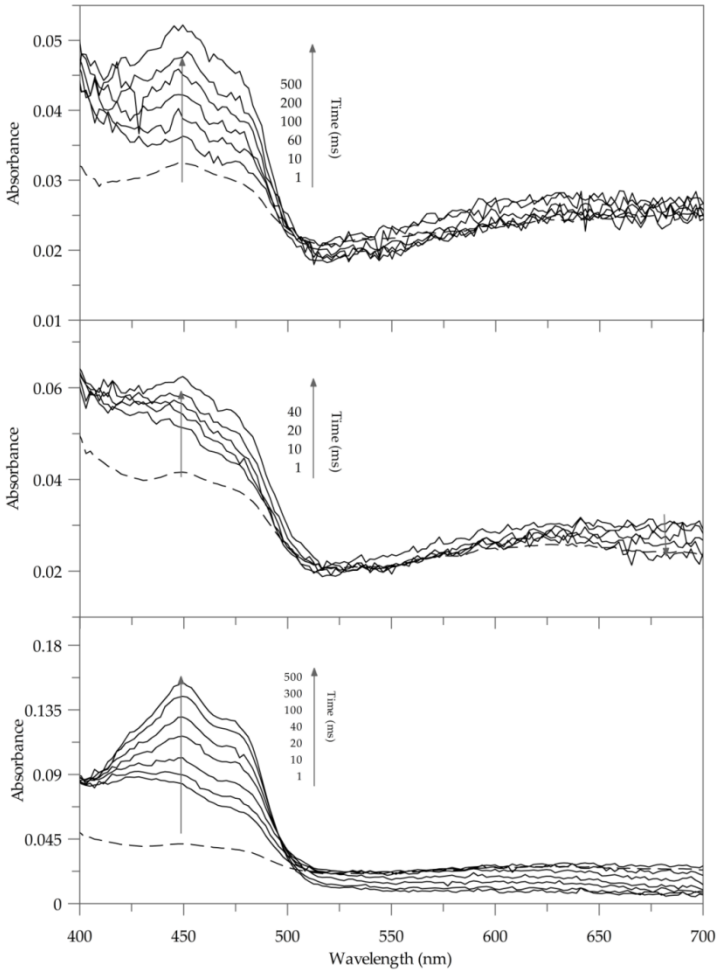

Figure 33. Reoxidation of NAD^+:reductase$_{TOL}^{CT}$ by ferricyanide. Spectra were recorded in 1 ms intervals. Only selected spectra are shown. The spectrum of NADH-reduced reductase$_{TOL}$ (dashed line) mixed buffer without ferricyanide was used as reference. Arrows indicate the directions of absorption changes. The upper figure shows time-dependent spectral changes of NAD^+:reductase$_{TOL}^{CT}$ mixed with sub-stoichiometric amount of ferricyanide (11.5 μM of enzyme, 3.5 μM of ferricyanide). The middle figure demonstrates time-dependent spectral changes of NAD^+:reductase$_{TOL}^{CT}$ mixed stoichiometric amount of ferricyanide (15 μM of enzyme, 15 μM of ferricyanide). Time-dependent spectral changes of reductase$_{TOL}$ mixed over-stoichiometric amount of ferricyanide changes are presented in the lower figure (15 μM of enzyme, 30 μM of ferricyanide).

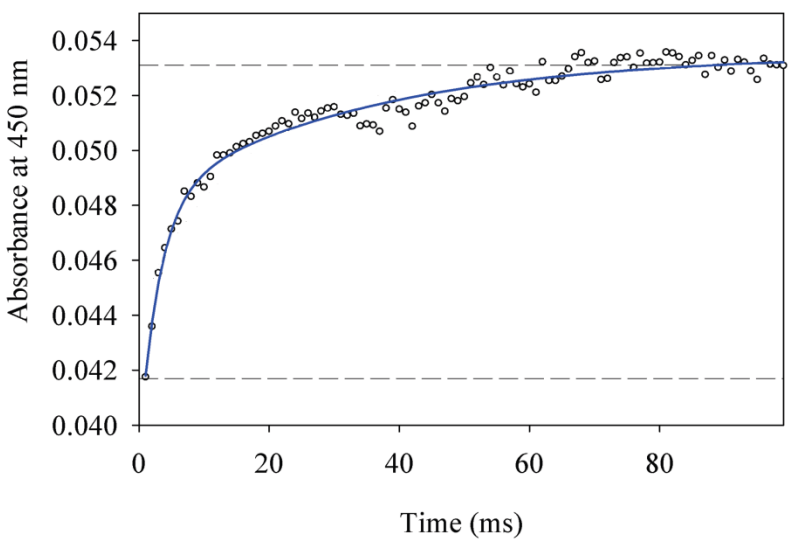

Figure 34. Reaction transients at 450 nm with sub-stoichiometric amount of ferricyanide. NADH-reduced reductase (11.5 μM) was reoxidized with a sub-stoichiometric amount of ferricyanide (3.5 μM). The reaction transients were fitted to a double exponential equation ($A\ (t) = A_{(1)} \exp(-k_{obs(1)}\ t) + A_{(2)}\ \exp(-k_{obs(2)}\ t) + c$), where $A_{(1)}$ and $A_{(2)}$ are amplitudes, $k_{obs(1)}$ and $k_{obs\ (2)}$ the observed rate constant and c the offset. The semiquinone formation of RED_{TOL}-$FADH^{-}$-NAD^{+} measured at 610 nm has a much higher $k_{obs(1)}$ value than the $k_{obs(2)}$ value, representing the decay. The semiquinone formation of RED_{TOL}-$FADH^{-}$ (species 2) has a $k_{obs(1)}$ value of higher than 300 s^{-1} and a $k_{obs(2)}$ value of ca. 30 s^{-1} representing the rate of reoxidation of semiquinone to quinone.

The oxidation of NAD^{+}:$reductase_{TOL}^{CT}$ with sub-stoichiometric amount of ferricyanide indicates a fast FAD reoxidation which is not accompanied by the dissociation of NAD^{+} recognizable by an unchanged CT absorbance band at 690 nm (Fig. 33, upper). A concomitant decrease of the CT absorbance band could be observed with stoichiometric amount of ferricyanide (Fig. 33, middle). This observation was more significant when NAD^{+}:$reductase_{TOL}^{CT}$ was mixed with over-stoichiometric amount of ferricyanide. The dissociation of the CT complex was completed at the end of the reaction (Fig. 33, lower).

The reoxidation of FAD could be divided into a fast step and a comparatively slow step (Fig. 33 lower). The fast reoxidation step is described by the comparison of the first spectrum after mixing to the reference spectrum. The resulting absorption

discontinuity (ΔA) at 450 nm is 0.04. This indicates that 23 % of reductase$_{TOL}$ (of 15 μM enzyme) is reoxidized within the dead time of the instrument. The charge transfer absorbance band remained unchanged. The higher $k_{obs(1)}$ value (formation of semiquinone) than $k_{obs(2)}$ value (formation of quinone) was observed (Fig. 34). The following slow reoxidation step was accompanied by the dissociation of the CT complex (Fig. 33, lower). The decay of the semiquinone was found to be slower than its formation (Fig. 35).

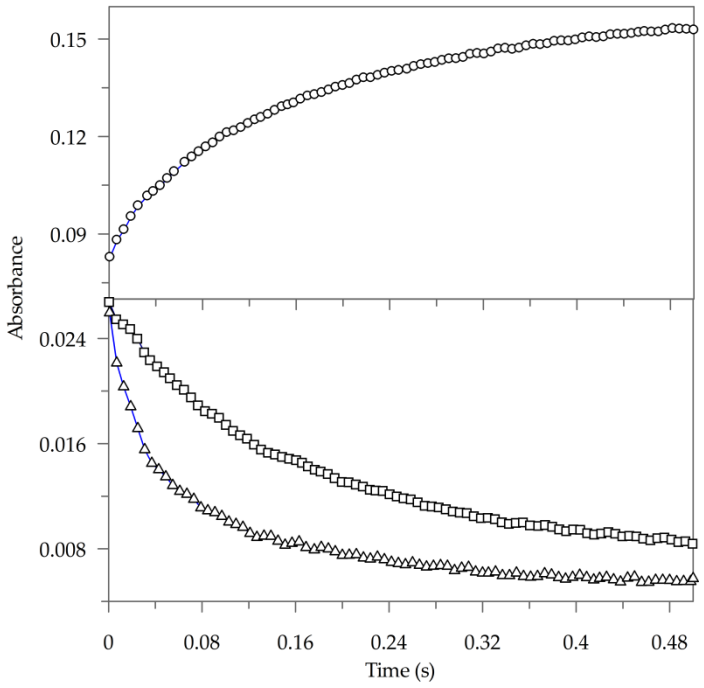

Figure 35. Reaction transients at 450, 610 and 690 nm with an excess of ferricyanide. NADH-reduced reductase (15 μM) was reoxidized with an over-stoichiometric amount of ferricyanide (30 μM). The reaction transients were fitted to a double exponential equation ($A\,(t) = A_{(1)}\ \exp(-k_{obs(1)}\ t) + A_{(2)}\ \exp(-k_{obs(2)}\ t)$ + c), where $A_{(1)}$ and $A_{(2)}$ are amplitudes, $k_{obs(1)}$ and $k_{obs\,(2)}$ the observed rate constant and c the offset. The formation and decay of semiquinone of RED$_{TOL}$-FADH^{-}-NAD^{+} (species 1) was measured at 450 nm. It has a higher $k_{obs(1)}$ value than the $k_{obs(2)}$ value. The dissociation of NAD^{+} has an observed rate constant of ca. 15 s^{-1}. The semiquinone formation of RED$_{TOL}$-FADH^{-} has a $k_{obs(1)}$ value of around 30 s^{-1} and a $k_{obs(2)}$ value of ca. 5 s^{-1} representing the rate of reoxidation of semiquinone to quinone. The change in absorbance at 450 nm (reoxidation of FAD) is shown as circles, at 610 nm (semiquinone oxidation) as triangles and at 690 nm (dissociation of the charge transfer complex) as squares.

The reoxidation of DT-reduced reductase$_{TOL}$ with over-stoichiometric amount of ferricyanide was almost completed within 1 ms and considerably faster than the reoxidation of NADH-reduced reductase$_{TOL}$ (Fig. 36). Experiments with sub-stoichiometric amount of ferricyanide demonstrate a fast formation and slow decomposition of neutral semiquinone (Fig. 37).

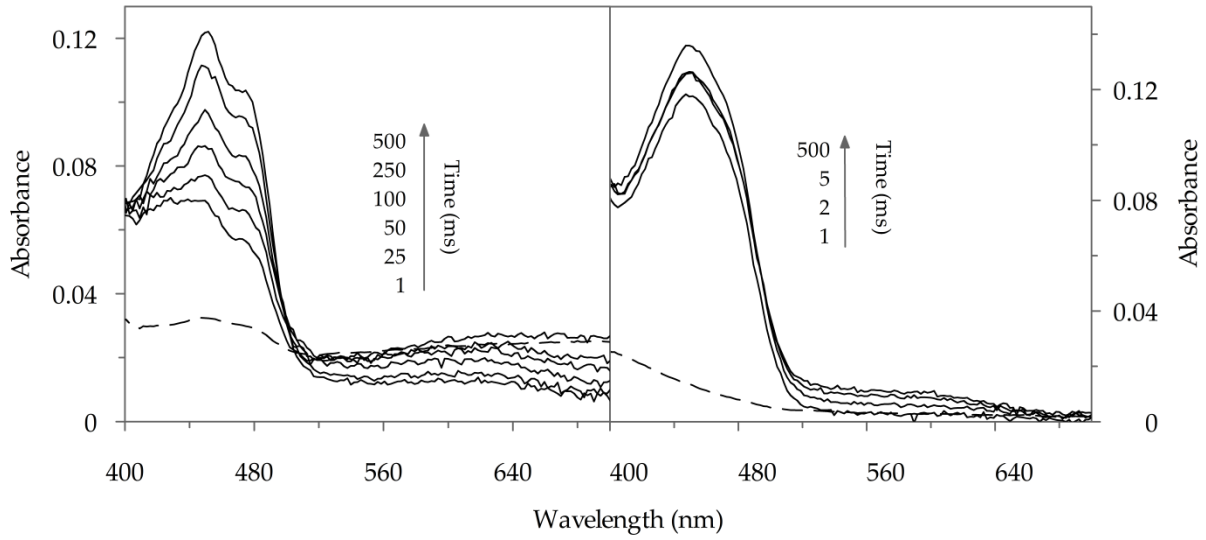

Figure 36. Reoxidation of NADH-reduced and DT-reduced reductase$_{TOL}$ with over-stoichiometric amount of ferricyanide. Time-dependent spectral changes of 11.5 μM NADH-reduced reductase$_{TOL}$ mixed with 40 μM ferricyanide are shown on the left side of the figure and of 14 μM DT-reduced reductase$_{TOL}$ mixed with 45 μM ferricyanide on the right side. Only selected spectra are shown.

The fast and slow reoxidation step noticed with the NADH-reduced reductase$_{TOL}$ can be explained under the assumption that two different species of reduced reductase$_{TOL}$ in solution exist, namely a reduced reductase$_{TOL}$ forming a CT complex with NAD^+ (RED_{TOL}-$FADH^-$-NAD^+, species 1) and a reduced reductase$_{TOL}$ which is not complexed with NAD^+ (RED_{TOL}-$FADH^-$, species 2). The reaction of species 1 with ferricyanide could account for the slow reoxidation step. Species 1 is reoxized by ferricyanide Fe(III) to generate a neutral semiquinone species and reduced ferricyanide Fe(II). Reoxidation of the semiquinone to quinone by another molecule of ferricyanide is

succeeded by the dissociation of NAD^+. This fits to the hypothesized model. The observation of the fast reoxidation could be attributed to the reaction of ferricyanide with species 2. The existence of species 2 is plausible taking the slow NAD^+ dissociation at the end of the reductive half reaction into consideration (Fig. 32). The fast reoxidation resembles the reoxidation of DT-reduced reductase$_{TOL}$ with ferricyanide (Fig. 36 and 37). It can be assumed that the reaction observed with species 2 follows the same reoxidation pattern. It does not exhibit a CT absorbance band (Fig. 36).

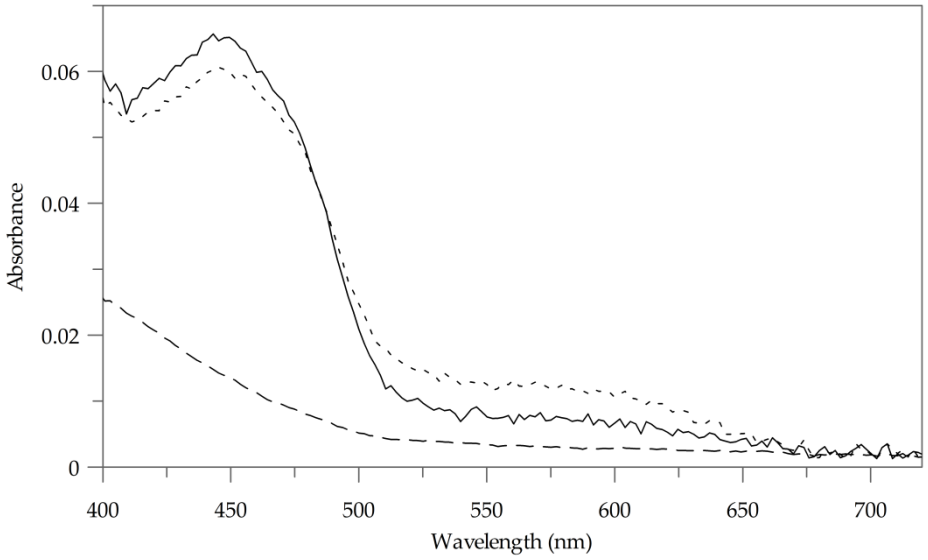

Figure 37. Oxidative half reaction of DT-reduced reductase$_{TOL}$ with sub stoichiometric amount of ferricyanide. Time-dependent spectral changes of 14 µM reductase$_{TOL}$ mixed with 10 µM ferricyanide. Only selected spectra are shown. The spectrum 1 ms after mixing is shown as a dotted line and 4 ms after mixing as a solid line. The spectrum of reduced reductase$_{TOL}$ (dashed line) has been recorded by mixing the enzyme with buffer without ferricyanide.

Experiments of reductase$_{TOL}$ (11.5 µM) mixed with sub stoichiometric amount of ferricyanide (3.5 µM) clarify the attribution of species 2 to the fast reoxidation under the assumption that ferricyanide has a higher affinity to species 2 than to species 1. Derived from the CT absorption band 27 % of reduced reductase$_{TOL}$ is in form of species 2 (3.1 µM). Under the given condition 3.5 µM of ferricyanide can reoxidize

1.75 µM of reductase$_{TOL}$ which leaves no ferricyanide to react with species 1. Consequently, no dissociation of NAD^+ but a slight increase of the semiquinone absorption band is detectable (Fig. 33, upper). The contribution of species 1 to the slow FAD reoxidation could be enlightened by experiments of reductase$_{TOL}$ (15 µM) mixed with stoichiometric amount of ferricyanide (15 µM). 15 µM of ferricyanide can reduce 7.5 µM reductase$_{TOL}$ (Fig. 33, middle). In this experiment 5 µM of enzyme are in the form of RED$_{TOL}$-FADH$^-$ species. 5 µM of RED$_{TOL}$-FADH$^-$ species are reoxidized first with no observable change in CT absorbance leaving 2.5 µM of ferricyanide exclusively to react with species 1. In that case, around 2.5 µM of CT complex should decay. The absorption change at 690 nm (ΔA_{690}) of 0.006 describes a diminishing of CT species of ca. 2.9 µM and underline the proposal that the decay of the CT complex is contributed to the reaction of ferricyanide with species 1 (Fig. 33, middle).

The reaction of ferricyanide with species 2 would not likely occur under physiological conditions. Similar to the notice of the NAD^+ dissociation at the end of the reductive half reaction the generation of species 2 could be prevented by the supplementation of additional NAD^+. Based on the findings in the oxidative half reaction the reaction cycle of reductase$_{TOL}$ can be completed (reaction scheme 2).

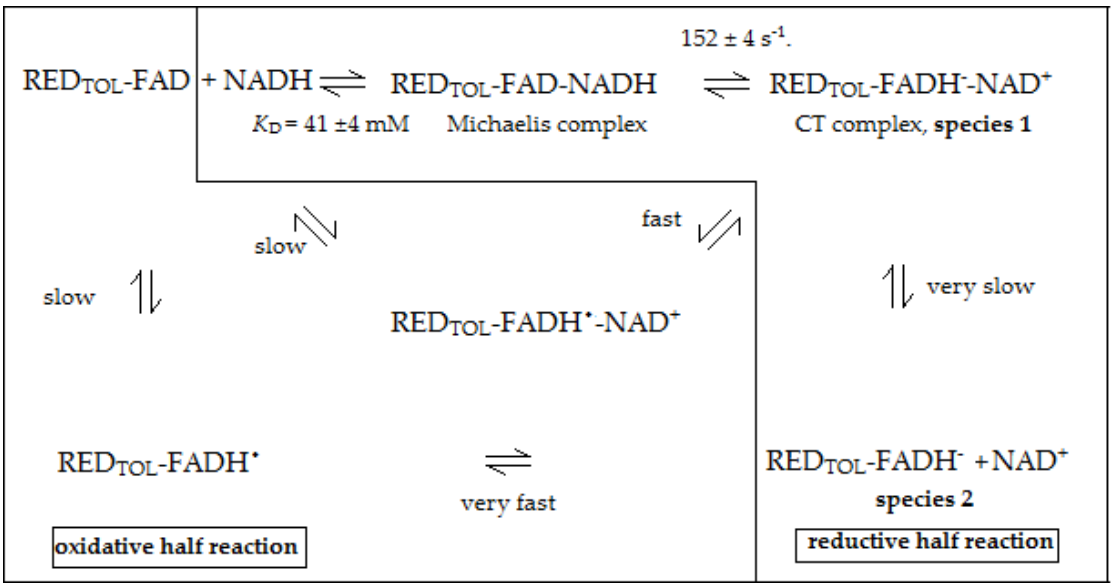

Reaction scheme 2. Reaction scheme of the reductive and oxidative half reaction of reductase$_{TOL}$.

The comparison of the transient kinetics investigations of DT-reduced reductase$_{TOL}$ to NAD$^+$:reductase$_{TOL}$ exemplifies that the rate of the electron transfer reaction is governed by the CT complex. This conclusion is supported by the experiment, at which the DT-reduced reductase$_{TOL}$ and NAD$^+$:reductase$_{TOL}^{CT}$ were each mixed with oxygen-saturated buffer to demonstrate that the reoxidation of NAD$^+$:reductase$_{TOL}^{CT}$ by oxygen was circa 100-fold slower than the reoxidation of DT-reduced reductase$_{TOL}$ (Fig. 38). This corresponds to the *circa* 100 times calculated decrease of the electron transfer rate upon NAD$^+$ binding (Δk = 106).

The results of this section are explainable by the results found in the structural characterization and determination of the redox potential and add weight to the supposition that the CT complex has a protective role in catalysis in so far as its presence minimizes the probability to waste reducing equivalents.

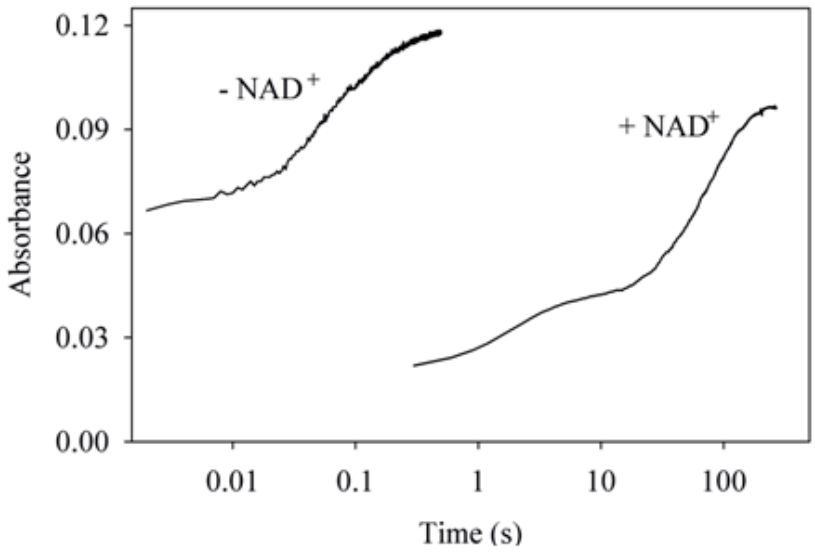

Figure 38. Time-dependent change in absorption at 450 nm. Reduced reductase$_{TOL}$ was mixed (1:1) with an air-saturated solution. The trace labeled -NAD$^+$ shows the reoxidation of DT-reduced reductase$_{TOL}$, while +NAD$^+$ indicates the recorded trace for NADH-reduced reductase$_{TOL}$, where the NAD$^+$:reductase$_{TOL}^{CT}$ is found in solution.

SUMMARY

The toluene dioxygenase from *Pseudomonas putida* F1 is a three-component Rieske non-heme iron dioxygenase comprising of a reductase, ferredoxin and an oxygenase component. It catalyzes the initial step in the aerobic degradation of the aromatic hydrocarbon toluene, the conversion of toluene to *cis*-toluene dihydrodiol by the incorporation of two hydroxyl groups from molecular oxygen into the aromatic nucleus. A smooth interaction between all three components needs to be ensured to efficiently transfer the electrons derived from NADH oxidation to the terminal oxygenase component where molecular oxygen is activated and used for the hydroxylation of the aromatic hydrocarbon.

Based on the results of the kinetic studies of the reductive half reaction of reductase NADH rapidly reduces the reductase, resulting in the formation of a stable charge transfer complex between NAD^+ and $FADH^-$. Oxidation of the charge transfer complex by an electron acceptor proceeds *via* the neutral semiquinone to the quinone state of FAD. It is shown that the charge transfer complex affects the oxidation of $FADH^-$ and suppresses the reaction of the reductase with dioxygen. An explanation for this change in reactivity can be deduced from the structure of the charge transfer complex. The crystal structure of the charge transfer complex reveals that its slower reaction with dioxygen results from a) NAD^+ lying coplanar above the *Re*-face of the FAD shielding the reactive N5-C4a locus of the FAD, the site where oxygen attacks the flavin, b) the planarity of the isoalloxazine ring forced by a π-π donor-acceptor interaction in the charge transfer complex.

The increased redox potential of the FAD/$FADH^-$ couple in the charge transfer complex, which is shifted to a 60 mV more positive value in comparison with the reductase without charge transfer complex also explains the slower reaction with dioxygen.

The formation of the reductase-ferredoxin complex allows efficient electron transfer from reductase to ferredoxin because a) the oppositely charged interacting surfaces

of both proteins facilitate the pre-orientation of the ferredoxin on the reductase, b) a hydrophobic region surrounding the two redox centers in the complex acts as an exit/entrance port for electrons and c) the short edge-to-edge distance between both cofactors of 11.7 Å guarantees a fast electron transfer.

The results of this thesis demonstrate that the electron transfer between reductase and ferredoxin is governed by the formation of a stable charge transfer and of a reductase-ferredoxin complex with which the problem of an unwanted side reaction with dioxygen is obviated.

ZUSAMMENFASSUNG

Die Toluol-Dioxygenase von *Pseudomonas putida* F1 gehört zur Familie der Rieske-Dioxygenasen und katalysiert den ersten Schritt im aeroben Abbau des aromatischen Kohlenwasserstoffes Toluol. Sie besteht aus Reduktase-, Ferredoxin- und Oxygenase-Komponente und katalysiert die Umwandlung von Toluol zum *cis*-Toluol-Dihydrodiol, indem sie zwei Hydroxylgruppen in den aromatischen Kern einbaut. Ein effizienter Elektronentransfer zur terminalen Oxygenase-Komponente - an der die Sauerstoffaktivierung und Umwandlung des aromatischen Kohlenwasserstoffs stattfindet - setzt eine reibungslose Interaktion aller Komponenten miteinander voraus.

Die Ergebnisse der Stopped-flow-Messungen in der reduktiven Halbreaktion zeigen, dass NADH die Reduktase mittels Hydridtransfer reduziert, wodurch ein stabiler Ladungstransfer-Komplex zwischen NAD^+ und $FADH^-$ entsteht. In der oxidativen Halbreaktion wird dieser dann durch einen Elektronenakzeptor über das blaue Semichinon zum Chinon oxidiert. Dabei zeigt sich, dass der Ladungstransfer-Komplex Einfluss auf die Flavin-Oxidation hat und die Reaktion der Reduktase mit Sauerstoff unterdrückt. Eine Erklärung hierfür liefert die Kristallstruktur des Ladungstransfer-Komplexes. Aus ihr ist ersichtlich, dass die Reaktion mit Sauerstoff dadurch unterdrückt wird, dass a) das NAD^+ koplanar mit dem Isoalloxazinring ist und dabei den reaktiven N5-C4a Teil des FADs schützt, der Teil des Flavins der mit molekularem Sauerstoff reagiert, und dadurch, dass b) das NAD^+-Molekül den Isoalloxazinring in eine planare, weniger sauerstoffempfindliche Konformation zwängt.

Aus der Bildung des Ladungstransfer-Komplexes resultiert ein um 60 mV erhöhtes Redoxpotential des FAD/$FADH^-$-Überganges im Vergleich zur Reduktase ohne Ladungstransferkomplex, welches ebenso die verlangsamte Reaktion der Reduktase mit molekularem Sauerstoff erklärt.

Durch die Bildung des Reduktase-Ferredoxin-Komplexes wird ein effizienter

Elektronentransfer folgendermaßen ermöglicht: a) das Ferredoxin bindet an die Reduktase aufgrund elektrostatischer Anziehung entgegengesetzter Oberflächenladungen beider Proteine, b) die hydrophobe Region, die die beiden Redoxzentren umgibt, fungiert als Ein- und Ausgang für Elektronen und c) die geringe Entfernung von 11.7 Å zwischen beiden Kofaktoren erlaubt einen schnellen Elektronentransfer.

Die Ergebnisse dieser Arbeit zeigen, dass der Elektronentransfer zwischen Reduktase und Ferredoxin durch die Bildung eines stabilen Ladungstransfer- und Reduktase-Ferredoxin-Komplexes beeinflusst wird und dadurch das Problem einer ungewollten Reaktion mit molekularem Sauerstoff umgangen wird.

REFERENCES

Adams P.D., Afonine P.V., Bunkóczi G., Chen V.B., Davis I.W., Echols N., Headd J.J., Hung L.W., Kapral G.J., Grosse-Kunstleve R.W., McCoy A.J., Moriarty N.W., Oeffner R., Read R.J., Richardson D.C., Richardson J.S., Terwilliger T.C., Zwart P.H. (2010). PHENIX: a comprehensive Python-based system for macromolecular structure solution. *Acta Crystallogr D Biol Crystallogr*. **66**, 213-221.

Aliverti A., Curti B., Vanoni M.A. (1999). Identifying and Quantitating FAD and FMN in Simple and in Iron-Sulfur-Containing Flavoproteins. *Methods in Molecular Biology: Flavoprotein Protocols* **131,** 9-23.

Atkins P.W., The Elements of Physical Chemistry, 3rd Edition, *Oxford University Press* (1993), 114.

Axcell B.C., Geary P.J. (1975). Purification and some properties of a soluble benzene-oxidizing system from a strain of Pseudomonas. *Biochem J*. **146**, 173-183.

Batie C.J., Ballou D.P., Correll C.J. (1991). Phthalate dioxygenase reductase and related flavin-iron-sulfur containing electron transferases. *Chemistry and Biochemistry of Flavoenzymes*, 544-554.

Beil S., Mason J.R., Timmis K.N., Pieper D.H. (1998), Identification of chlorobenzene dioxygenase sequence elements involved in dechlorination of 1,2,4,5 tetrachlorobenzene. *J Bacteriol*. **180**, 5520-5528.

Benen J.A. , Van Berkel W.J., Van Dongen W.M. , Müller F., De Kok A. (1989).

Molecular cloning and sequence determination of the *lpd* gene encoding lipoamide dehydrogenase from *Pseudomonas fluorescens*. *J Gen Microbiol*. **135**, 1787-1797.

Bradford M.M. (1976). A Rapid and Sensitive Method for the Quantitation of microgram quantities of protein utilizing the principle of protein-dye binding. *Analytical Biochemistry* **72**, 248-254.

Brown E.N., Friemann R., Karlsson A., Parales, J.V., Couture, M.M., Eltis L.D., Ramaswamy, S. (2008). Determining Rieske cluster reduction potentials. *J.Biol.Inorg.Chem*. **13**, 1301–1313.

Cammack R., Gay E., Shergill J.K. (1999). Studies of hyperfine interactions in [2Fe–2S] proteins by EPR and double resonance spectroscopy. *Coordin. Chem. Rev.* **192** 1003-1022.

Cerniglia C.E. (1992). Biodegradation of polycyclic aromatic hydrocarbons. *Biodegradation* **3**, 351-368.

Chen W., Kuo T. (1993). A simple and rapid method for the preparation of gram-negative bacterial genomic DNA. *Nucleic Acids Research* **21**, 2260.

Chenna R., Sugawara H., Koike T., Lopez R., Gibson T.J., Higgins D.G., Thompson J.D. (2003). Multiple sequence alignment with the Clustal series of programs. *Nucleic Acids Res.* **31**, 3497-3500.

Clark, W. M. (1960) Oxidation-Reduction Potentials of Organic Systems (Williams and Wilkins, Baltimore, Md.).

Cline J.F., Hoffman B.M., Mims W.B., LaHaie E., Ballou D.P., Fee J.A. (1985). Evidence for N coordination to Fe in the [2Fe-2S] clusters of Thermus Rieske protein and phthalate dioxygenase from *Pseudomonas*. *J Biol Chem.* **260,** 3251 - 3254.

Colbert C.L., Couture M.M., Eltis L.D., Bolin J.T. (2000). A cluster exposed: structure of the Rieske ferredoxin from biphenyl dioxygenase and the redox properties of Rieske Fe-S proteins. *Structure* **8**, 1267-1278.

Cosper N.J., Eby D.M., Kounosu A., Kurosawa N., Neidle E.L., Kurtz D.M. Jr., Iwasaki T., Scott R.A. (2002). Redox-dependent structural changes in archaeal and bacterial Rieske-type [2Fe-2S] clusters. *Protein Sci.* **12**, 2969-2973.

DeLano W.L. (2002). The PyMol Molecular Graphics System. In ed^eds. DeLano Scientific, San Carlos, CA, USA.

Edwards A. (2006). General properties of flavins. *Flavins: Photochemistry and Photobiology* **6**, 1-11.

Emsley P., Cowtan K. (1987). Coot: model-building tools for molecular graphics. *Acta Crystallogr D Biol Crystallogr*. **60**, 2126-2132.

Ensley B.D., Gibson, D.T. (1983). Naphthalene dioxygenase: purification and properties of a terminal oxygenase component. *J. Bacteriol*. **155**, 505-511.

Entsch B., Ballou D.P., Massey V. (1976). Flavin–oxygen derivatives involved in hydroxylation by p-hydroxybenzoate hydroxylases. *J. Biol. Chem.* **251,** 2550-2563.

Entsch B., Van Berkel W.J.H. (1995)- Structure and mechanism of p-hydroxybenzoate hydroxylases. *FASEB J.* **9**, 476–483.

Ferraro D.J., Gakhar L., Ramaswamy S. (2005). Rieske business: structure-function of Rieske non-heme oxygenases. *Biochem Biophys Res Commun.* **338**, 175-190.

Fish, W.W. (1988). Rapid colorimetric micromethod for the quantitation of complexed iron in biological samples. *Methods Enzymol.* **158,** 357-364.

Fraaije M.W., Mattevi A. (2000). Flavoenzymes: diverse catalysts with recurrent features. *Trends Biochem. Sci.* **25**, 126-132.

Friemann R., Ivkovic-Jensen M.M., Lessner D.J., Yu C.L., Gibson D.T., Parales R.E., Eklund H., Ramaswamy S. (2005). Structural insight into the dioxygenation of nitroarene compounds: the crystal structure of nitrobenzene dioxygenase. *J Mol Biol.* **348**, 1139-1151.

Friemann R., Lee K., Brown E.N., Gibson D.T., Eklund H., Ramaswamy S. (2009). Structures of the multi-component Rieske non-heme iron toluene 2,3-dioxygenase enzyme system. *Acta Crystallogr D Biol Crystallogr.* **65**, 24-33.

Fritsche W., Hofrichter M. (1999). Aerobic degradation by microorganisms. *Biotechnology* **11b**, 145-167.

Furusawa Y., Nagarajan V., Tanokura M., Masai E., Fukuda M., Senda T. (2004). Crystal structure of the terminal oxygenase component of biphenyl dioxygenase derived from *Rhodococcus sp.* strain RHA1. *J Mol Biol* **342**, 1041-1052.

Ghisla S., Massey V. (1989). Mechanisms of flavoprotein-catalyzed reactions. *Eur. J. Biochem.* **181**, 1–17.

Gibson, D. T., Koch J.R., Kallio, R.E. (1968). Oxidative degradation of aromatic hydrocarbons by microorganisms I. Enzymatic formation of catechol from benzene. *Biochemistry* **7**, 2653-2661.

Gibson D.T., Hensley M., Yoshioka H., Mabry T.J. (1970). Formation of (+)-*cis*-2,3-dihydroxy-1-methylcyclohexa-4,6-diene from toluene by *Pseudomonas putida*. *Biochemistry* **9**, 1626-1630.

Gibson D.T., Parales R.E. (2000). Aromatic hydrocarbon dioxygenases in environmental biotechnology. *Curr Opin Biotechnol*. **3**, 236-243.

Haigler B.E., Gibson D.T. (1990). Purification and properties of ferredoxin$_{NAP}$, a component of naphthalene dioxygenase from *Pseudomonas sp*. strain. *J. Bacteriol*. **172**, 465-468.

Hanukoglu I., Gutfinger T. (1989). cDNA Sequence of adrenodoxin reductase-identification of NADP binding sites in oxidoreductases. *Eur. J. Biochem* **180**, 479-484.

Harayama S., Timmis K.N. (1992). Aerobic biodegradation of aromatic hydrocarbons by bacteria. In: Sigel H, Sigel A (eds) *Metal ions in biological systems. Marcel Dekker, New York*, **28**, 99-156.

Heelis P.F. (1982). The photophysical and photochemical properties of flavins (isoalloxazines). *Chem. Soc. Rev*. **11**, 15–39.

Hegg E.L., Que L. Jr.. (1997). The 2-His-1-carboxylate facial triad - an emerging structural motif in mononuclear non-heme iron(II) enzymes. *Eur J Biochem*. **250**, 625-629.

Jerina D.M., Daly J.W., Jeffrey A.M., Gibson D.T. (1971). *Cis*-1,2-dihydroxy-1,2-dihydronaphthalene: a bacterial metabolite from naphthalene. *Arch Biochem Biophys* **142**, 394-396.

Jiang H., Parales R.E., Lynch N.A., Gibson D.T. (1996). Site-directed mutagenesis of conserved amino acids in the alpha subunit of toluene dioxygenase: potential mononuclear non-heme iron coordination sites. *J Bacteriol*. **178**, 3133 – 3139.

Jiang H., Parales R.E., Gibson D.T. (1999). The alpha subunit of toluene dioxygenase from *Pseudomonas putida* F1 can accept electrons from reduced ferredoxin$_{TOL}$ but is catalytically inactive in the absence of the beta subunit. *Appl Environ Microbiol.* **65**, 315-318.

Karlsson A., Beharry Z.M., Matthew Eby D., Coulter E.D., Neidle E.L., Kurtz D.M. Jr., Eklund H., Ramaswamy S. (2002). X-ray crystal structure of benzoate 1,2 dioxygenase reductase from *Acinetobacter sp.* strain ADP1. *J Mol Biol* **318**, 261-272.

Karplus P.A., Schulz G.E. (1987). Refined structure of glutathione reductase at 1.54 Å resolution. *J Mol Biol* **195**, 701-729.

Kauppi B., Lee K., Carredano E., Parales R.E., Gibson D.T., Eklund H., Ramaswamy S. (1998). Structure of an aromatic-ring-hydroxylating dioxygenase - naphthalene 1,2-dioxygenase. *Structure* **6**, 571-586.

Kemal C., Chan T.W., Bruice R.C. (1977). Reaction of $^3O_2$ with dihydroflavins. 1. N3,5-dimethyl-1,5-dihydrolumiflavin and 1,5-dihydroisoalloxazines. *J Am Chem Soc*. **99**, 7272-7286.

Kim J.J.P., Wang M., Paschke R. (1993). Crystal structures of medium-chain acyl-CoA dehydrogenase from pig liver mitochondria with and without substrate. *Proc. Natl. Acad. Sci. U. S. A*. **90**, 7523-7527.

Kuila D., Fee J.A. (1986). Evidence for a redox-linked ionizable group associated with the [2Fe-2S] cluster of Thermus Rieske protein. *J Biol Chem.* **261**, 2768-2771.

Kurowski B., Ludwig B. (1987). The genes of the *Paracoccus denitrificans* bc1 complex. Nucleotide sequence and homologies between bacterial and mitochondrial subunits. *J. Biol. Chem.* **262**, 13805–13811.

Leatherbarrow R.J. (2001). *GraFit Version 5*, Horley, U.K.

Lee, K., Friemann, R., Parales, J. V., Gibson, D. T. & Ramaswamy, S. (2005). Purification, crystallization and preliminary X-ray diffraction studies of the three components of the toluene 2,3-dioxygenase enzyme system. *Acta Crystallogr Sect F Struct Biol Cryst Commun* **61**, 669-672.

Loach, P. A. (1973) Oxidation-reduction potentials: Absorbance bands and molar absorbance of compounds used in biochemical studies. In Handbook of Biochemistry Selected Data for Molecular Biology (Sorber, H. A., Ed.) pp J33-J40, CRC Press, Cleveland, OH.

Lockridge O., Massey V., Sullivan P.A. (1972). Mechanism of the flavoenzyme

lactate oxidase, *J. Biol. Chem*. **247**, 8097-8106.

Macheroux P. (1999). UV-visible spectroscopy as a tool to study flavoproteins. *Methods in Molecular Biology: Flavoprotein Protocols* **131**, 1-8.

Maeda-Yorita K., Russell G.C., Guest J.R., Massey V., Williams C.H. Jr. (1994). Modulation of the oxidation-reduction potential of the flavin in lipoamide dehydrogenase from *Escherichia coli* by alteration of a nearby charged residue, K53R. *Biochemistry*. **33**, 6213-6220.

Malmström B.G. (1982). Enzymology of oxygen. *Annu Rev Biochem*. **51**, 21-59.

Mason, J.R. (1988). Oxygenase catalyzed hydroxylation of aromatic compounds: simple chemistry by complex enzymes. *Int. Ind. Biotechnol*. **8**, 19-24.

Mason J.R., Cammack R. (1992). The electron-transport proteins of hydroxylating bacterial dioxygenases. *Annu Rev Microbiol.* **46,** 277-305.

Massey V. (1994). Activation of molecular oxygen by flavins and flavoproteins. *J Biol Chem.* **269**, 22459-22462.

Massey V. (1995). Introduction: flavoprotein structure and mechanism. *FASEB J.* **9**, 473–475.

Massey V. (2000). The Chemical and Biological Versatility of Riboflavin. *Biochemical Society Transactions* **28**, 283 – 296.

Massey V. (2002). The reactivity of oxygen with flavoproteins. *International Congress Series* **1233**, 3-11.

Massey V., Veeger C. (1961). Studies on the reaction mechanism of lipoyl dehydrogenase. *Biochim Biophys Acta*. **48**, 33-47.

Massey V., Palmer G. (1966). On the existence of spectrally distinct classes of flavoprotein semiquinones. A new method for the quantitative production of flavoprotein semiquinones, *Biochemistry* **10**, 3181-3189.

Massey V., Ghisla S. (1974). Role of charge transfer interactions in flavoproteins catalysis. *Annals of the New York Academy of Sciences* **227**, *The Mechanism of Energy Transduction in Biological Systems*, 446-465.

Massey V., Hemmerich P. (1978). Photoreduction of flavoproteins and other biological compounds catalyzed by deazaflavins. *Biochemistry* **17**, 9-16.

Mattevi A. (2006). To be or not to be an oxidase: challenging the oxygen reactivity of flavoenzymes. *Trends Biochem Sci*. **31**, 276-273.

Mayhew S. (1999). The effect of pH and semiquinone formation on the oxidation-reduction potentials of flavin mononucleotide: a reppraisal. *Eur J. Biochem*. **264**, 698-702.

McCoy A.J., Grosse-Kunstleve R.W., Adams P.D., Winn M.D., Storoni L.C., Read R.J. (2007). Phaser crystallographic software. *J Appl Crystallogr.* **40**, 658-674.

Moser C.C., Keske J.M., Warncke K., Farid R.S., and Dutton P.L. (1992). Nature of biological electron transfer. *Nature* **355**, 796-802.

Müller F., Brüstlein M., Hemmerich P., Massey V., Walker W.H. (1972). Light-absorption studies on neutral flavin radicals. *Eur. J. Biochem*. **25**, 573–580.

Müller J.J, Lapko A., Bourenkov G., Ruckpaul K., Heinemann U. (2001). Adrenodoxin Reductase-Adrenodoxin complex structure suggests electron transfer path in steroid biosynthesis. *J. Biol. Chem* **276**, 2786-2979.

Page C.C., Moser C.C., Chen X., Dutton P.L. (1999). Natural engineering principles of electron tunneling in biological oxidation-reduction. *Nature* **402**, 47-52.

Pai E.F., Schulz G.E. (1983). The catalytic mechanism of glutathione reductase as derived from x-ray diffraction analyses of reaction intermediates. *J Biol Chem*. **258**, 1752-1757.

Painter J., Merritt E.A. (2006). Optimal description of a protein structure in terms of multiple groups undergoing TLS motion. *Acta Crystallogr D Biol Crystallogr*. **62**, 439-450.

Parales J.V., Parales R.E., Resnick S.M., Gibson D.T. (1998). Enzyme specificity of 2-nitrotoluene 2,3-dioxygenase from *Pseudomonas sp*. strain JS42 is determined by the C-terminal region of the alpha subunit of the oxygenase component. *J Bacteriol*. **180**, 1194-1199.

Parales R.E., Parales J.V., Gibson D.T. (1999). Aspartate 205 in the catalytic domain of naphthalene dioxygenase is essential for activity. *J Bacteriol.* **181**, 1831-1837.

Powell P.J., Lau S.M., Killian D., Thorpe C. (1987). Interaction of acyl coenzyme A substrates and analogues with pig kidney medium-chain acyl-CoA dehydrogenase. *Biochemistry* **26**, 3704- 3710.

Prudêncio M., Ubbink M. (2004). Transient complexes of redox proteins: structural and dynamic details from NMR studies. *J Mol Recognit*. **17**, 524-539.

Que L. Jr. (2000). One motif - many different reactions. *Nat Struct Biol*. **7**, 182-184.

Reipa V., Holden M.J., Vilker V.L. (2007). Association and redox properties of the putidaredoxin reductase-nicotinamide adenine dinucleotide complex. *Biochemistry* **45**, 13235-13244.

Rieske J.S., Maclennan D.H., Coleman R. (1964). Isolation and properties of an iron-protein from the (reduced coenzyme Q)-cytochrome C reductase complex of the respiratory chain. *Biochem. Biophys. Res. Commun* **15**, 338–344.

Roome P.W., Jr., Philley J.C., Peterson J.A. (1983). Purification and properties of Putida redoxinreductase. *J Biol. Chem.* **4**, 2593- 2598.

Rossmann M.G. (1990). The molecular replacement method. *Acta Crystallogr A.* **46**, 73-82.

Sakurai T., Hosoya H. (1966). Charge transfer complexes of nicotinamide-adenine dinucleotide analogues and flavin mononucleotide. *Bibl Laeger*. **112**, 459-468.

Sambrook J, E. F. Fritsch & T. Maniatis (1989). *Molecular Cloning: a laboratory Manual*, Vol. 2nd edn: Cold Spring Harbor, NY: Cold spring Harbor Laboratory.

Sauber K., Fröhner C., Rosenberg G., Eberspächer J., Lingens F. (1977). Purification

and properties of pyrazon dioxygenase from pyrazon-degrading bacteria. *Eur J Biochem.* **74**, 89-97.

Schulz G.E., Schirmer R.H., Sachsenheimer W., Pai E.F. (1978). The structure of the flavoenzyme glutathione reductase. *Nature* **273**, 120-124.

Scrutton N.S., Berry A., Deonarain M.P., Perham R.N. (1990). Active site complementation in engineered heterodimers of *Escherichia coli* glutathione reductase created *in vivo*. *Proc. Biol. Sci.* **242**, 217-224.

Senda T., Yamada T., Sakurai N., Kubota M., Nishizaki T., Masai E., Fukuda M., Mitsuidagger Y. (2000), Crystal structure of NADH-dependent ferredoxin reductase component in biphenyl dioxygenase. *J Mol Biol* **304**, 397-410.

Senda M., Kishigami S., Kimura S., Fukuda M., Ishida T., Senda T. (2007). Molecular mechanism of the redox-dependent interaction between NADH-dependent ferredoxin reductase and Rieske-type [2Fe-2S] ferredoxin. *J Mol Biol* **373**, 382-400.

Sevrioukova I.F., Li H., Poulos T.L. (2004). Crystal structure of putidaredoxin reductase from *Pseudomonas putida*, the final structural component of the cytochrome P450cam monooxygenase. *J Mol Biol* **336**, 889-902.

Stankovich M.T. (1980). An anaerobic spectroelectrochemical cell for studying the spectral and redox properties of flavoproteins. *Anal Biochem*. **109**, 295-308.

Strickland S., Massey V. (1973). The mechanism of action of the flavoprotein melilotate hydroxylase. *J Biol. Chem.* **248**, 2953-2962.

Subramanian V, Liu TN, Yeh WK, Serdar CM, Wackett LP & Gibson DT (1985). Purification and properties of ferredoxinTOL. A component of toluene dioxygenase from *Pseudomonas putida* F1. *J Biol Chem* **260**, 2355-2363.

Subramanian, S., Liu, T.-N., Yeh, W.-K., Narro, M., Gibson, D. (1981). Purification and properties of NADH-ferredoxinTOL reductase. *J Biol Chem* **256**, 2723-2730.

Sucharitakul J., Chaiyen P., Entsch B., Ballou D.P. (2005). The reductase of p-hydroxyphenylacetate 3-hydroxylase from *Acinetobacter baumannii* requires p-hydroxyphenylacetate for effective catalysis. *Biochemistry* **44**, 10434-10442.

Susin S.A., Lorenzo H.K., Zamzami N., Marzo I., Snow B.E., Brothers G.M., Mangion J., Jacotot E., Costantini P., Loeffler M., Larochette N., Goodlett D.R., Aebersold R., Siderovski D.P., Penninger J.M., Kroemer G. (1999). Molecular characterization of mitochondrial apoptosis-inducing factor, *Nature* **6718**, 441-446.

Sun W., Williams C.H., Massey V. (1997). The role of glycine 99 in L-lactate monooxygenase from *Mycobacterium smegmatis*. *J. Biol. Chem*. **272**, 27065-27076.

Tarasev M. and Ballou D.P. (2006). The "Bridging" Aspartate 178 in Phthalate Dioxygenase Facilitates Interactions between the Rieske Center and the Iron(II)-Mononuclear Center. Biochemistry **45**, 10208-10216.

Wood P.W. (1988). The potential diagram for oxygen at pH 7. *Biochem. J.* **253**, 287-289.

Zylstra G.J., Gibson D.T. (1989). Toluene degradation by *Pseudomonas putida* F1. Nucleotide sequence of the *todC1C2BADE* genes and their expression in *Escherichia coli. J Biol Chem* **264,** 14940-14946.

APPENDIX

A Experimental part

1 Appendix molecular biology

Table A1. Cloning and expression strains used in the thesis.

Strain	Derivative	Genotyp	Antibiotic Resistance
DH5α	K-12	F⁻ Φ80d*lac*Z_M15 *nup*G *gln*V44 (*lac*ZYA-*arg*F) U169 *deo*R *rec*A1 *end*A1 *thi*-1 *hsd*R17 (r_{K^-}, m_{K^+} *phoA sup*E44 *gyr*A96 relA1 λ– *rel*A1	none
XL-1blue	K-12	e*nd*A1 *gyr*A96(nal^R) *thi-1 rec*A1 *rel*A1 *lac gln*V44 *F'[::Tn10 pro*AB$^+$ *lac*I^q Δ(*lac*Z)*M15] hsd*R17(r_{K^-}, m_{K^+})	none
BL21	B	F⁻ *omp*T *hsd*S(r_{B^-} m_{B^-}) dcm$^+$ Tet^r *gal*	
CodonPlus		λ(DE3) *end*A Hte [*argU ileY leuW* Cam^r]	Cam

CAM is the abbreviation for chloramphenicol and was used with a final concentration of 50 µg/ml solved in 100% ethanol.

Table A2. Vectors, into which *todA* and *todB* were cloned, and the names of new cloned plasmids.

Vector	insert (gene)	T7lac	Antibiotics Resistance	His-Tag
pET-11a	none	yes	Amp/Cb	none
pET-15 b	none	yes	Amp/Cb	N
pET15b*todA*	*todA*	yes	Amp/Cb	N
pET11a*todB*	*todB*	yes	Amp/Cb	none
pET15b*to*	*todB*	yes	Amp/Cb	N

Amp stands for ampicillin(100 µg/ml), Cb for Carbenillin (50 µg/ml). N stands for N-Terminal His6-Tag.

Table A3. Primers used in cloning of reductase$_{TOL}$ and ferredoxin$_{TOL}$.

Name	Sequence	(°C)
pput*todA_fw*:	5′- GAC CAT ATG GCT ACC CAT GTG GCG AT - 3′	64
pput*todA_rv*:	5′- GAG GAT CCT CAC GTT AGG TCT CCT CCA -3′	63
pput*todB_fw*:	5′- GAC CAT ATG ACT TGG ACA TAC ATA TTG CGG -3′	62
pput*todB_rv*:	5′- GCG GAT CCT CAC TTC AAC TCC CCG TTG T- 3′	65

Recognition site for *Nde*I is colored in yellow, the recognition site for *Bam*HI is depicted in blue. *fw* stands for forward primer, *rv* for reverse primer. Tm is the melting temperature of the primers in °C.

Table A4. PCR reaction material and thermoycler condition of PCR reactions of cloning of reductase$_{TOL}$ and ferredoxin$_{TOL}$

PCR reaction material

dNTP Mix: 200 nM

Forward primer 500

Reverse Primer: 500

Genomic DNA *P.putida F:* 25 ng

Pfu Polymerase: 0.25 U.

10 x Pfu Polymerase buffer: 1 x

Step	Temperature	Time (min)
1. Initial denaturation	95 °C	5
2. Denaturation	95 °C	2
3. Annealing	63 °C	2
4. Extension	74 °C	3
5. Final extension	74 °C	10

For thermocycling conditions steps 2 to 4 were repeated 20 x with a final extension step at the end.

Table A5. Loading dye for 1 % agarose electrophoresis.

Loading dye (6x)	0.25 % (w/v) bromphenol blue
	0.25 % (w/v) xylene cyanol FF
	30 % (w/v) glycerol

2 Appendix expression and purification

Table A6. Recipe for ten 12 % SDS-PAGE gels.

Name	concentration	chemical/biochemical
SDS loading buffer (4 x)	200 mM	Tris pH 6.8
(DTT+)	8 % (w/v)	SDS
	0.4 % (w/v)	bromphenol blue
	40 % (v/v)	DTT
Running buffer (10 x)	144 g	glycine
	3 g	Tris
	10 g	SDS
		ad 1000 ml H_2O
Staining solution	0.125 g	SERVA BLUE G
	50 ml	acetic acid
		ad 500 ml H_2O
Destaining solution	100 ml	acetic acid
		ad 500 ml H_2O
Polyacrylamide (12 %)	21 ml	ddH_2O
stacking gel	40 ml	Rotiphorese Gel 30
	37.5 ml	1 M Tris pH 8.8
	1 ml	10 % (v/v) SDS
	80 µl	TEMED

	0.5 ml	10 % (w/v) APS
Polyacrylamide (6 %)	36.5 ml	ddH_20
running gel	10 ml	Rotiphorese Gel 30
	2.5 ml	2.5 M Tris pH 6.8
	0.5 ml	10 % (w/v) SDS
	40 ml	TEMED
	0.5 ml	10 % (w/v) APS

Table A7. Media and solutions used for cloning and expression.

LB Medium :	10 g/l	trypton
	5 g/l	yeast extract
	5 g/l	NaCl
TB Medium:	12 g/l	trypton
	24 g/l	yeast extract
	10 ml/l	87 % glycerol
dYT Medium:	16 g/l	trypton
	5 g/l	yeast extract
	5 g/l	NaCl
SOB Medium:	20 g/l	trypton
	5 g/l	yeast extract
	0.5 g/l	NaCl
	2.5 mM	KC
		pH adjusted to 7.0 with NaOH
	10 mM	$MgCl_2$
LB Agar:	10 g/	trypton
	5 g/l	yeast extract
	5 g/l	NaCl

	15 g/l	bacto agar
Lysis buffer:	40 mM	Tris-HCl pH 8.0
	20 mM	sodium acetate
	1 mM	EDTA
	1 % (w/v)	SDS
TAE buffer (50x):	2 M	Tris
	1 ml	acetic acid
	50 mM	EDTA pH 8.0

Table A8. Buffers used for the purification of reductase$_{TOL}$.

Buffer A:	50 mM	Tris-HCl pH 8.5
	20 mM	NaCl
	20 mM	Imidazole
	1 mM	PMSF
Buffer B:	50 mM	Tris-HCl pH
	20 mM	NaCl
	varying concentration of imidazole	
Buffer C:	50 mM	Tris-HCl pH 8.0
Buffer D:	50 mM	Tris-HCl pH 8.0
	150 mM	NaCl

Table A9. Buffers used for the purification of ferredoxin$_{TOL}$.

Breaking buffer:	50 mM	Tris-HCl pH 6.9
	1 mM	DTT
	1 mM	PMSF

Buffer E1:	50 mM	Tris-HCl pH 6.9
	1 mM	DTT
Buffer E2:	50 mM	Tris-HCl pH 6.9
	1 mM	DTT
	0.5 M	NaCl
Buffer F1:	5 mM	KH_2PO_4 pH 6.9
	1 mM	DTT
	1 mM	DTT
Buffer G:	50 mM	Tris-HCl pH 6.9
	1 mM	DTT
	150 mM	NaCl

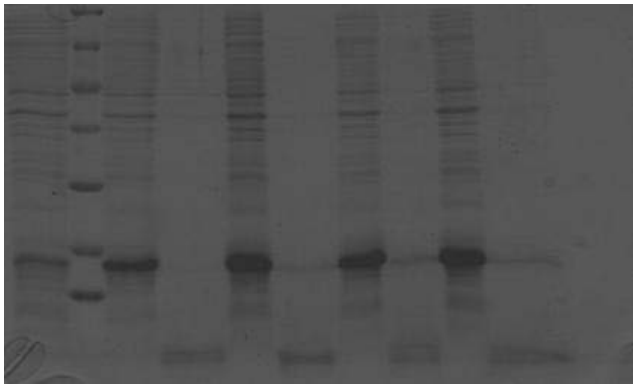

Figure A1. Test expression of ferredoxin$_{TOL}$ in *E. coli* BL21CodonPlus-(DE3) at 18 °C expression temperature after induction. Lane 1 = 0 h before induction, lane 3 = 3 h after induction, lane 4 = supernatant 3 h after induction, lane 5 = 6 h after induction, lane 6 = supernatant 6h after induction, lane 7 = 8 h after induction, lane 8 = supernatant 8 h after induction, lane 9 = 18 h after induction lane 10 = supernatant 18 h after induction, M = unstained molecular weight marker from Fermentas.

3 Appendix spectroscopic characterization

Table A10. Extinction coefficients of reductase$_{TOL}$, ferredoxin$_{TOL}$ and redox dyes used for the calculation of the redox potential.

$mM^{-1}cm^{-1}$	$\varepsilon_x^{RED, ox}$	$\varepsilon_x^{FER, ox}$	$\varepsilon_x^{PS, ox}$	$\varepsilon_x^{S T, ox}$	$\varepsilon_x^{IDS, ox}$
450 nm	11.3	–	9.29	5.95	–
460 nm		7.6	–	–	–
521 nm	0.3	–	44.7	–	–
522 nm	0.287	–	–	28.457	–
610 nm	–	–	–	–	19.375

RED = reductase$_{TOL}$, FER = ferredoxin$_{TOL}$, PS = phenosafranine, ST = Safranin T, IDS = indigo-disulfonate

B Acknowledgment

Ich danke Herrn Prof. Dr. Holger Dobbek für die Bereitstellung des interessanten und facettenreichen Themas, für seine Unterstützung und Bereitschaft, sich geduldig diverser Problematiken anzunehmen und vor allem die Geduld, die er für mich als Person aufgebracht hat.

Weiterhin danke ich Dr. Jae-Hun Jeoung für die zahlreichen Tricks und Kniffe, die er mir im Labor beigebracht hat sowie für die vielen hilfreichen Gespräche.

Ich bedanke mich bei Dr. Tobias Werther für die informative und spaßige Zeit während der Messungen an dem *Stopped-Flow* Spektrophotometer.

Mein Dank gilt ebenso meinen Mitstreitern/-innen in Berlin Sebastian, Jochen, Sandra, Martin, Brinda und Silke, mit denen ich eine angenehme Zeit im und ausserhalb des Labor verbracht habe. Auch die Kollegen aus Bayreuther Zeit möchte ich nicht unerwähnt lassen und mich für die lehrreiche und interessante Zeit bedanken.

Ich danke Sina, die mir stets Mut zugesprochen und mir in jeglicher Weise geholfen hat.

Und nicht zuletzt danke ich meinen Eltern und meiner Schwester für all ihre Unterstützung und Liebe.

Publication list

Lin T.Y., Werther T., Jeoung J.H., Dobbek H. (2012). Suppression of electron-transfer to dioxygen by charge-transfer and electron-transfer complexes in the FAD-dependent reductase component of toluene dioxygenase. *Submitted to JBC*.

Jeoung J.H., Lin T.Y., Bommer M., Dobbek H. (2012). Monodentate binding of homogentisate on mononuclear non-heme Fe(II) site of homogentisate 1,2-dioxygenase: the role of Tyr346. *In preparation*.

C Statement

Hiermit erkläre ich, dass ich die Arbeit selbständig verfasst und keine anderen als die von mir angegebenen Quellen und Hilfsmittel benutzt habe.

Hereby, I declare the fact that I wrote this work independently and used no different data than the sources presented by me.

Ferner erkläre ich, dass ich anderweitig mit oder ohne Erfolg nicht versucht habe, diese Dissertation einzureichen. Ich habe keine gleichartige Doktorprüfung an einer anderen Hochschule endgültig nicht bestanden.

Furthermore, I declare that I did not attempt to submit this thesis elsewhere with or without success. I did not have an equivalent doctor examination at another university

Berlin, den